EFFECT OF SPECTRAL BAND SELECTION AND BANDWIDTH ON WEED DETECTION IN AGRICULTURAL FIELDS USING HYPERSPECTRAL REMOTE SENSING

by

Samuel Bryant Tittle

A thesis submitted in partial fulfillment
of the requirements for the degree

of

Master of Science

in

Environmental Science

MONTANA STATE UNIVERSITY
Bozeman, Montana

November 2017

ACKNOWLEDGEMENTS

I would like to than Rick Lawrence my advisor for all the time and effort he put into helping me on this path. I would like to thank my Committee members Bruce Maxwell and Kevin Repasky for their thoughts, encouragement, and support. Cooper McCann that took time out of his research to sit down and help with processing of the imagery. The folks of the Spatial Sciences Center- including Michael Oldham, Rachel Ulrich, Emma Bode, Emery Three Irons, Paul Bodalski, Mikindra Morin – our shared experience in our windowless world was grand and I thank you all for your contributions to helping me on this journey. I would like to thank the Vandyke and Merja farms for the opportunity to collect data in their fields and Chris Boyer of Kestrel Aviation for flying the sensor. The funding for this research is thanks to the Montana Research & Economic Development Initiative and principal investigator Joe Shaw who headed up the project I was on. Finally all the friends and family that had to deal with my long nights and missed plans in the name of science, thank you.

TABLE OF CONTENTS

TABLE OF CONTENTS CONTINUED

LIST OF TABLES

Table Page

LIST OF FIGURES

Figure Page

LIST OF FIGURES CONTINUED

Figure Page

LIST OF EQUATIONS

Equation Page

ABSTRACT

Presence of weeds in agricultural fields affects farmers' economic returns by increasing herbicide input. Application of herbicides traditionally consists of uniform application across fields, even though weed locations can be spatially variable within a field. The concept of spot spraying seeks to reduce farmers' costs and chemical inputs to the environment by only applying herbicides to infested areas. Current spot spraying technology relies on broad spectral bands with limited ability to differentiate weed species from crops. Hyperspectral remote sensing (many narrow, contiguous spectral bands) has been shown in previous research to successfully distinguish weeds from other vegetation. Hyperspectral sensor technology, however, might not currently be practical for on-tractor applications. The research objectives were to determine (1) the utility of using a limited number of narrow spectral bands as compared to a full set of hyperspectral bands and (2) the relative accuracy of narrow spectral bands compared to wider spectral bands. Answers to these objectives have the potential for improving on-tractor weed detection sensors. Reference data was provided by field observations of 224 weed infested and 304 uninfested locations within two winter wheat fields in Gallatin County, Montana, USA. Airborne hyperspectral data collected concurrently with the reference data provided 6-nm spectral bands that were used in varying combinations and artificially widened to address the research objectives. Band selection was compared using Euclidean, divergence, transformed divergence, and Jefferies-Matusita signature separability measures. Certain three and four narrow band combinations produced accuracies with no statistical difference from the full set of hyperspectral bands (based on kappa statistic analysis, alpha = 0.05). Bands that were artificially widened to 96 nm also showed no statistically significant difference from the use of 6-nm bands for both all bands and select band combinations. Results indicate the potential for bands that can differentiate weed species from crops and that the narrowest spectral bands available might not be necessary for accurate classification. Further research is needed to determine the robustness of this analysis, including whether a single set of spectral bands can be used effectively across multiple crop/weed systems, or whether band selection is site or system specific.

CHAPTER ONE

INTRODUCTION

The goal of this research was to explore techniques that may enhance spot spraying technology for weed management. Managing large or damaging weed populations without over-spraying requires a paradigm shift from traditional, uniform application, toward improved methods of spot spraying. The spatial variation of weeds across a field means that application of consistent herbicide levels result in over-spraying to occur in areas with low weed densities (Thorp and Tian, 2004). Remote sensing has the power to help in location of weeds for spot spraying. This research seeks to investigate the use of narrow spectral bands for weed infestation classification.

The introduction of herbicides into an ecosystem can detrimentally affect the overall function of environmental systems (DeNoyelles et al., 1982; Rohr and Crumrine, 2005; Solomon et al., 1996). Patch spraying has the ability to reduce herbicide inputs to the surrounding environment and lower treatment costs by spraying only where weeds are present (Weis et al., 2008). Site specific application of herbicides has been shown to reduce herbicide application by 25% to 100% (Bongiovanni and Lowenberg-Deboer, 2004; Brown and Steckler, 1993; Laursen et al., 2016; Weis et al., 2008). Remote sensing has seen improvement and reduction in cost of GPS, GIS, computers, sensors, and related technology. The largest issue for most agricultural producers is the expense and inaccessibility of technology, with systems costing tens or hundreds of thousands of dollars (Grains Research & Development Corporation, 2010; Kondinin Group, 2013).

Simplification of sensors and computing has the potential to further reduce the cost of technology.

One of the current shortcomings of on-tractor weed sensors is the inability to differentiate between crop and weeds. Systems like the Weedseeker PhD600 look between rows, spraying any vegetation detected against the soil background (Sui et al., 2008), limiting the time of year a system can be effective and crop cover types in which it can be used. Understanding the aspects of weeds' spectral signatures for precision weed control can improve weed classification and the field of remote sensing as whole.

Large data sets can to be collected and analyzed along with ancillary data to understand what parts of spectral signatures discriminate weeds and crop targets. Airborne platforms can cover a large swath of land, providing high spatial resolution with proper preprocessing, in a short time frame compared to ground-based methods. Flights can be planned for the specific missions taking into account time of day and target areas to control for cloud cover, observation angle, and sun angle. Logistics of planning a flight can make multiple flights expensive and time consuming however. Logistics and inherent drawbacks of airborne platforms, like roll, pitch, and yaw errors and limitations from aviation laws, permitting, fuel capacities, and airfield locations, make flying feasible for data collection but not for extensive monitoring plans like those that agriculture producers would require.

The addition of a hyperspectral sensor to a flight provides higher analytical power. Hyperspectral sensors divide the electromagnetic (EM) spectrum in to many narrow, contiguous spectral bands. Based on the width of these bands, as small as 1.7 nm,

and the spectral range, these sensors can have over 200 bands (Resonon Inc., 2016; Spectral Imaging Ltd., 2014). This high spectral resolution provides the ability to identify portions of the EM spectrum that can be used to differentiate weeds.

The high dimensionality of hyperspectral data, however, means that data reduction is required to remove volume and redundancy for processing and analysis (Su et al., 2014; Sun et al., 2015). Excessive data can cause over classification and collection across a large spectral range can increase the cost of sensor equipment. Improvements in processing time and reduction of storage requirements can be made by reducing data to only the bands necessary while still identifying the target. Knowing the narrow bands that can be used to differentiate weeds can reduce the price of sensors by only collecting data in the necessary range; this reduction of the data is called band selection.

Hyperspectral data was collected in this research to address two questions of the potential for applying narrow spectral bands to weed identification. (1) Can hyperspectral data be reduced to only a few bands and still maintain accuracies found using all bands? (2) How necessary are narrow bands to identification of a target and to what extent can they be widened without negative effects on accuracy? Chapter 3 addresses the first of these questions, while Chapter 4 addresses the second question. Chapter 2 reviews the state of the science with respect to hyperspectral and multispectral weed detection and band selection algorithms. Chapter 5 summarizes the research and proposes future research needed to more fully explore the research questions.

References Cited

Bongiovanni, R., Lowenberg-Deboer, J., 2004. Precision Agriculture and Sustainability. Precision Agriculture 5, 359–387. doi:10.1023/B:PRAG.0000040806.39604.aa

Brown, R.B., Steckler, J.-P.G.A., 1993. Weed Patch Identification in No-Till Corn Using Digital Imagery. Canadian Journal of Remote Sensing 19, 088–091. doi:10.1080/07038992.1993.10855155

DeNoyelles, F., Kettle, W.D., Sinn, D.E., 1982. The Responses of Plankton Communities in Experimental Ponds to Atrazine, the Most Heavily Used Pesticide in the United States. Ecology 63, 1285–1293. doi:10.2307/1938856

Du, Q., Yang, H., 2008. Similarity-Based Unsupervised Band Selection for Hyperspectral Image Analysis. IEEE Geoscience and Remote Sensing Letters 5, 564–568. doi:10.1109/LGRS.2008.2000619

Gao, B.-C., Montes, M.J., Davis, C.O., Goetz, A.F.H., 2009. Atmospheric correction algorithms for hyperspectral remote sensing data of land and ocean. Remote Sensing of Environment, Imaging Spectroscopy Special Issue 113, S17–S24. doi:10.1016/j.rse.2007.12.015

Grains Research & Development Corporation, 2010. Why We Purchased a Header and Weedseeker [WWW Document]. www.grdc.com.au. URL https://www.grdc.com.au/Research-and-Development/GRDC-Update-Papers/2010/09/WHY-WE-PURCHASED-A-HEADER-AND-WEEDSEEKER (accessed 2.6.16).

Kondinin Group, 2013. Weedseeker upgrade looks the goods [WWW Document]. Farming Ahead. URL http://www.farmingahead.com.au/articles/1/9196/2013-10-18/news/weedseeker-upgrade-looks-the-goods (accessed 2.6.16).

Laursen, M.S., Jørgensen, R.N., Midtiby, H.S., Jensen, K., Christiansen, M.P., Giselsson, T.M., Mortensen, A.K., Jensen, P.K., 2016. Dicotyledon Weed Quantification Algorithm for Selective Herbicide Application in Maize Crops. Sensors 16, 1848. doi:10.3390/s16111848

Resonon Inc., 2016. Hyperspectral Imaging Cameras Datasheet [WWW Document]. www.resonon.com. URL http://www.resonon.com/data-sheets/ResononHyperspectralCameras.Datasheet.pdf (accessed 2.5.16).

Rohr, J.R., Crumrine, P.W., 2005. Effects of an herbicide and an insecticide on pond community structure and processes. Ecological Applications 15, 1135–1147. doi:10.1890/03-5353

Solomon, K.R., Baker, D.B., Richards, R.P., Dixon, K.R., Klaine, S.J., La Point, T.W., Kendall, R.J., Weisskopf, C.P., Giddings, J.M., Giesy, J.P., others, 1996. Ecological risk assessment of atrazine in North American surface waters. Environmental Toxicology and Chemistry 15, 31–76.

Spectral Imaging Ltd., 2014. SPECIM Datasheets [WWW Document]. URL http://www.specim.fi/files/pdf/aisa/datasheets/AisaOWL_ver1-2014.pdf (accessed 2.5.16).

Su, H., Du, Q., Chen, G., Du, P., 2014. Optimized Hyperspectral Band Selection Using Particle Swarm Optimization. IEEE Journal of Selected Topics in Applied Earth Observations and Remote Sensing 7, 2659–2670. doi:10.1109/JSTARS.2014.2312539

Sui, R., Thomasson, J.A., Hanks, J., Wooten, J., 2008. Ground-based sensing system for weed mapping in cotton. Computers and Electronics in Agriculture 60, 31–38. doi:10.1016/j.compag.2007.06.002

Sun, K., Geng, X., Ji, L., 2015. A New Sparsity-Based Band Selection Method for Target Detection of Hyperspectral Image. IEEE Geoscience and Remote Sensing Letters 12, 329–333. doi:10.1109/LGRS.2014.2337957

Thorp, K.R., Tian, L.F., 2004. A Review on Remote Sensing of Weeds in Agriculture. Precision Agriculture 5, 477–508. doi:10.1007/s11119-004-5321-1

Weis, M., Gutjahr, C., Ayala, V.R., Gerhards, R., Ritter, C., Schölderle, F., 2008. Precision farming for weed management: techniques. Gesunde Pflanzen 60, 171–181. doi:10.1007/s10343-008-0195-1

CHAPTER TWO

LITERTURE REVIEW

Corrections

Radiometric Corrections

Images collected with passive optical sensors rely on the reflection of radiation from objects. This radiation must travel through the Earth's atmosphere before and after reflecting off an object (Fraser and Kaufman, 1985). Variations in the atmosphere resulting from gases, aerosol, water particles (King et al., 1992), the angle and level of illumination, sensor viewing angle (Andújar et al., 2015; Dozier and Warren, 1982), and sensor noise can affect the data values collected. Changes in these conditions can cause reflectance values to be different for the same target signature and sensor. The data necessary to correct for these variations in reflectance can in many cases be collected and algorithms used to correct the image. Corrections for atmospheric conditions are challenging however, as aerosol particles can vary across space and time, making them hard to model and account for in imagery (Xia et al., 2016). The atmospheric conditions in images collected with scanning sensors may change as data is collected over extended time, causing inconsistent variation across the image (Coppin and Bauer, 1994). Images must be normalized for variations in atmosphere for comparison within and between images.

The correction of images is accomplished through modeling of the atmosphere and applying the estimates of the model to the pixels of the image. The model can be a

simple solar constant (Gueymard, 2004) or more advanced . Flat field correction (FFC) is a common method to correct for non-uniform response (Davidson et al., 2003). FFC can be used in an image to correct for differences in irradiance assumed to be caused by the atmosphere. The correction is based in a uniform, spectrally homogeneous, Lambertian surface known as a flat field. A correction factor is generated for the imagery assuming that any deviance from the expected uniform surface is not related to the spectral properties of the object (Kelcey and Lucieer, 2012). The FFC can be modified to use an area of the image with known spectral properties to correct the rest of the image (Green et al., 1990).

Other methods rely on using a second, already corrected image to correct the first (McCann et al., 2017). This approach normalizes the two images and can be accomplished either through a universal correction for the entire image to be corrected, if it is assumed that atmospheric conditions are constant across the image, or on a localized basis if it is necessary to correct for atmospheric variation within the image to be corrected. This allows a correction method unavailable in one image to be used in another.

Geometric Corrections

Geometric corrections are necessary to compare two data sources such as in pixel-based changed detection (Hussain et al., 2013) or locate an image in three dimensional space (Toutin, 2004). Correct geometric registration can solve many geometric errors and is even more important for data extraction of small targets. The selection of the wrong pixel can cause unreliable analysis if targets are only contained in very specific pixels.

The integration of datasets that are not properly geo-located can cause errors (Mouginot et al., 2017).

Increased error can be introduced with higher spatial resolution (Toutin, 2004) as errors are compounded, for example a 0.5-m pixel positively classified as infested with a maximum error of 5 m could be 10 pixels from its true location when compared to actual ground location, causing low user accuracies (Glenn et al., 2005). Inconsistent movement quantified as roll, pitch, and yaw of aircraft as data is collected can vary across the image, casing unknown levels error and bringing into question if pixel locations are correct and if it is feasible to compare between datasets (Aspinall et al., 2002).

Sensor Platforms for Weed Identification

The on-tractor platform has little issue with atmospheric and geo-referencing since the sensor is directly above the ground and spraying can occur in real time, making synchronization of weeds maps, true ground locations, and spraying less complicated (Plant, 2001; Senay et al., 1998). On-tractor real time sensing and spraying are major advantages but limit the computing time and sensors size. A sprayer will not have time to spray the weed before the tractor has passed if the process takes too long. The computing unit and sensor must fit on the tractor, limiting the size and weight (Sui et al., 2008). Data collection is also limited with a sensor close to the ground, causing a relatively small field of view (FOV). Sensors therefore must be driven back and forth to collect data (Campbell and Wynne, 2011).

The use of space-borne platform sensors has the advantage of collecting large swaths with limited logistics of flight planning and restrictions from topography or local

government for the end user at a relatively low costs (Röser and von Schönermark, 1996). Excessive platform movement from turbulence or maneuvering is also limited (Lunetta et al., 1991). Space platform sensors do have drawbacks that limit sensing of weed populations in individual fields (Steven, 1993). The drawbacks include reduced spatial resolution, potential for cloud cover on collection dates, inflexibility in mission planning, and issues with speed of delivery.

Airborne platforms share some of the advantages of space-borne platforms while reducing some drawbacks (Röser and von Schönermark, 1996). Airborne platforms can cover large swaths of land in a short time compared to ground based methods (Pradeep K. Goel et al., 2003a). The airborne sensor can be flown closer to the ground, providing the ability for higher spatial resolution and less atmospheric error (Slater and Jackson, 1982). Flights can be planned to target specific times of day and areas, thereby controlling cloud cover, observation angle, and sun angle.

Airborne platforms have drawbacks. Georeferencing the image to actual ground locations can be difficult because roll, pitch, and yaw of the aircraft must be accurately measured and accounted for in the image (Aspinall et al., 2002). Limitations from aviation laws, permitting regulations, fuel capacities, and airfield locations can cause data collection in some areas to not be feasible (Röser and von Schönermark, 1996). Multiple missions increase costs with a premium placed on professional's time and equipment. Airborne sensors are common for reconnaissance and research data collection for vegetation, and have seen an increased use with unmanned aerial vehicles (UAV) (Berni

et al., 2009; Casbeer et al., 2005; Domingues Franceschini et al., 2017; Kelcey and Lucieer, 2012; Natividade et al., 2017; Torres-Sánchez et al., 2013; Villa et al., 2016).

Multispectral Weed Sensing

The variability of multispectral sensors makes them numerous. Multispectral sensors range from government sponsored satellite campaigns like Landsat that can be used to collect regional land use data (Zhang and Weng, 2016) to more common and easily accessible sensors like retrofitted point and shoot cameras, often mounted in UAVs (Fornace et al., 2014). The power of multispectral sensing is in the relatively low cost data and wide availability of sensors. Research requiring examination of spectral signatures with large changes in certain regions of the EM spectrum are common; examples include land cover change (Sankey et al., 2012) and biomass mapping (Roy and Ravan, 1996). Due to the large number of available sensors, using multiple sensors is an option to collected data in regions not covered by a single sensor (Skakun et al., 2017). The ability for multispectral sensors to collect wide bands in the visible and near infrared (NIR), has led to its use in vegetation research like rangeland monitoring (Sankey et al., 2009; Todd et al., 1998) using indexes such as the normalized difference vegetation index (NDVI) that use bands from the visible red and NIR spectrum.

Current UAS technology are capable of using point-and-shoot cameras adapted to be triggered by software for visible spectrum and NIR multispectral sensing (Colomina and Molina, 2014; Goebel et al., 2015). More robust airborne systems are available for use with larger sensors and can be used for forest fires monitoring where safety concerns limit manned flight (Casbeer et al., 2005; Yuan et al., 2015).

The ability to use NIR or visible portions of the spectrum has led to use of multispectral sensing in the search for weeds in various crops including corn (*Zea mays*) (Peña et al., 2013), sunflowers (*Helianthus annuus L.*) (López-Granados et al., 2016), wheat (*Triticum spp.*) (Lamb, 2000; López-Granados et al., 2008), rice (*Oryza sativa*) (Barrero et al., 2016), and soybeans (*Glycine max*) (Gibson et al., 2004; Gray et al., 2008).

Current use of multispectral weed identification suffers from one or both of two short falls; spatial resolution and spectral resolution (López-Granados, 2011). The spatial resolution required for sensing of plants is based on the Linear Mixing Model (LMM). The LMM in an agricultural field can be visualized like a checker board where light hits the reflects off weeds, crops, bare soil, roads, or other structures in the field (Gao et al., 2015). Mixing of the spectral response of a pixel occurs because the sensor does not have enough spatial resolution to separate different pure spectral components (Liaghat and Balasundram, 2010). Increasing the spatial resolution can improve differentiation by allowing individual pixels to contain only one class or allow object-based image analysis.

Object-based image analysis allows classification of weed species with limited spectral separation (López-Granados et al., 2016; Peña et al., 2013), however the pattern recognition while accurate can require large amounts of processing time not reasonable on-tractor (Barrero et al., 2016). When plots were experimentally planted in monoculture or predetermined crop/weed mixes, multispectral sensors could classify weed plots and crop plots sided by side (Gibson et al., 2004; Gray et al., 2008). The more complex issue is when the co-occurring vegetation are not separable but a mixture of species, creating a

mixed signature, an issue more prevalent in airborne and space borne sensing due to spatial resolution common to these sensors (Kruse et al., 2003; Zhu et al., 2015). Multispectral sensors can lack the spectral resolution to separate crop and weed species when they are mixed within pixels (Lamb, 2000).

Spectral

Plants Spectra

The spectral signature of all plants are similar due to morphology (Zwiggelaar, 1998). It has been concluded that vegetation canopy reflectance varies with hemispherical reflectance, area, orientation, and transmittance of the leaves in a canopy, along with supporting structure hemispherical reflectance, hemispherical reflectance transmittance, background reflectance, solar zenith angle, viewing angle, and azimuth angle (Colwell, 1974). Plant signatures change as they grow and mature, making timing of image acquisition important to vegetation differentiation. Canopy reflectance changes with sun angle as the proportion of illuminated to shaded vegetation and soil change (Bauer, 1985). The proportions of illuminated and shaded areas visible also change as the viewing angle of the sensor changes. Crop row direction, height, and species affect the role sun angle has on plant spectra (Lord et al., 1988). Image acquisition occurring at the same times of day and year can minimize variability in light and shadow patterns caused by sun angle.

The characteristic spectral properties of plants have high absorption in the visible spectrum caused by chlorophyll for photosynthesis (Chappelle et al., 1992; Mackinney, 1941). The transition from the visible red to the NIR shows an increase in reflectance

termed the red edge (Horler et al., 1983). The NIR portion of the spectrum is reflected by structures within the leaves and stems of plants, creating potential variation in spectral curves for individual plants (Zwiggelaar, 1998). Vegetation indexes like NDVI use the high NIR and lower visible reflectance as inputs. Identifying differences in vegetation for land cover with NDVI is popular (Lamb et al., 1999; Rouse et al., 2010), and NDVI is used as metric for biomass in hard to access areas (Goswami et al., 2015). NDVI however cannot differentiate plant species unless difference in biomass or spectral temporal variations are appropriate indicators of species (Zheng et al., 2015).

Weed and Crop Spectra

Co-occurring vegetation, like crop and weed species, make detecting weed populations complex. This phenomenon can be described by a nonlinear mixing model (NLMM), and these mixtures must be considered as individual spectral signatures (Gao et al., 2015). Understanding how the spectral properties of weed and crop mix allow varying spectra to be classified without 100% coverage of the target class (McGwire et al., 2000; Somers et al., 2011).

Articles pertaining to the sensing of weeds are found in the literature as far back as the 1970s, with extensive articles in the 1980s, most early reported research related to the use of aerial photography and the basic spectral properties of weeds (Bauer, 1985; Colwell, 1974; Huete et al., 1985; Knipling, 1970). The sensing of weeds against bare ground, where green vegetation is compared to soil back grounds, is the simplest form of measurement (Haggar et al., 1983; MacDonald and Hall, 1980). Weeds were identified 90% of the time against soil backgrounds as early as the 1980s using a use a modified

Oxford Precision sprayer with a sensor to detect NIR and red reflectance (Haggar et al., 1983).

Soil spectral properties greatly differ from those of plants (Haggar et al., 1983; Scotford and Miller, 2005), allowing weeds to be identified against a soil background. Classifying weeds in the inter-row spacing or with imagery flown at an altitude such that the young crop species are indistinguishable from the soil background allows weeds to be classified (Lamb et al., 1999). Active sensors for weed identification like the Weedseeker PhD600 are capable of reducing spraying by looking between the crop rows and spraying any detected vegetation against the soil background (Sui et al., 2008). Once crops have grown to a certain size or mixed with weeds, these types of sensors are not able to differentiate the species, causing these techniques to only be useful part of the growing season (Haun, 1973; Nieto et al., 1968; Vanderlip and Reeves, 1972).

The sensing of weeds and distinguishing them from crops must rely on varying spectral properties caused by differences in structure (Zwiggelaar, 1998). Farmers' planting and spraying calendars, along with the life cycle of the weeds, are deciding factors for when images are collected for spraying purposes. Weeds are more susceptible to spraying at certain life stages (Tidemann et al., 2016), requiring spraying to occur at specific times before which mapping must occur. Real time sensors must also account for changes in detectable limits with different stages of plant growth. Physiological variability can occur in the weed species and co-occurring vegetation throughout sites, making clear spectral signatures for a species unlikely (Lawrence et al., 2006). It is possible that patches of weeds or crops' spectral signatures will also differ across the

field due to differing levels of competition, available sunlight, soil conditions, and water (Khokhar et al., 2017).

Hyperspectral Weed Sensing

Multispectral imagery does not provide enough spectral resolution to resolve narrow absorption and reflection features that might be needed to distinguish some weed species from co-occurring crops (Brown and Noble, 2005; Glenn et al., 2005). Hyperspectral imagery consists of many contagious narrow spectral bands for high spectral resolution and the ability to isolate small parts of the spectral signature to be compared (Aspinall et al., 2002).

Hyperspectral imagery with the ability to analyze small sections of the EM spectrum has been shown to classify weed species in multiple agricultural settings including cabbage (*Brassica oleracea*) (Deng et al., 2016), corn (*Zea mays*) (Goel et al., 2002; Lin et al., 2017; Moshou et al., 2013; Wendel and Underwood, 2016), soybeans (*Glycine max*) (Goel et al., 2002; Huang et al., 2016), sugar beet (*Beta vulgaris*) (Okamoto et al., 2007), tomatoes (*Solanum lycopersicum*) (Staab et al., 2009), and wheat (*Triticum spp.*) (Herrmann et al., 2013).

Majority of research relating to hyperspectral sensors for weed identification in planted crops has either used ground based stationary or handheld sensors (Deng et al., 2016; Herrmann et al., 2013; Lin et al., 2017; Moshou et al., 2013; Okamoto et al., 2007) with only a limited amount integrated on vehicles with the potential for spot spraying, or airborne sensing (Goel et al., 2002; P. K Goel et al., 2003b, 2003a; Huang et al., 2007). Use of hyperspectral for vegetation indices in crops is more common (Pradeep K. Goel et

al., 2003b; Haboudane et al., 2004; Thenkabail, 2017; Thenkabail et al., 2002, 2000; Yang et al., 2007; Ye et al., 2006). Accuracies as high as 100% were recorded in a laboratory study with a hyperspectral sensor (Deng et al., 2016), however in-lab studies cannot replicated variability introduced by infield conditions (Huang et al., 2016). Hyperspectral imaging requires a combination of high data storage, processing, and relatively expensive sensors systems that result in limited feasibility of their use on tractor (Uto et al., 2016).

Hyperspectral sensing outputs large amounts of data, all of which might not be necessary for classification of targets (Riedmann and Milton, 2003). The high dimensionality of hyperspectral data means that data reduction is often preferred to remove volume and redundancy (Su et al., 2014; Sun et al., 2015). An issue that must be considered with hyperspectral image classification is over classification, as within class variation of spectra contain unnecessary noise that is not related to the spectral properties of the target (Yang et al., 2012).

Methods for optimizing narrow spectral bands has seen progress in recent years as hyperspectral data becomes more economical and computer technology improves. Unsupervised and supervised selection methods are available. Unsupervised methods do not require reference data and are based on evaluation of various statistical measures or clustering quality assessment (MartÍnez-UsÓMartinez-Uso et al., 2007). Supervised selection is based on class separability using reference data that includes spectral information related to the classes of interest (Li et al., 2012; Sugiyama, 2007). The classification of certain plant species would fall under supervised classification where

certain target classes are identified. Options for supervised band selection, from now on referred to as band selection, vary but maintain some similarities.

Hyperspectral data can contain bands that are distinct but not revealing in classification of the target class. These distinct bands need to be removed or they may adversely affect results (Gao et al., 2009). Wavelengths known to be absorbed by atmospheric aerosols and water, or that have low signal to noise ratio (SNR) (Czanner et al., 2015) could potentially overpower the target signal and should be removed based on prior knowledge and research (Du and Yang, 2008).

Once data has been processed, the process of optimization must start with determining the number of bands for which to optimize. This can be done in a number of different ways and can be integrated into models or designated by the analyst. The more complicated the image or relatively similar the targets, the more dimensionality is needed to detect or classify the desired targets (Du and Yang, 2008).

Classes within a hyperspectral image are assumed to contain certain spectral properties that make them distinctive, enabling classification. When the reflectance of these classes are placed in multidimensional space, clusters will form (Jia et al., 2016). This can be visualized in two dimensions as a scatter plot where each axis is a spectral band. Spectral separability is the measurement of the distance between points or clusters of points. The more separation between clusters, the more power those bands will have in differentiating the classes represented by the clusters. The measurement of the distance between spectral clusters is achieved with band selection algorithms, with the difference in algorithms consisting of how this distance is measured.

Current Band Selection Algorithms

Band selection algorithms rely on different methods of calculating statistical separation. Examples of common methods are Euclidean minimum distance, divergence, transform divergence, and Jefferies-Matusita.

Euclidean minimum distance is the simplest method, based on the length of a straight line between the centers of spectral clusters (Davis et al., 1978). Applying this concept in two dimensions it can be visualized as the hypotenuse of a right triangle with corners defined by the centers of clusters of pixels for different classes, and this concept is readily extended to *n*-dimensional space for any number of spectral bands. Euclidean minimum distance has been used for band selection in palm print detection (Guo et al., 2012) and change vector analysis of land cover (Berberoglu and Akin, 2009).

Euclidean distance does not, however, take into account any of the variability within clusters (Davis et al., 1978). Euclidean minimum distance applied to signature clusters calculates separability by averaging the distance for every possible pair of points from each signature cluster (Keshava, 2004). Other methods use a probability density function to measure separability. The greater the common probability of the clusters, the closer to zero the distance measurement, indicating poor separation. The distance measurement is based on the statistical separation of two clusters using the logarithmic likelihood ratio.

Divergence measures the likelihood a classifier will correctly place a measurement in a class defined by each cluster with values constrained to greater than 0 (Chang and Wang, 2006). Divergence has shown to produce band combinations from

AVIRIS data with accuracies above 70% with 4 bands and near 80% accuracy with 6 bands (Huang and He, 2005). A transformation can be performed on the divergence calculation to increase separation, creating values from 0 to 2000 (Davis et al., 1978). The advantage is that the transformation contains a negative exponential function creating a saturating effect. The saturating effect creates an exponential decrease as distance values get smaller, so that, when averaged, a few widely separated values in a cluster no longer make a disproportionate difference in the distance metric. Transform divergence was shown to produce accuracies over 92% for as few as 3 bands in research using HYDICE data reducing 191 bands (Yang et al., 2011).

Jeffries-Matusita measures statistical separability using the distance between density functions and contains a negative exponential to create a saturating effect as well, however it requires one more matrix inversion for each feature combination evaluated (Swain and King, 1973). Jeffries-Matusita values range from 0 to 1414 and requires more computing power than transformed divergence to select bands (Davis et al., 1978). Jefferies-Matusita selecting as few as four bands was shown to produce accuracies above the use of all bands with HYDICE data and correlated heavy with all band classifications of AVIRIS data (Yang et al., 2011).

Band Selection for Vegetation

Vegetation has certain spectral aspects and sections of the EM spectrum are consistently found to differentiate vegetation (Thenkabail et al., 2004). Different vegetation types among 27 salt march species showed statistical separability in different regions of the EM spectrum, regions which shared detectable differences were the bands within the visible and red edge (500 – 750 nm), and in the SWIR near 2000 nm (Schmidt and Skidmore, 2003). Results for looking at hyperspectral data in agricultural field showed benefits from bands in blue (462 nm), red edge (708 and 723 nm), and NIR (1157–1419 nm) (Verrelst et al., 2016). The SWIR region (1300–1900 nm) provided the best bands for classification in research looking at differences of vegetation ecotypes (Chan and Paelinckx, 2008)

New Band Selection Algorithms

Research is currently applying the concept of distance metrics and band selection to optimize the use of hyperspectral data. Methods like ant colony optimization (ACO) (Gao et al., 2015), particle swarm optimization (PSO) (Su et al., 2014), and a machine learning method based on Gaussian processes regression (GPR) (Verrelst et al., 2016) seek to streamline the process of band selection. The trend is integration of selection for the number needed bands and location of those bands in the EM spectrum for classification (Gao et al., 2015; Su et al., 2014; Verrelst et al., 2016).

ACO is a swarm intelligence algorithm that imitates pheromone patterns of ants. As an ant searches for food, it releases a pheromone that other ants are attracted to and follow. Pheromones dissipate as time passes causing longer and less used routes to

receive less traffic. Shorter routes receive more traffic, causing more pheromones to remain and attract ants, and selection by positive feed-back. This principal is applied to band selection by plotting all band in space with routes between them. Equations dictate how a pseudo ant decides which route to select and dissipation factor for "pheromones." The algorithm can be programmed to stop at a predetermined number of iterations or when a designated number of bands have been selected (Gao et al., 2014).

PSO is an evolutionary searching approach, where the solutions are projected as a randomly generated swarm of particles that is repeatedly updated. Each new generation's particles move based on a criterion function and velocity determined by an equation that takes into account; the particles location, historically best global solution, and previous velocity scaled by inertia weight (Yang et al., 2012). The criterion function is used to reduce computation cost and gauge class separability. PSO integrates the number of bands selected by using one swarm to optimize bands within a second swarm that tries to optimize the number of bands after each iteration of the internal swarm (Su et al., 2014). This provides a streamlined and objective solution to the number of bands selected without analyst bias.

The GPR procedure also includes an automated selection of the optimal number of bands. The GPR uses a Bayesian model to estimate variance and find the most informative band by progressively removing the least contributing band, highest variance, with a regression model. The last band is then added to a subset of band and the subset of bands is revaluated using the GPR to find the band that has the highest variance and removing it and providing least number of bands.

These individual methods, however, are not yet well established, shown effective in diverse applications, or rigorously compared to established methods discussed above, and further research is need on their use before they can be embraced. Distance metrics form the base of these methods as criterion functions (Gao et al., 2014). Use of these methods to automate and compare various band selection and classification techniques in research seems promising with accuracies over 90% (Gao et al., 2014; Su et al., 2014; Yang et al., 2012), but increased processing times (Ding et al., 2012; Gao et al., 2015).

References Cited

Andújar, D., Fernández-Quintanilla, C., Dorado, J., 2015. Matching the Best Viewing Angle in Depth Cameras for Biomass Estimation Based on Poplar Seedling Geometry. Sensors 15, 12999–13011. doi:10.3390/s150612999

Aspinall, R.J., Marcus, W.A., Boardman, J.W., 2002. Considerations in collecting, processing, and analysing high spatial resolution hyperspectral data for environmental investigations. J Geograph Syst 4, 15–29. doi:10.1007/s101090100071

Barrero, O., Rojas, D., Gonzalez, C., Perdomo, S., 2016. Weed detection in rice fields using aerial images and neural networks, in: 2016 XXI Symposium on Signal Processing, Images and Artificial Vision (STSIVA). Presented at the 2016 XXI Symposium on Signal Processing, Images and Artificial Vision (STSIVA), pp. 1–4. doi:10.1109/STSIVA.2016.7743317

Bauer, M.E., 1985. Spectral inputs to crop identification and condition assessment. Proceedings of the IEEE 73, 1071–1085. doi:10.1109/PROC.1985.13238

Berberoglu, S., Akin, A., 2009. Assessing different remote sensing techniques to detect land use/cover changes in the eastern Mediterranean. International Journal of Applied Earth Observation and Geoinformation 11, 46–53. doi:10.1016/j.jag.2008.06.002

Berni, J.A.J., Zarco-Tejada, P.J., Suarez, L., Fereres, E., 2009. Thermal and Narrowband Multispectral Remote Sensing for Vegetation Monitoring From an Unmanned Aerial Vehicle. IEEE Transactions on Geoscience and Remote Sensing 47, 722–738. doi:10.1109/TGRS.2008.2010457

Brown, R.B., Noble, S.D., 2005. Site-specific weed management: sensing requirements—what do we need to see? Weed Science 53, 252–258. doi:10.1614/WS-04-068R1

Campbell, J.B., Wynne, R.H., 2011. Introduction to Remote Sensing, Fifth Edition, 5th edition. ed. The Guilford Press, New York.

Casbeer, D.W., Beard, R.W., McLain, T.W., Li, S.-M., Mehra, R.K., 2005. Forest fire monitoring with multiple small UAVs, in: American Control Conference, 2005. Proceedings of the 2005. Presented at the American Control Conference, 2005. Proceedings of the 2005, pp. 3530–3535 vol. 5. doi:10.1109/ACC.2005.1470520

Chan, J.C.-W., Paelinckx, D., 2008. Evaluation of Random Forest and Adaboost tree-based ensemble classification and spectral band selection for ecotope mapping using airborne hyperspectral imagery. Remote Sensing of Environment 112, 2999–3011. doi:10.1016/j.rse.2008.02.011

Chang, C.-I., Wang, S., 2006. Constrained band selection for hyperspectral imagery. IEEE Transactions on Geoscience and Remote Sensing 44, 1575–1585. doi:10.1109/TGRS.2006.864389

Chappelle, E.W., Kim, M.S., McMurtrey, J.E., 1992. Ratio analysis of reflectance spectra (RARS): An algorithm for the remote estimation of the concentrations of chlorophyll A, chlorophyll B, and carotenoids in soybean leaves. Remote Sensing of Environment 39, 239–247. doi:10.1016/0034-4257(92)90089-3

Colomina, I., Molina, P., 2014. Unmanned aerial systems for photogrammetry and remote sensing: A review. ISPRS Journal of Photogrammetry and Remote Sensing 92, 79–97. doi:10.1016/j.isprsjprs.2014.02.013

Colwell, J.E., 1974. Vegetation canopy reflectance. Remote Sensing of Environment 3, 175–183. doi:10.1016/0034-4257(74)90003-0

Coppin, P.R., Bauer, M.E., 1994. Processing of multitemporal Landsat TM imagery to optimize extraction of forest cover change features. IEEE Transactions on Geoscience and Remote Sensing 32, 918–927. doi:10.1109/36.298020

Czanner, G., Sarma, S.V., Ba, D., Eden, U.T., Wu, W., Eskandar, E., Lim, H.H., Temereanca, S., Suzuki, W.A., Brown, E.N., 2015. Measuring the signal-to-noise ratio of a neuron. PNAS 112, 7141–7146. doi:10.1073/pnas.1505545112

Davidson, D.W., Fröjdh, C., O'Shea, V., Nilsson, H.-E., Rahman, M., 2003. Limitations to flat-field correction methods when using an X-ray spectrum. Nuclear Instruments and Methods in Physics Research Section A: Accelerators, Spectrometers, Detectors and Associated Equipment, Proceedings of the 4th Internatonal Workshop on Radiation Imaging Detectors 509, 146–150. doi:10.1016/S0168-9002(03)01563-8

Davis, S.M., Landgrebe, D.A., Phillips, T.L., Swain, P.H., Hoffer, R.M., Lindenlaub, J.C., Silva, L.F., 1978. Remote sensing: The quantitative approach. McGraw-Hill International Book Company.

Deng, W., Huang, Y., Zhao, C., Chen, L., Wang, X., 2016. Bayesian discriminant analysis of plant leaf hyperspectral reflectance for identification of weeds from cabbages. AJAR 11, 551–562. doi:10.5897/AJAR2015.10395

Ding, S., Qin, Q., Chen, L., Zhang, H., 2012. Hyperspectral Classification with Swarm Intelligence Optimization Algorithms. Sensor Letters 10, 1759–1767.

Domingues Franceschini, M.H., Bartholomeus, H., van Apeldoorn, D., Suomalainen, J., Kooistra, L., 2017. Intercomparison of Unmanned Aerial Vehicle and Ground-Based Narrow Band Spectrometers Applied to Crop Trait Monitoring in Organic Potato Production. Sensors 17, 1428. doi:10.3390/s17061428

Dozier, J., Warren, S.G., 1982. Effect of viewing angle on the infrared brightness temperature of snow. Water Resour. Res. 18, 1424–1434. doi:10.1029/WR018i005p01424

Du, Q., Yang, H., 2008. Similarity-Based Unsupervised Band Selection for Hyperspectral Image Analysis. IEEE Geoscience and Remote Sensing Letters 5, 564–568. doi:10.1109/LGRS.2008.2000619

Fornace, K.M., Drakeley, C.J., William, T., Espino, F., Cox, J., 2014. Mapping infectious disease landscapes: unmanned aerial vehicles and epidemiology. Trends in Parasitology 30, 514–519. doi:10.1016/j.pt.2014.09.001

Fraser, R.S., Kaufman, Y.J., 1985. The relative importance of aerosol scattering and absorption in remote sensing. IEEE Transactions on Geoscience and Remote Sensing 625–633.

Gao, B.-C., Montes, M.J., Davis, C.O., Goetz, A.F.H., 2009. Atmospheric correction algorithms for hyperspectral remote sensing data of land and ocean. Remote Sensing of Environment, Imaging Spectroscopy Special Issue 113, S17–S24. doi:10.1016/j.rse.2007.12.015

Gao, J., Du, Q., Gao, L., Sun, X., Zhang, B., 2014. Ant colony optimization-based supervised and unsupervised band selections for hyperspectral urban data classification. J. Appl. Remote Sens 8, 085094–085094. doi:10.1117/1.JRS.8.085094

Gao, L., Gao, J., Li, J., Plaza, A., Zhuang, L., Sun, X., Zhang, B., 2015. Multiple Algorithm Integration Based on Ant Colony Optimization for Endmember Extraction From Hyperspectral Imagery. IEEE Journal of Selected Topics in Applied Earth Observations and Remote Sensing 8, 2569–2582. doi:10.1109/JSTARS.2014.2371615

Gibson, K.D., Dirks, R., Medlin, C.R., Johnston, L., 2004. Detection of Weed Species in Soybean Using Multispectral Digital Images. Weed Technology 18, 742–749. doi:10.1614/WT-03-170R1

Glenn, N.F., Mundt, J.T., Weber, K.T., Prather, T.S., Lass, L.W., Pettingill, J., 2005. Hyperspectral data processing for repeat detection of small infestations of leafy spurge. Remote Sensing of Environment 95, 399–412. doi:10.1016/j.rse.2005.01.003

Goebel, M.E., Perryman, W.L., Hinke, J.T., Krause, D.J., Hann, N.A., Gardner, S., LeRoi, D.J., 2015. A small unmanned aerial system for estimating abundance and size of Antarctic predators. Polar Biol 38, 619–630. doi:10.1007/s00300-014-1625-4

Goel, P.K., Prasher, S.O., Landry, J.A., Patel, R.M., Bonnell, R.B., Viau, A.A., Miller, J.R., 2003a. Potential of airborne hyperspectral remote sensing to detect nitrogen deficiency and weed infestation in corn. Computers and Electronics in Agriculture 38, 99–124. doi:10.1016/S0168-1699(02)00138-2

Goel, P.K., Prasher, S.O., Landry, J.-A., Patel, R.M., Viau, A.A., 2003a. Hyperspectral image classification to detect weed infestations and nitrogen status in corn. Transactions of the ASAE 46, 539.

Goel, P.K., Prasher, S.O., Landry, J.-A., Patel, R.M., Viau, A.A., Miller, J.R., 2003b. Estimation of crop biophysical parameters through airborne and field hyperspectral remote sensing. Transactions of the ASAE 46, 1235.

Goel, P.K., Prasher, S.O., Patel, R.M., Landry, J.A., Bonnell, R.B., Viau, A.A., 2003b. Classification of hyperspectral data by decision trees and artificial neural networks to identify weed stress and nitrogen status of corn. Computers and Electronics in Agriculture 39, 67–93. doi:10.1016/S0168-1699(03)00020-6

Goel, P.K., Prasher, S.O., Patel, R.M., Smith, D.L., DiTommaso, A., 2002. Use of airborne multi–spectral imagery for weed detection in field crops. Transactions of the ASAE 45, 443.

Goswami, S., Gamon, J., Vargas, S., Tweedie, C., 2015. Relationships of NDVI, Biomass, and Leaf Area Index (LAI) for six key plant species in Barrow, Alaska. PeerJ PrePrints.

Gray, C.J., Shaw, D.R., Gerard, P.D., Bruce, L.M., 2008. Utility of Multispectral Imagery for Soybean and Weed Species Differentiation. Weed Technology 22, 713–718. doi:10.1614/WT-07-116.1

Green, R.O., Conel, J.E., Carrere, V., Bruegg, C.J., Margolis, J.S., Rast, M., Hoover, G., 1990. Determination of the In-Flight Spectral and Radiometric Characteristics of the Airborne Visible/Infrared Imaging Spectrometer (AVIRIS). AVIRIS Proceedings June 4 - 5, 1990 (JPL Publication) 90–54.

Gueymard, C.A., 2004. The sun’s total and spectral irradiance for solar energy applications and solar radiation models. Solar Energy 76, 423–453. doi:10.1016/j.solener.2003.08.039

Guo, Z., Zhang, D., Zhang, L., Liu, W., 2012. Feature Band Selection for Online Multispectral Palmprint Recognition. IEEE Transactions on Information Forensics and Security 7, 1094–1099. doi:10.1109/TIFS.2012.2189206

Haboudane, D., Miller, J.R., Pattey, E., Zarco-Tejada, P.J., Strachan, I.B., 2004. Hyperspectral vegetation indices and novel algorithms for predicting green LAI of

crop canopies: Modeling and validation in the context of precision agriculture. Remote Sensing of Environment 90, 337–352. doi:10.1016/j.rse.2003.12.013

Haggar, R.J., Stent, C.J., Isaac, S., 1983. A prototype hand-held patch sprayer for killing weeds, activated by spectral differences in crop/weed canopies. Journal of Agricultural Engineering Research 28, 349–358. doi:10.1016/0021-8634(83)90066-5

Haun, J.R., 1973. Visual Quantification of Wheat Development. Agronomy Journal 65, 116–119. doi:10.2134/agronj1973.00021962006500010035x

Herrmann, I., Shapira, U., Kinast, S., Karnieli, A., Bonfil, D.J., 2013. Ground-level hyperspectral imagery for detecting weeds in wheat fields. Precision Agriculture 14, 637–659. doi:10.1007/s11119-013-9321-x

Horler, D.N.H., Dockray, M., Barber, J., 1983. The red edge of plant leaf reflectance. International Journal of Remote Sensing 4, 273–288. doi:10.1080/01431168308948546

Huang, R., He, M., 2005. Band selection based on feature weighting for classification of hyperspectral data. IEEE Geoscience and Remote Sensing Letters 2, 156–159. doi:10.1109/LGRS.2005.844658

Huang, W., Lamb, D.W., Niu, Z., Zhang, Y., Liu, L., Wang, J., 2007. Identification of yellow rust in wheat using in-situ spectral reflectance measurements and airborne hyperspectral imaging. Precision Agric 8, 187–197. doi:10.1007/s11119-007-9038-9

Huang, Y., Lee, M.A., Thomson, S.J., Reddy, K.N., 2016. Ground-based hyperspectral remote sensing for weed management in crop production. International Journal of Agricultural and Biological Engineering; Beijing 9, 98–109. doi:http://dx.doi.org/10.3965/j.ijabe.20160902.2137

Huete, A.R., Jackson, R.D., Post, D.F., 1985. Spectral response of a plant canopy with different soil backgrounds. Remote Sensing of Environment 17, 37–53. doi:10.1016/0034-4257(85)90111-7

Hussain, M., Chen, D., Cheng, A., Wei, H., Stanley, D., 2013. Change detection from remotely sensed images: From pixel-based to object-based approaches. ISPRS Journal of Photogrammetry and Remote Sensing 80, 91–106. doi:10.1016/j.isprsjprs.2013.03.006

Jia, S., Tang, G., Zhu, J., Li, Q., 2016. A Novel Ranking-Based Clustering Approach for Hyperspectral Band Selection. IEEE Transactions on Geoscience and Remote Sensing 54, 88–102. doi:10.1109/TGRS.2015.2450759

Kelcey, J., Lucieer, A., 2012. Sensor Correction of a 6-Band Multispectral Imaging Sensor for UAV Remote Sensing. Remote Sensing 4, 1462–1493. doi:10.3390/rs4051462

Keshava, N., 2004. Distance metrics and band selection in hyperspectral processing with applications to material identification and spectral libraries. IEEE Transactions on Geoscience and Remote Sensing 42, 1552–1565. doi:10.1109/TGRS.2004.830549

Khokhar, J.S., Sareen, S., Tyagi, B.S., Singh, G., Chowdhury, A.K., Dhar, T., Singh, V., King, I.P., Young, S.D., Broadley, M.R., 2017. Characterising variation in wheat traits under hostile soil conditions in India. PLOS ONE 12, e0179208. doi:10.1371/journal.pone.0179208

King, M.D., Kaufman, Y.J., Menzel, W.P., Tanre, D., 1992. Remote sensing of cloud, aerosol, and water vapor properties from the moderate resolution imaging spectrometer (MODIS). IEEE Transactions on Geoscience and Remote Sensing 30, 2–27. doi:10.1109/36.124212

Knipling, E.B., 1970. Physical and physiological basis for the reflectance of visible and near-infrared radiation from vegetation. Remote Sensing of Environment 1, 155–159. doi:10.1016/S0034-4257(70)80021-9

Kruse, F.A., Boardman, J.W., Huntington, J.F., 2003. Comparison of airborne hyperspectral data and EO-1 Hyperion for mineral mapping. IEEE Transactions on Geoscience and Remote Sensing 41, 1388–1400. doi:10.1109/TGRS.2003.812908

Lamb, D.W., 2000. The use of qualitative airborne multispectral imaging for managing agricultural crops-a case study in south-eastern Australia. Australian Journal of Experimental Agriculture 40, 725–738.

Lamb, Weedon, Rew, 1999. Evaluating the accuracy of mapping weeds in seedling crops using airborne digital imaging: Avena spp. in seedling triticale. Weed Research 39, 481–492. doi:10.1046/j.1365-3180.1999.00167.x

Lawrence, R.L., Wood, S.D., Sheley, R.L., 2006. Mapping invasive plants using hyperspectral imagery and Breiman Cutler classifications (randomForest). Remote Sensing of Environment 100, 356–362. doi:10.1016/j.rse.2005.10.014

Li, W., Prasad, S., Fowler, J.E., Bruce, L.M., 2012. Locality-Preserving Dimensionality Reduction and Classification for Hyperspectral Image Analysis. IEEE Transactions on Geoscience and Remote Sensing 50, 1185–1198. doi:10.1109/TGRS.2011.2165957

Liaghat, S., Balasundram, S.K., 2010. A review: The role of remote sensing in precision agriculture. American journal of agricultural and biological sciences 5, 50–55.

Lin, F., Zhang, D., Huang, Y., Wang, X., Chen, X., 2017. Detection of Corn and Weed Species by the Combination of Spectral, Shape and Textural Features. Sustainability 9, 1335. doi:10.3390/su9081335

López-Granados, F., 2011. Weed detection for site-specific weed management: mapping and real-time approaches. Weed Research 51, 1–11. doi:10.1111/j.1365-3180.2010.00829.x

López-Granados, F., Peña-Barragán, J.M., Jurado-Expósito, M., Francisco-FERNÁNDEZ, M., Cao, R., Alonso-Betanzos, A., Fontenla-Romero, O., 2008. Multispectral classification of grass weeds and wheat (Triticum durum) using linear and nonparametric functional discriminant analysis and neural networks. Weed Research 48, 28–37. doi:10.1111/j.1365-3180.2008.00598.x

López-Granados, F., Torres-Sánchez, J., Serrano-Pérez, A., Castro, A.I. de, Mesas-Carrascosa, F.-J., Peña, J.-M., 2016. Early season weed mapping in sunflower using UAV technology: variability of herbicide treatment maps against weed thresholds. Precision Agric 17, 183–199. doi:10.1007/s11119-015-9415-8

Lord, D., Desjardins, R.L., Dubé, P.A., 1988. Sun-Angle Effects on the Red and near Infrared Reflectances of Five Different Crop Canopies. Canadian Journal of Remote Sensing 14, 46–55. doi:10.1080/07038992.1988.10855118

Lunetta, R.S., Congalton, R.G., Fenstermaker, L.K., ensen, J.R., McGwire, K.C., Tinney, L.R., 1991. Remote sensing and geographic information system data integration: error sources and research issues.

MacDonald, R.B., Hall, F.G., 1980. Global Crop Forecasting. Science 208, 670–679.

Mackinney, G., 1941. Absorption of light by chlorophyll solutions. J. biol. Chem 140, 315–322.

MartÍnez-UsÓMartinez-Uso, A., Pla, F., Sotoca, J.M., GarcÍa-Sevilla, P., 2007. Clustering-Based Hyperspectral Band Selection Using Information Measures. IEEE Transactions on Geoscience and Remote Sensing 45, 4158–4171. doi:10.1109/TGRS.2007.904951

McCann, C., Repasky, K.S., Morin, M., Lawrence, R.L., Powell, S., 2017. Using Landsat Surface Reflectance Data as a Reference Target for Multiswath Hyperspectral Data Collected Over Mixed Agricultural Rangeland Areas. IEEE Transactions on Geoscience and Remote Sensing PP, 1–13. doi:10.1109/TGRS.2017.2699618

McGwire, K., Minor, T., Fenstermaker, L., 2000. Hyperspectral Mixture Modeling for Quantifying Sparse Vegetation Cover in Arid Environments. Remote Sensing of Environment 72, 360–374. doi:10.1016/S0034-4257(99)00112-1

Moshou, D., Kateris, D., Pantazi, X.E., Gravalos, I., 2013. Crop and weed species recognition based on hyperspectral sensing and active learning. Precision Agriculture 555–561.

Mouginot, J., Rignot, E., Scheuchl, B., Millan, R., 2017. Comprehensive Annual Ice Sheet Velocity Mapping Using Landsat-8, Sentinel-1, and RADARSAT-2 Data. Remote Sensing 9, 364. doi:10.3390/rs9040364

Natividade, J., Prado, J., Marques, L., 2017. Low-cost multi-spectral vegetation classification using an Unmanned Aerial Vehicle, in: 2017 IEEE International Conference on Autonomous Robot Systems and Competitions (ICARSC). Presented at the 2017 IEEE International Conference on Autonomous Robot Systems and Competitions (ICARSC), pp. 336–342. doi:10.1109/ICARSC.2017.7964097

Nieto, H.J., Brondo, M.A., Gonzalez, J.T., 1968. Critical Periods of the Crop Growth Cycle for Competition from Weeds. International Journal of Pest Management: Part C 14, 159–166. doi:10.1080/05331856809432576

Okamoto, H., Murata, T., Kataoka, T., Hata, S.-I., 2007. Plant classification for weed detection using hyperspectral imaging with wavelet analysis. Weed Biology and Management 7, 31–37. doi:10.1111/j.1445-6664.2006.00234.x

Peña, J.M., Torres-Sánchez, J., Castro, A.I. de, Kelly, M., López-Granados, F., 2013. Weed Mapping in Early-Season Maize Fields Using Object-Based Analysis of Unmanned Aerial Vehicle (UAV) Images. PLOS ONE 8, e77151. doi:10.1371/journal.pone.0077151

Plant, R.E., 2001. Site-specific management: the application of information technology to crop production. Computers and Electronics in Agriculture 30, 9–29. doi:10.1016/S0168-1699(00)00152-6

Riedmann, M., Milton, E.J., 2003. Supervised band selection for optimal use of data from airborne hyperspectral sensors, in: IGARSS 2003 IEEE International. Presented at the Geoscience and Remote Sensing Symposium, pp. 1770–1772. doi:10.1109/IGARSS.2003.1294245

Röser, H.P., von Schönermark, M., 1996. Comparison of remote sensing experiments from airborne and space platforms. Acta Astronautica, IAA International Symposium on Small Satellites for Earth Observation 39, 855–862. doi:10.1016/S0094-5765(97)00070-2

Rouse, J.H., Shaw, J.A., Lawrence, R.L., Lewicki, J.L., Dobeck, L.M., Repasky, K.S., Spangler, L.H., 2010. Multi-spectral imaging of vegetation for detecting CO2 leaking from underground. Environmental Earth Sciences 60, 313–323. doi:10.1007/s12665-010-0483-9

Roy, P.S., Ravan, S.A., 1996. Biomass estimation using satellite remote sensing data—an investigation on possible approaches for natural forest. Journal of biosciences 21, 535–561.

Sankey, J.B., Ravi, S., Wallace, C.S.A., Webb, R.H., Huxman, T.E., 2012. Quantifying soil surface change in degraded drylands: Shrub encroachment and effects of fire and vegetation removal in a desert grassland. J. Geophys. Res. 117, G02025. doi:10.1029/2012JG002002

Sankey, T.T., Sankey, J.B., Weber, K.T., Montagne, C., 2009. Geospatial Assessment of Grazing Regime Shifts and Sociopolitical Changes in a Mongolian Rangeland. Rangeland Ecology & Management 62, 522–530. doi:10.2111/.1/REM-D-09-00014.1

Schmidt, K.S., Skidmore, A.K., 2003. Spectral discrimination of vegetation types in a coastal wetland. Remote Sensing of Environment 85, 92–108. doi:10.1016/S0034-4257(02)00196-7

Scotford, I.M., Miller, P.C.H., 2005. Applications of Spectral Reflectance Techniques in Northern European Cereal Production: A Review. Biosystems Engineering 90, 235–250. doi:10.1016/j.biosystemseng.2004.11.010

Senay, G.B., Ward, A.D., Lyon, J.G., Fausey, N.R., Nokes, S.E., 1998. Manipulation of high spatial resolution aircraft remote sensing data for use in site-specific farming. Transactions of the ASAE 41, 489.

Skakun, S., Vermote, E., Roger, J.-C., Franch, B., 1 Department of Geographical Sciences, University of Maryland, College Park, MD 20742, USA, 2 NASA Goddard Space Flight Center Code 619, 8800 Greenbelt Road, Greenbelt, MD 20771, USA, 2017. Combined Use of Landsat-8 and Sentinel-2A Images for Winter Crop Mapping and Winter Wheat Yield Assessment at Regional Scale. AIMS Geosciences 3, 163–186. doi:10.3934/geosci.2017.2.163

Slater, P.N., Jackson, R.D., 1982. Atmospheric effects on radiation reflected from soil and vegetation as measured by orbital sensors using various scanning directions. Appl. Opt., AO 21, 3923–3931. doi:10.1364/AO.21.003923

Somers, B., Asner, G.P., Tits, L., Coppin, P., 2011. Endmember variability in Spectral Mixture Analysis: A review. Remote Sensing of Environment 115, 1603–1616. doi:10.1016/j.rse.2011.03.003

Staab, E.S., Slaughter, D.C., Zhang, Y., Giles, D.K., 2009. Hyperspectral imaging system for precision weed control in processing tomato, in: 2009 Reno, Nevada, June 21-June 24, 2009. American Society of Agricultural and Biological Engineers, p. 1.

Steven, M.D., 1993. Satellite remote sensing for agricultural management: opportunities and logistic constraints. ISPRS Journal of Photogrammetry and Remote Sensing 48, 29–34. doi:10.1016/0924-2716(93)90029-M

Su, H., Du, Q., Chen, G., Du, P., 2014. Optimized Hyperspectral Band Selection Using Particle Swarm Optimization. IEEE Journal of Selected Topics in Applied Earth Observations and Remote Sensing 7, 2659–2670. doi:10.1109/JSTARS.2014.2312539

Sugiyama, M., 2007. Dimensionality reduction of multimodal labeled data by local fisher discriminant analysis. Journal of machine learning research 8, 1027–1061.

Sui, R., Thomasson, J.A., Hanks, J., Wooten, J., 2008. Ground-based sensing system for weed mapping in cotton. Computers and Electronics in Agriculture 60, 31–38. doi:10.1016/j.compag.2007.06.002

Sun, K., Geng, X., Ji, L., 2015. A New Sparsity-Based Band Selection Method for Target Detection of Hyperspectral Image. IEEE Geoscience and Remote Sensing Letters 12, 329–333. doi:10.1109/LGRS.2014.2337957

Swain, P., King, R., 1973. Two Effective Feature Selection Criteria for Multispectral Remote Sensing. LARS Technical Reports.

Thenkabail, P., 2017. Hyperspectral Remote Sensing of Vegetation and Agricultural Crops. Photogrammetric Engineering & Remote Sensing (PE&RS);80,(2014) Pagination 697,723.

Thenkabail, P.S., Enclona, E.A., Ashton, M.S., Van Der Meer, B., 2004. Accuracy assessments of hyperspectral waveband performance for vegetation analysis applications. Remote Sensing of Environment 91, 354–376. doi:10.1016/j.rse.2004.03.013

Thenkabail, P.S., Smith, R.B., De Pauw, E., 2002. Evaluation of narrowband and broadband vegetation indices for determining optimal hyperspectral wavebands for agricultural crop characterization. Photogrammetric Engineering and Remote Sensing 68, 607–622.

Thenkabail, P.S., Smith, R.B., De Pauw, E., 2000. Hyperspectral Vegetation Indices and Their Relationships with Agricultural Crop Characteristics. Remote Sensing of Environment 71, 158–182. doi:10.1016/S0034-4257(99)00067-X

Tidemann, B.D., Hall, L.M., Harker, K.N., Alexander, B.C.S., 2016. Identifying Critical Control Points in the Wild Oat (Avena fatua) Life Cycle and the Potential Effects of Harvest Weed-Seed Control. Weed Science 64, 463–473. doi:10.1614/WS-D-15-00200.1

Todd, S.W., Hoffer, R.M., Milchunas, D.G., 1998. Biomass estimation on grazed and ungrazed rangelands using spectral indices. International Journal of Remote Sensing 19, 427–438. doi:10.1080/014311698216071

Torres-Sánchez, J., López-Granados, F., Castro, A.I.D., Peña-Barragán, J.M., 2013. Configuration and Specifications of an Unmanned Aerial Vehicle (UAV) for Early Site Specific Weed Management. PLOS ONE 8, e58210. doi:10.1371/journal.pone.0058210

Toutin, T., 2004. Review article: Geometric processing of remote sensing images: models, algorithms and methods. International Journal of Remote Sensing 25, 1893–1924. doi:10.1080/0143116031000101611

Uto, K., Seki, H., Saito, G., Kosugi, Y., Komatsu, T., 2016. Development of a Low-Cost, Lightweight Hyperspectral Imaging System Based on a Polygon Mirror and Compact Spectrometers. IEEE Journal of Selected Topics in Applied Earth Observations and Remote Sensing 9, 861–875. doi:10.1109/JSTARS.2015.2472293

Vanderlip, R.L., Reeves, H.E., 1972. Growth Stages of Sorghum [Sorghum bicolor, (L.) Moench.]. Agronomy Journal 64, 13–16. doi:10.2134/agronj1972.00021962006400010005x

Verrelst, J., Rivera, J.P., Gitelson, A., Delegido, J., Moreno, J., Camps-Valls, G., 2016. Spectral band selection for vegetation properties retrieval using Gaussian processes regression. International Journal of Applied Earth Observation and Geoinformation 52, 554–567. doi:10.1016/j.jag.2016.07.016

Villa, T.F., Gonzalez, F., Miljievic, B., Ristovski, Z.D., Morawska, L., 2016. An Overview of Small Unmanned Aerial Vehicles for Air Quality Measurements: Present Applications and Future Prospectives. Sensors 16, 1072. doi:10.3390/s16071072

Wendel, A., Underwood, J., 2016. Self-supervised weed detection in vegetable crops using ground based hyperspectral imaging, in: 2016 IEEE International Conference on Robotics and Automation. Presented at the 2016 IEEE International Conference on Robotics and Automation (ICRA), pp. 5128–5135. doi:10.1109/ICRA.2016.7487717

Xia, X., Che, H., Zhu, J., Chen, H., Cong, Z., Deng, X., Fan, X., Fu, Y., Goloub, P., Jiang, H., Liu, Q., Mai, B., Wang, P., Wu, Y., Zhang, J., Zhang, R., Zhang, X., 2016. Ground-based remote sensing of aerosol climatology in China: Aerosol optical properties, direct radiative effect and its parameterization. Atmospheric Environment, Air Pollution in the Beijing – Tianjin – Hebei (BTH) region, China 124, 243–251. doi:10.1016/j.atmosenv.2015.05.071

Yang, C., Everitt, J.H., Bradford, J.M., 2007. Airborne hyperspectral imagery and linear spectral unmixing for mapping variation in crop yield. Precision Agric 8, 279–296. doi:10.1007/s11119-007-9045-x

Yang, H., Du, Q., Chen, G., 2012. Particle Swarm Optimization-Based Hyperspectral Dimensionality Reduction for Urban Land Cover Classification. IEEE Journal of Selected Topics in Applied Earth Observations and Remote Sensing 5, 544–554. doi:10.1109/JSTARS.2012.2185822

Yang, H., Du, Q., Su, H., Sheng, Y., 2011. An Efficient Method for Supervised Hyperspectral Band Selection. IEEE Geoscience and Remote Sensing Letters 8, 138–142. doi:10.1109/LGRS.2010.2053516

Ye, X., Sakai, K., Garciano, L.O., Asada, S.-I., Sasao, A., 2006. Estimation of citrus yield from airborne hyperspectral images using a neural network model. Ecological Modelling 198, 426–432. doi:10.1016/j.ecolmodel.2006.06.001

Yuan, C., Zhang, Y., Liu, Z., 2015. A survey on technologies for automatic forest fire monitoring, detection, and fighting using unmanned aerial vehicles and remote sensing techniques. Can. J. For. Res. 45, 783–792. doi:10.1139/cjfr-2014-0347

Zhang, L., Weng, Q., 2016. Annual dynamics of impervious surface in the Pearl River Delta, China, from 1988 to 2013, using time series Landsat imagery. ISPRS Journal of Photogrammetry and Remote Sensing 113, 86–96. doi:10.1016/j.isprsjprs.2016.01.003

Zheng, B., Myint, S.W., Thenkabail, P.S., Aggarwal, R.M., 2015. A support vector machine to identify irrigated crop types using time-series Landsat NDVI data. International Journal of Applied Earth Observation and Geoinformation 34, 103–112. doi:10.1016/j.jag.2014.07.002

Zhu, Z., Wang, S., Woodcock, C.E., 2015. Improvement and expansion of the Fmask algorithm: cloud, cloud shadow, and snow detection for Landsats 4–7, 8, and Sentinel 2 images. Remote Sensing of Environment 159, 269–277. doi:10.1016/j.rse.2014.12.014

Zwiggelaar, R., 1998. A review of spectral properties of plants and their potential use for crop/weed discrimination in row-crops. Crop Protection 17, 189–206. doi:10.1016/S0261-2194(98)00009-X

CHAPTER THREE

NARROW SPECTRAL BAND SELECTION FOR PRECISION WEED DETECTTION IN AGRICULTRAL FIELDS USING HYPERSPECTRAL REMOTE SENSING

Introduction

Weed identification and mapping can be used to minimize the use of pesticides by providing target areas for treatment. Producers can reduce costs and environmental impacts by treating only the targeted areas where weeds have been identified (Stafford and Miller, 1996). Treating weeds by spraying with pesticides can be accomplished using weed maps created prior to spraying or using real time information generated from on-tractor sensors. On-tractor sensing for real time spraying offers a versatile platform for spot spraying. Not only can weeds be sprayed efficiently, but real time monitoring of weed species in crops can be achieved. An important question to address is what combination of spectral bands works best for a specific combination of crops and weeds, potentially reducing herbicide waste and minimizing environmental impacts.

Continuous narrow spectral bands across the visible and NIR region of the EM spectrum collected by hyperspectral sensors allow the spectral response of each band to be analyzed (Goetz et al., 1985). The ability of hyperspectral sensors to provide spectral information in many narrow spectral bands allows researchers to differentiate species based on differences in internal characteristics of individual plant's structure and absorption dynamics of canopies created by many plants across space (Huete et al., 1985; Knipling, 1970; Lord et al., 1988; Marchant and Onyango, 2002). The continuous narrow

spectral bands of hyperspectral sensors give a more representative view of the spectral response than broader segregated bands associated with multispectral sensors. Increased information, however, related to the increased number of spectral bands associated with hyperspectral imagers must be weighed against the cost and complexity of data analysis.

Hyperspectral sensors have been used to locate and classify weed species. Aerial monitoring of noxious weeds has allowed researchers to identity weed locations against similar native background vegetation. Chinese bushclover (*Lespedeza cuneata L.),* for example, was mapped in pasture lands of Missouri with an accuracy of 89% (Wang et al., 2008). Leafy spurge (*Euphorbia esula*) was classified in southern Montana with an overall accuracy of 86% and spotted knapweed (*Centaurea maculosa*) classified with 84% overall accuracy (Lawrence et al., 2006). Cabbage *(Brassica oleracea)* against a background of 5 weeds was correctly classified 100% of the time (Deng et al., 2016). Spotted knapweed was identified in southern Montana at 95% to 99% correct classification with coverages as low as five to ten plants per 5x5-m pixel (Lass et al., 2002).

Spectral irradiance collected by ground based sensors is less affected by atmospheric conditions such as water vapor or aerosols than aerial based sensors (King et al., 1992) because of the shorter optical path length from the target to the sensor . Aerosol loading and molecular species concentrations vary both spatially and temporally, making the exact makeup of the atmosphere at the time of sensing difficult to determine (Xia et al., 2016). Hyperspectral sensors therefore have also been applied to ground-based sensing systems where real time sensors would be used to detect weeds and trigger

a spraying mechanism. Ground based systems have the advantage of requiring minimal atmospheric corrections compared to flight-based sensors but must be mounted on vehicles to cover larger areas.

A stationary ground-based hyperspectral sensor placed in a wheat field showed an overall accuracy as high as 90% for identifying weeds (Herrmann et al., 2013). In a comparison of various machine learning techniques using hyperspectral data collected with a ground vehicle mounted sensor recognition in corn (*Zea mays*) of creeping buttercup (*Ranunculus repens),* Canada thistle *(Cirsium arvense) ,* wild mustard *(Sinapis arvensis) ,* chickweed *(Stellaria media),* common dandelion *(Tarraxacum officinale) ,* annual bluegrass *(Poa annua),* lady's thumb *(Poligonum persicaria),* common nettle *(Urtica dioica),* common yellow woodsorrel *(Oxalis europaea),* and black medick *(Medicago lupulina)* were located with accuracies as high as 94% (Pantazi et al., 2016). Classification of caltrop (Tribulus terrestris), curly dock (Rumex crispus), red dock (rumex sanguineus), and barnyardgrass (Echinochloa crusgalli) in corn with a ground based hyperspectral sensor reached accuracies over 95% (Wendel and Underwood, 2016). The classification accuracies of wild buckwheat (*Fallopia convolvulus),* field horsetail *(Equisetum arvense),* green foxtail *(Setaria viridis),* and common chickweed (*Stellaria media)* in a field of sugar beets ranged between 74.7% and 97.3% accuracies using a stationary overhead hyperspectral sensors (Okamoto et al., 2007).

On-tractor sensors rarely use hyperspectral data due to the high cost of the sensors and the difficulty in processing the large amounts of data associated with hyperspectral imagers. Current commercial spot spraying sensors rely on multispectral bands centered

in the visible and NIR spectral region (Holland Scientific, 2017; NTech Industies, Inc., 2017; Topcon Positioning Systems, Inc., 2017). Spot spraying systems using these limited spectral bands are used in fallow fields, between rows, or in pre-emergent crops where any vegetation detected using the characteristic red edge signal (Horler et al., 1983) associated with vegetation is assumed to be weeds, drastically limiting the flexibility and usefulness of the spot spraying systems.

An accurate sensor for on-tractor weed detection needs to maintain some of spectral fidelity of the hyperspectral imager to differentiate between weeds and crops but must maintain the cost competitiveness and simplicity of the multispectral imager. The question arises how to reduce the number of narrow spectral bands found in hyperspectral technology and to produce a simple multispectral sensor capable of on-tractor weed detection. The high dimensionality of hyperspectral data means that spectral channels contain redundant information and therefore potential for removing bands without deteriorating the classification power (Su et al., 2014; Sun et al., 2015). The data contained in a single band is directly correlated to the bands immediately around it, and removal of bands might not remove substantial information. Narrow spectral bands could be applied to current on-tractor sensors to improve in crop spot spraying once specific bands are known to differentiate weed species from a crop. A known target can be used to remove bands that do not add new information, reducing required processing power and speeding up classification.

Proprietary software packages (*e.g.* ERDAS Imagine, Harris Geospatial ENVI) contain options for band selection using distance metrics for measuring spectral

separability. Distance metrics place the spectral responses of interest in multi-dimensional space with each band on an axis (Davis et al., 1978). The distance metrics compute the distance among spectral responses for various numbers of band combinations, providing a reference for comparing the similarity of two signatures. A particular crop spectral response and weed spectral response, for example, can be compared across all possible three band combinations to determine which three band combination provides the greatest distance between the two spectra.

A common and simple approach to determining spectral differences is Euclidean minimum distance, a measurement of the shortest distance between points representing spectral responses in one band of the spectra (Davis et al., 1978). Applying this concept in two dimensions it can be visualized as the hypotenuse of a triangle, and this concept is readily extended to *n*-dimensional space for any number of spectral bands.

Methods like divergence, transformed divergence, and Jeffries-Matusita exist for measuring the distance between groups of points, or clusters (Davis et al., 1978). The divergence, transformed divergence, and Jeffries-Matusita are normalized distance measures accounting for in-group variability when calculating distance.

Divergence measures the likelihood a classifier will correctly place a measurement in a class defined by each cluster (Davis et al., 1978). The distance measurement is based on the statistical separation of two clusters using the logarithmic likelihood ratio $\left(L'_{ji}\right)$ and values constrained to greater than 0 (Equation 1). The more similar the probability density function of the clusters, the closer to zero the distance

measurement, indicating poor separation. To calculate divergence a mean vector U_i and covariance matrix $\mathbf{\Sigma}_I$ are used to express divergence with no integrals (Equation 2).

$$D_{ij} = E\left[L'_{ij}(X)|\omega_i\right] + E\left[L'_{ji}(X)\middle|\omega_j\right]$$

where

$$E\left[L'_{ij}(X)|\omega_i\right] = \int_x L'_{ij}(X)p\left(X\middle|\omega_j\right)dX$$

and $$E\left[L'_{ij}(X)|\omega_i\right] = \int_x L'_{ij}(X)p\left(X\middle|\omega_j\right)dX$$

Equation 3.1. Divergence defined in terms of the logarithmic likelihood ratio.

$$D_{ij} = \frac{1}{2}tr\left[(\Sigma_i - \Sigma_j)\left(\Sigma_j^{-1} - \Sigma_i^{-1}\right)\right] + \frac{1}{2}tr\left[\left(\Sigma_i^{-1} + \Sigma_j^{-1}\right)\left(U_i - U_j\right)\left(U_i - U_j\right)^T\right]$$

Equation 3.2. Divergence defined in terms of means and covariance using no integrals.

A transformation can be performed on the divergence calculation to increase separation (Equation 3), creating values from 0 to 2000 (Davis et al., 1978). The advantage is that the transformation contains a negative exponential function creating a saturating effect. The saturating effect creates an exponential decrease as distance values get smaller, so that, when averaged, a few widely separated outlier values in a cluster no longer make a disproportionate difference in the distance metric.

$$D_{ij}^T = 2\left[1 - exp\left(D_{ij}/8\right)\right]$$

Equation 3.3. Transform divergence equation using divergence value

Jeffries-Matusita measures statistical separability using the distance between density functions and contains a negative exponential to create a saturating effect as well (Equation 4) (Davis et al., 1978). Jeffries-Matusita values range from 0 to 1414 and is one of the most complicated to calculate, requiring more computing power than transformed divergence to select bands.

$$J_{ij} = [2(1 - e^{-\alpha})]^{1/2}$$

where

$$\alpha = \frac{1}{8}(U_i - U_j)^T \left(\frac{\Sigma_i + \Sigma_j}{2}\right)^{-1} (U_i - U_j) + \frac{1}{2}\log_e \left[\frac{\left|(\Sigma_i + \Sigma_j)/2\right|}{\left(|\Sigma_i| * |\Sigma_j|\right)^{1/2}}\right]$$

Equation 3.4. Jefferies-Matusita Equation

The more complicated the image or relatively similar the target is to the background, the more information is needed to detect or classify targets. The spectral signatures of crops and weeds are very similar. More information can be achieved by adding more and more bands if the number of bands is not limited (Du and Yang, 2008). It is important that selection of bands not replicate information if the number of bands is limited to only a few. Narrow spectral bands could potentially differentiate between crops and weeds based on a few specific morphological differences (Zwiggelaar, 1998).

The covariance of bands is calculated before adding additional bands for multiple band separability, to not duplicate information from band to band. Each of the four distance metrics are calculated differently, resulting in various band combinations for

identifying the same target and require comparison to determine which performs best in practice.

Performance of the selected band combinations can be evaluated by conducting image classifications and comparing the output overall accuracies to the full, non-reduced set of spectral bands. Many classification algorithms are available (*e.g.* C5.0, support vector machines (with either linear, polynomial, or radial kernels), random forest, neural networks, and linear discriminant analysis (a maximum likelihood classifier) (Bandos et al., 2009; Lawrence, 2004; Maggiori et al., 2017)). We tested and compared algorithms using sets of training and validation data. Random forest consistently produced comparatively high accuracies for separation of weeds and crops. Random forest generates multiple classification trees. A portion of data, the bagged data, is used to create a predictor function and the error of the prediction function is generated using data not within the bag. Averaging the error estimates for each prediction of the out of bag data is used to estimate the error of the classification. This allows all the data collected to be used for training, which with a small sample size has the potential to improve accuracy. Random forest outputs the internally estimated out-of-bag error that can be used as an accuracy metric, provided the data are not biased (i.e., if there is bias in the data, out-of-bag accuracy cannot detect errors not represented in the data) (Breiman, 1996, 2001; Lawrence, 2004). The use of out-of-bag accuracy is unavailable in other classification techniques, making random forest the best option.

We evaluated whether it might be possible to select a small number of bands from hyperspectral data while maintaining accuracies that can be achieved when using the

entire data set. A successful result would enable the use of sensors similar in design to those currently employed, with only alteration in filter bands and classification algorithms. The research focuses on broadleaf weed species within spring wheat, however the workflow could be applied to any cropping system with minor adjustments.

Methods

Location

The study site included two agricultural fields southwest of Bozeman, Montana at approximately 1675 m above sea level, in the north foothills of the Gallatin Range (Figure 3.1). Both fields were planted with winter wheat in 2015 in a mix of clay and silt loam soils, formed on well drained stream terraces and harvested in August of 2016. Based on 2017 U.S. climate data the Bozeman area receives approximately 41 cm of rain a year with highest average rain falls being concentrated in the spring and early summer months of April, May, and June. Based on averages from 1981 through 2010, the frost free growing season is late May to middle of September, just over 100 days. The weed infested areas were dominated by broadleaf weeds; Canada thistle (*Cirsium arvense*), prickly lettuce (*Lactuca serriola*), and bedstraw (*Galium aparine*). No grass weed locations large enough to be mapped from the air were found.

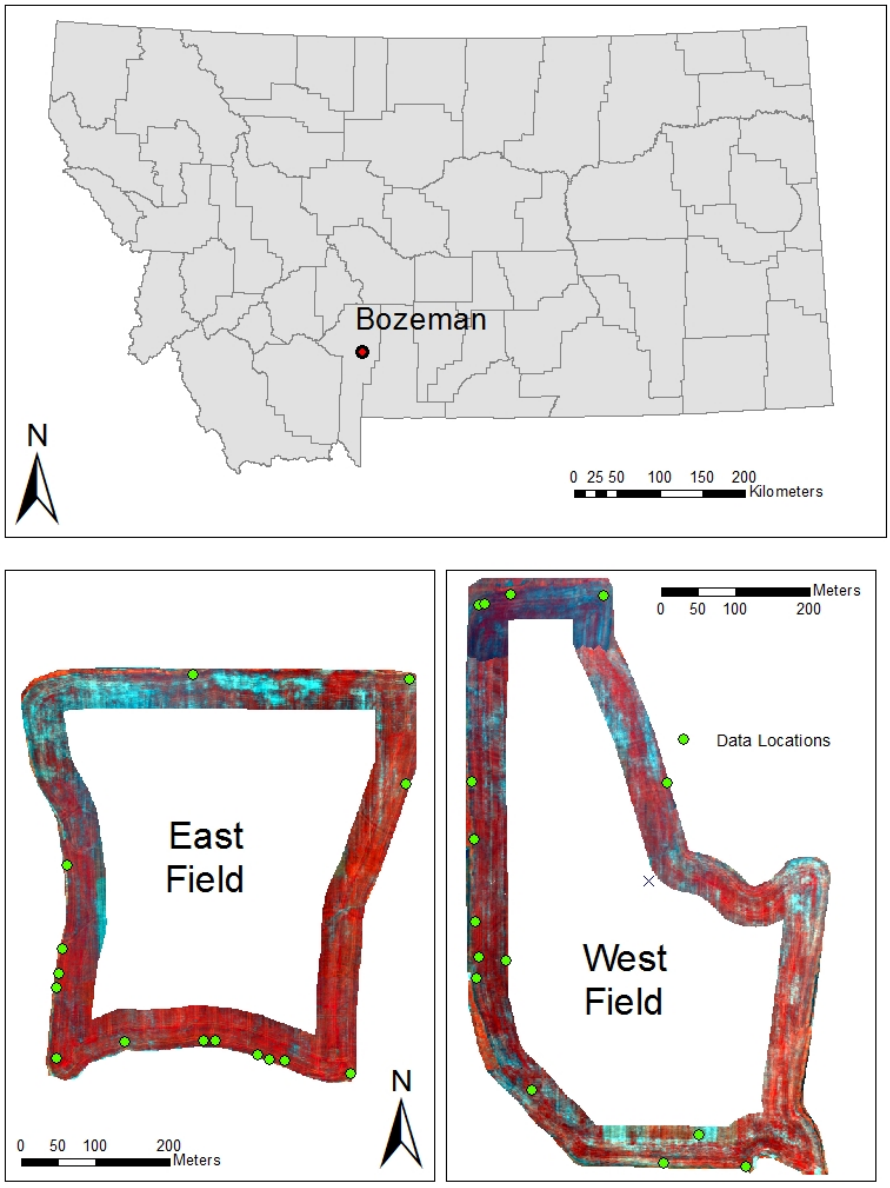

Figure 3.1. Research fields 15 km southwest of Bozeman, Montana where flights to collect hyperspectral data were conducted on June 2, 2016. Fields shown in false color infrared and data collection points in green. Center of field were removed due to a lack of data in these areas for analysis.

Reference Data

Weed locations were selected due to the requirements for visibility from the air. These weed locations had to be large enough that 0.5-m pixels would contain weeds. Roll, pitch, and yaw caused uncertainty in geolocation error of individual pixels during the aerial survey, requiring tarps be placed as reference to locate the weed locations in the image. Locations large enough to be selected were found within the wheat field 50 m or less from the field edges, concentrating data collection and analysis to this area.

Locations were visually selected as having at least a 2x2-m area of more than 75% weed coverage for infested locations (hereafter referred to as infested) (Figure 3.2a) and 2x2-m area free of weeds for uninfested locations (hereafter referred to as uninfested) 2b (Figure 3.2b). Locations corresponded to 224 infested and 184 uninfested pixels in the collected imagery, after initial analysis 30 uninfested locations or 120 pixels within the image were added to the training data. The added uninfested locations were selected based on firsthand knowledge of the field. Blue tarps were centered among infested and uninfested locations (Figure 3.2c) with each tarp identifying two infested and two uninfested locations. Tarp center points were the reference for field data collection. The infested and uninfested locations were documented as a distance and azimuth from tarp center (Figure 3.3) and marked with an orange flag. The azimuth was taken with a Lietz pocket transit in degrees from north from the tarp center.

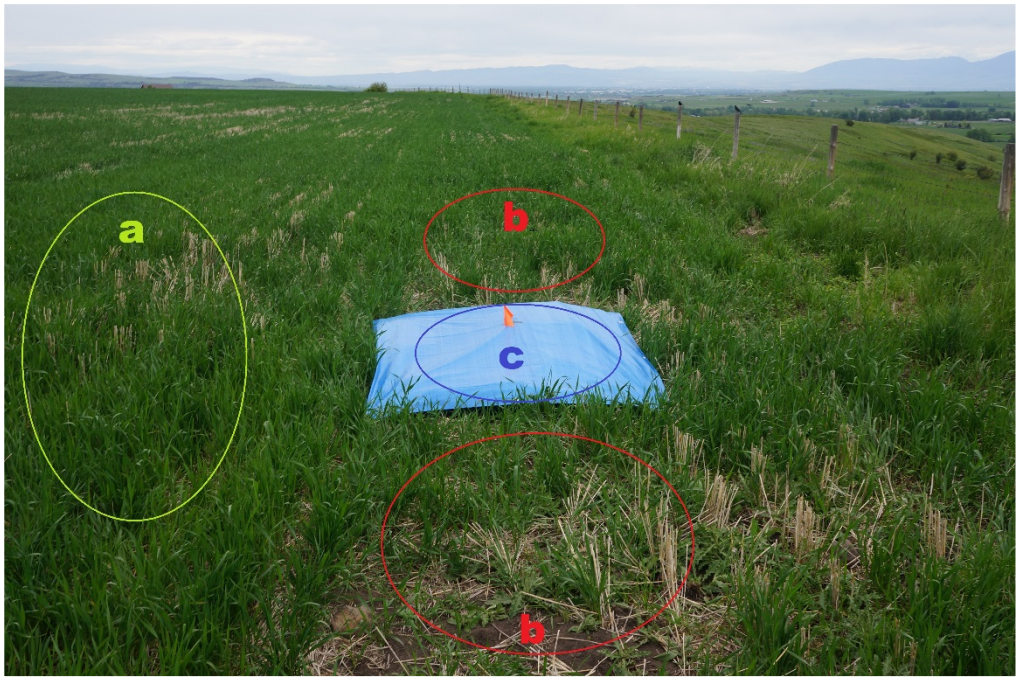

Figure 3.2. *a)* Infested area with high weed ground cover for which infested data was collected is seen in the foreground and beyond the tarp with red circles. *b)* Uninfested area free of weeds for which data was collected is to the left of the image in green circles. *c)* Tarp placed in field to locate data points on hyperspectral data. Blue tarps also provided reference for atmospheric correction.

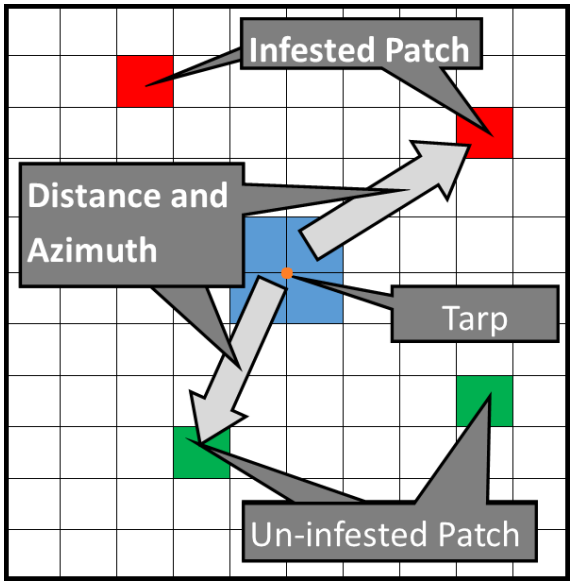

Figure 3.3. Distance and azimuth recorded for each infested and uninfested locations from the tarp center point. Field data allowed specific pixels to be selected as infested and un-infested signatures in the image for analysis.

Image Collection

A Pika II imaging spectrometer (Resonon, Inc., Bozeman, MT, USA) was flown at approximately 800 m above the ground on June 2nd, 2016, collecting 0.5-m resolution hyperspectral data. The flight date was selected to minimize shifting light conditions and coincided with the farmer's weed spraying schedule. Flight paths were planned to collect swaths that overlapped 50%, allowing common ground control points to be identified. The Pika collects 80 spectral bands with 6.39-nm spectral resolution from 425–925 nm. The imaging spectrometer was calibrated in the factory at the time of manufacture.

Processing

Data from the spectrometer was post processed as outlined by McCann et al. (2017), using data collected by the global positioning system and internal navigation system. Swaths were radiometrically normalized using areas contained in both swaths to smooth irradiance values. Each swath was georeferenced to a 2015 NAIP image of the area, projected, and mosaicked to create a single image for each field. The internal regions of the field were removed for analysis.

Three separate atmospheric corrections were performed on the images. ASTM was a model correction based on industry standard ASTM G173-03. This model simulated a basic arbitrary air mass using bands near 760 and 820 nm. The air mass was selected to minimize the O_2 absorption features and calculate a ground level solar irradiance (McCann et al., 2017).

The second method used field-based spectra of tarps as reference for atmospheric correction. Tarp spectral responses were collected with a FieldSpec Pro spectrometer

(ASD Inc., Longmont, Colorado, USA). Tarp pixels collected by the Pika and irradiance of the tarps from the FieldSpec were compared for each wavelength. An atmospheric correction was applied to the image using the Modified Flat Field Correction (MFFC) technique (Seibert et al., 1998).

The final atmospheric correction method was Landsat based, using Landsat surface reflectance (LaSRC) as a reference target for the hyperspectral data (McCann et al., 2017). A linear model was used to radiometrically correct the hyperspectral image with the Landsat surface reflectance data. Both images where resampled to a common spatial resolution using bicubic interpolation. The hyperspectral data was spectrally resampled to directly correspond to the Landsat bands. The LaSRC and hyperspectral data was compared on a pixel-by-pixel basis, using a linear model to minimize the difference between the spectral curves of each data set. The correction values calculated by the linear model to best match the hyperspectral data to the LaSRC data were then resampled back to the hyperspectral data spatial resolution and applied to the hyperspectral data as a linear global spectral correction.

Spectral Extraction and Analysis

The four pixels closest to infested or uninfested points were selected and spectral signatures extracted. The 224 infested and 304 uninfested spectra samples from each of the 528 identified pixels were merged to represent one infested and one uninfested spectra. These merged spectra potentially masked spectral variability within each class, but was appropriate for the purpose of the analysis, which intended to distinguish infested from uninfested locations as a two class problem.

A total of 27 datasets (each dataset consisting of a different configuration of band combinations) were tested in the analysis. Classification using all 80 bands for each of the three atmospheric corrections gave the baseline of expected accuracy. The infested and uninfested signatures were compared using four signature separability measures; Euclidean, divergence, transformed divergence, and Jefferies-Matusita. Separability measures were used to find expected three and four band optimal combinations since most current multispectral sensors that could be modified with filters use three or four bands, creating 12 three band and 12 four band combinations, one combination for each atmospherically corrected image method using the four separability measures. With the addition of the three all 80 bands combinations 27 datasets were used.

Each of the 27 datasets was classified using the random forest algorithm. The entire dataset was used for training in each of the 27 cases, and accuracies were assessed using out-of-bag error estimations (Breiman, 2001). Comparisons were made based on overall accuracy (i.e., pixels correctly classified divided by total pixels analyzed). Statistical significance between classifications were based on comparisons of kappa statistics at an alpha of 0.05. Output maps were also visually compared for correspondence with field observations (i.e., were weeds being predicted where they were known to be present?).

Results

The ASD spectra for both infested and uninfested locations show similarities (Figure 3.4). The green area of the spectrum and the majority of the NIR is higher for the infested locations. The areas of the highest variability in the NIR are notably above 1000 nm which is not covered by our aerial sensor.

Comparing the three 80 band overall accuracy results, the highest was the MFFC corrected image with an estimated overall accuracy of 77% (Table 3.1). The ASTM and LaSRC 80 band classifications had similar results at 74-75% estimated overall accuracy.

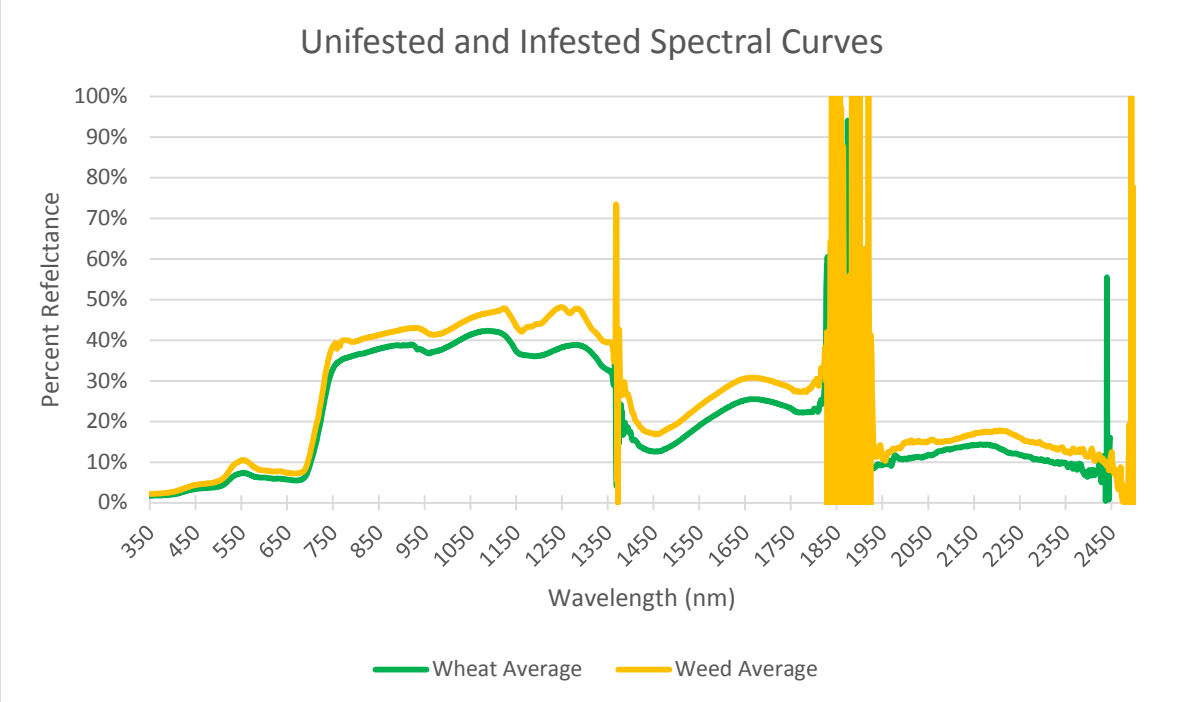

Figure 3.4 Average spectral curves of the 15 infested and 15 uninfested locations collected with the ASD ground based sensor.

Table 3.1. Classification overall estimated accuracy results. Each row represents an individual optimization method performed. Each column represents the method for atmospheric correction. Kappa statistics were calculated from each confusion matrix output by random forest. Results indicated with * vary statistically from the 80 band kappa results (alpha = 0.05).

Estimated Accuracy Results			
3 Bands			
	ASTM	LaSRC	MFFC
Transform Divergence	71.2%	64.9%	70.2%
Jeffries-Matusita	68.6%	68.1%	73.3%
Divergence	70.2%	56.5%	67.0%
Euclidean	54.5%	70.2%	62.8%
4 Bands			
Transform Divergence	73.8%	70.2%	70.2%
Jeffries-Matusita	64.9%	73.8%	71.2%
Divergence	69.6%	59.7%	64.9%
Euclidean	57.6%	70.2%	63.9%
All Bands			
All Bands	74.4%	75.4%	77.0%

Kappa Results			
3 Bands			
*Significant variability**	ASTM	LaSRC	MFFC
Transform Divergence	0.421	0.295*	0.399
Jeffries-Matusita	0.370	0.359	0.464
Divergence	0.398	0.125*	0.338*
Euclidean	0.083*	0.396	0.254*
4 Bands			
Transform Divergence	0.473	0.402	0.400
Jeffries-Matusita	0.295*	0.474	0.421
Divergence	0.389	0.194*	0.296*
Euclidean	0.144*	0.397	0.274*
All Bands			
All Bands	0.49	0.50	0.54

Atmospheric Correction Results

Averaged results by atmospheric correction technique (Table 3.2) were 66%, 67%, and 68% for ASTM, LaSRC, and MFFC, respectively. The MFFC corrected image was marginally higher on average than the LaSRC and ASTM correction. MFFC also was higher in each case when averaged separately for both three and four bands. LaSRC, however, displayed greater variability in results; when averaged for all band combinations it was the second highest, but it resulted in the lowest three band average and the highest four band average. The ASTM correction was the lowest combined average but was consistent between 3 and 4 bands.

Table 3.2. Average 3 and 4 band estimated accuracy for each atmospheric processing technique.

Correction Average	ASTM	LaSRC	MFFC
3 Band	66.11%	64.92%	68.32%
4 Band	66.49%	68.46%	67.54%
Combined	66.30%	66.69%	67.93%

Band Selection Methods Results

Averaging the results based on band selection technique (Table 3.3), the results show two groups. The higher group contains transformed divergence and Jefferies-Matusita, both with averages approximating 70%, regardless of number of bands analyzed. Transformed divergence and Jefferies-Matusita each contain one band combination result with a statistically significantly lower kappa statistic than the 80 band results; the transformed divergence with three bands using LaSRC correction had an

overall estimated accuracy of 65%, and four band Jefferies-Matusita an estimated accuracy of 65% when used with the ASTM correction.

Table 3.3. Averages for 3 band, 4 band, and combination of both 3 and 4 band for the band selection techniques.

Optimization Average	3 Band Average	4 Band Average	Combined Average
Transform Divergence	68.76%	71.38%	70.07%
Jeffries-Matusita	69.98%	69.98%	69.98%
Divergence	64.57%	64.75%	64.66%
Euclidean	62.50%	63.87%	63.19%

Transformed divergence and Jefferies-Matusita both outperformed divergence and Euclidean band selection, which had combined overall estimated accuracy averages of 65% and 63%, respectively. Euclidean and divergence had consistently statistically significantly lower kappa statistics for all correction methods, with results more than 5% lower than transformed divergence and Jefferies-Matusita. Euclidean and divergence band selection techniques each showed two band combinations with no statistically detectable change in estimated accuracy compared to 80 bands (Table 3.1). Divergence performed best with the ASTM correction, with both 3 and 4 bands estimated accuracy of 70%. Euclidean showed the best results when used with the LaSRC correction with 70% estimated accuracy for both 3 and 4 bands. Both Euclidean and divergence showed low estimated accuracy results with the MFFC correction.

Band Reduction Results

Overall estimated accuracy results were lower for 3-band combinations than for all 80 bands (Figure 3.4). Seven three-band combinations, however, resulted in kappa statistics that were not statistically significantly lower than the 80 band datasets, with accuracies ranging from 68% to 73%. These seven results included two transformed divergence combinations, three Jefferies-Matusita combinations, one Euclidean combination, and one divergence combination. The highest result was Jefferies-Matusita with the MFFC correction, which showed an estimated accuracy 3.7% lower than using all 80 bands.

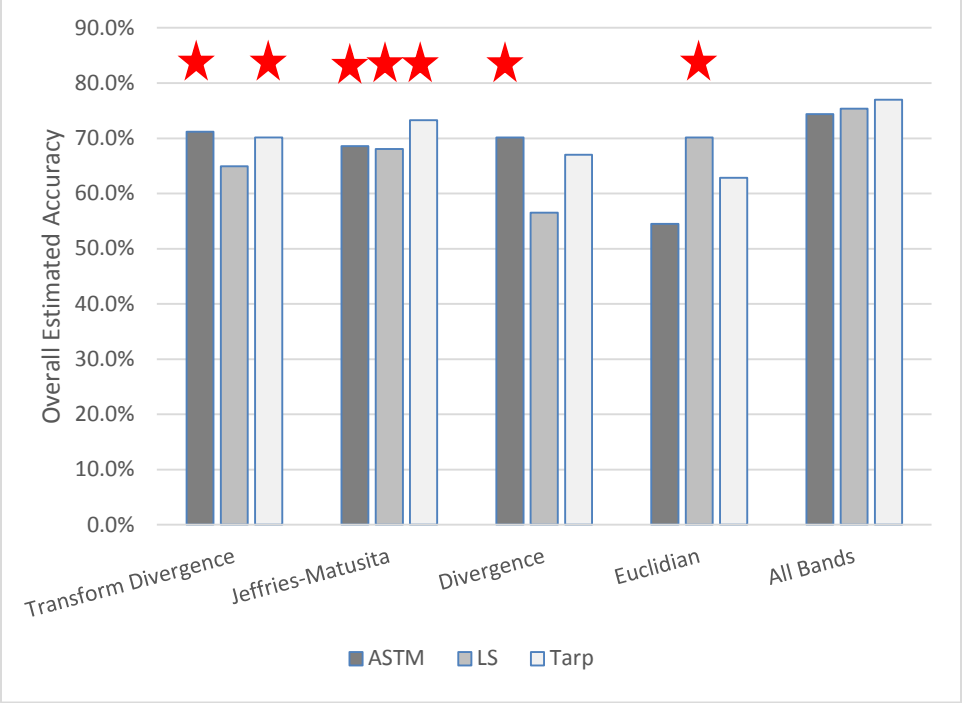

Figure 3.5. Comparison of 3 band results grouped by band selection method compared to 80 band results. Red stars indicate results with kappa statistics not significantly lower from the use of all 80 bands.

Comparing four band combinations to results from all 80 bands, five of the four band combinations show a detectable reduction in estimated accuracy (Figure 3.5). Seven of the 12 iterations with four bands showed kappa statistics without a detectable reduction from 80 bands accuracies. The results where a reduction in estimated accuracy was not detected ranged from 70 to 74%; including three transform divergence combinations, two Jefferies-Matusita combinations, one divergence combination, and one Euclidean combination. The highest result with four bands was transform divergence with the ASTM correction, 0.6% lower than using all 80 bands.

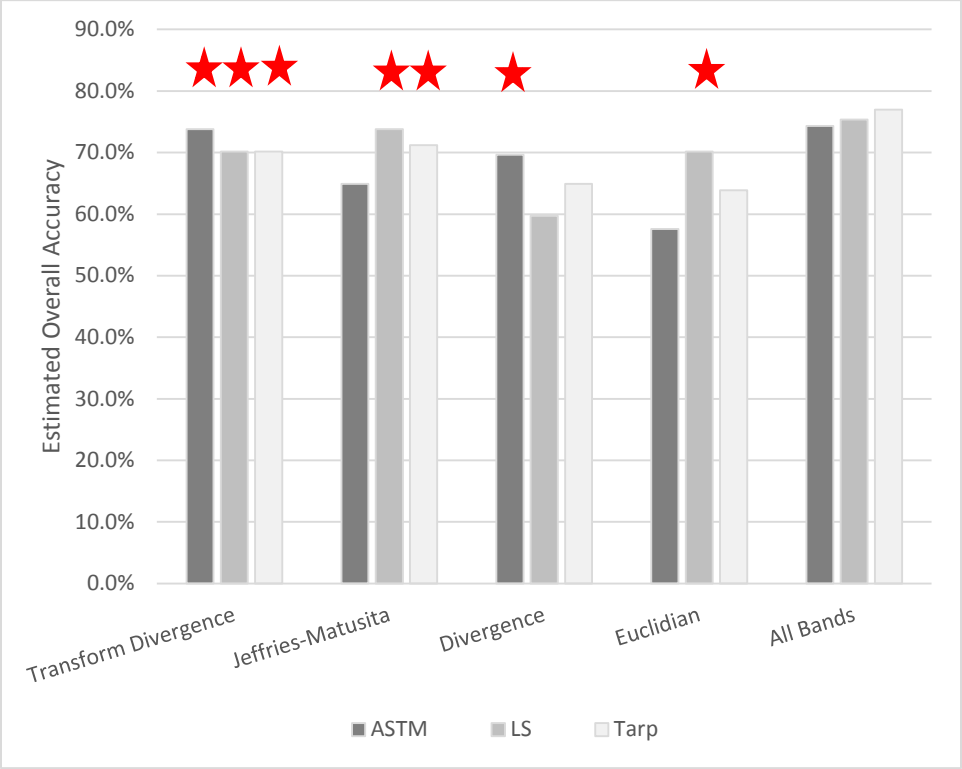

Figure 3.6. Comparison of 4 band results broken grouped by band selection method. Red stars indicate results with kappas not significantly lower from the use of all 80 bands.

Three and four band results had an average difference of 1%. The least consistent atmospheric correction technique was the LaSRC correction with the highest and lowest averages overall (Figure 3.6), the LaSRC four band average is five percent higher than the three band average. The MFFC and ASTM correction are more consistent with no statistical difference detected between three and four band results. By band selection technique there is no detected statistical difference in results between three and four bands within each band selection technique (Figure 3.7).

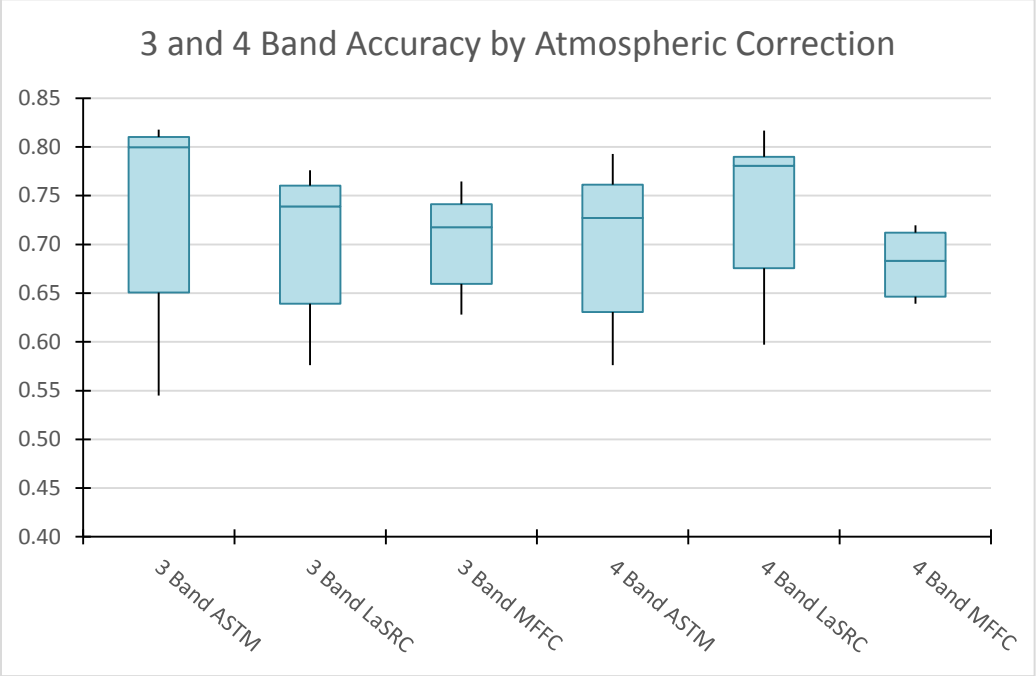

Figure 3.7. Comparison of 3 band and 4 band classification accuracies grouped by processing method.

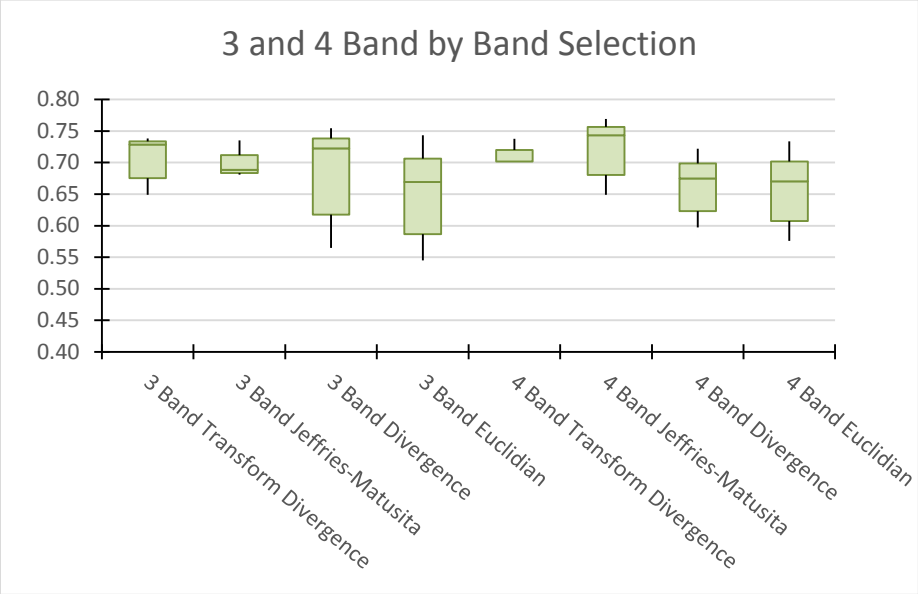

Figure 3.8. Comparison of 3 band and 4 band classification accuracies grouped by band selection method.

Map Results

Each random forest iteration output a map of estimated weed locations. The weed map output by all 80 bands using the highest estimated accuracy results, MFFC correction, estimated 38%, or 150,042 pixels of 394,458 pixels, of the west field was infested (Figure 3.8a), and 49%, 197,132 pixels of 404,630 pixels, of the east field being infested (Figure 3.8b). The highest estimated accuracy three band classification, Jeffries-Matusita with MFFC, estimated 25%, or 99,295 pixels of 394,458 pixels, of the west field infested (Figure 3.8c), and 46%, or 184,545 pixels of 404,630 pixels, of the east field infested (Figure 3.8d). The best 4-band classification, Jeffries-Matusita with the LaSRC correction, estimated 42%, or 167,067 pixels of 394,458 pixels, of the west field (Figure 3.8e) and 44%, or 178,364 pixels of 404,630 pixels, of the east field (Figure 3.8f) was infested with weeds.

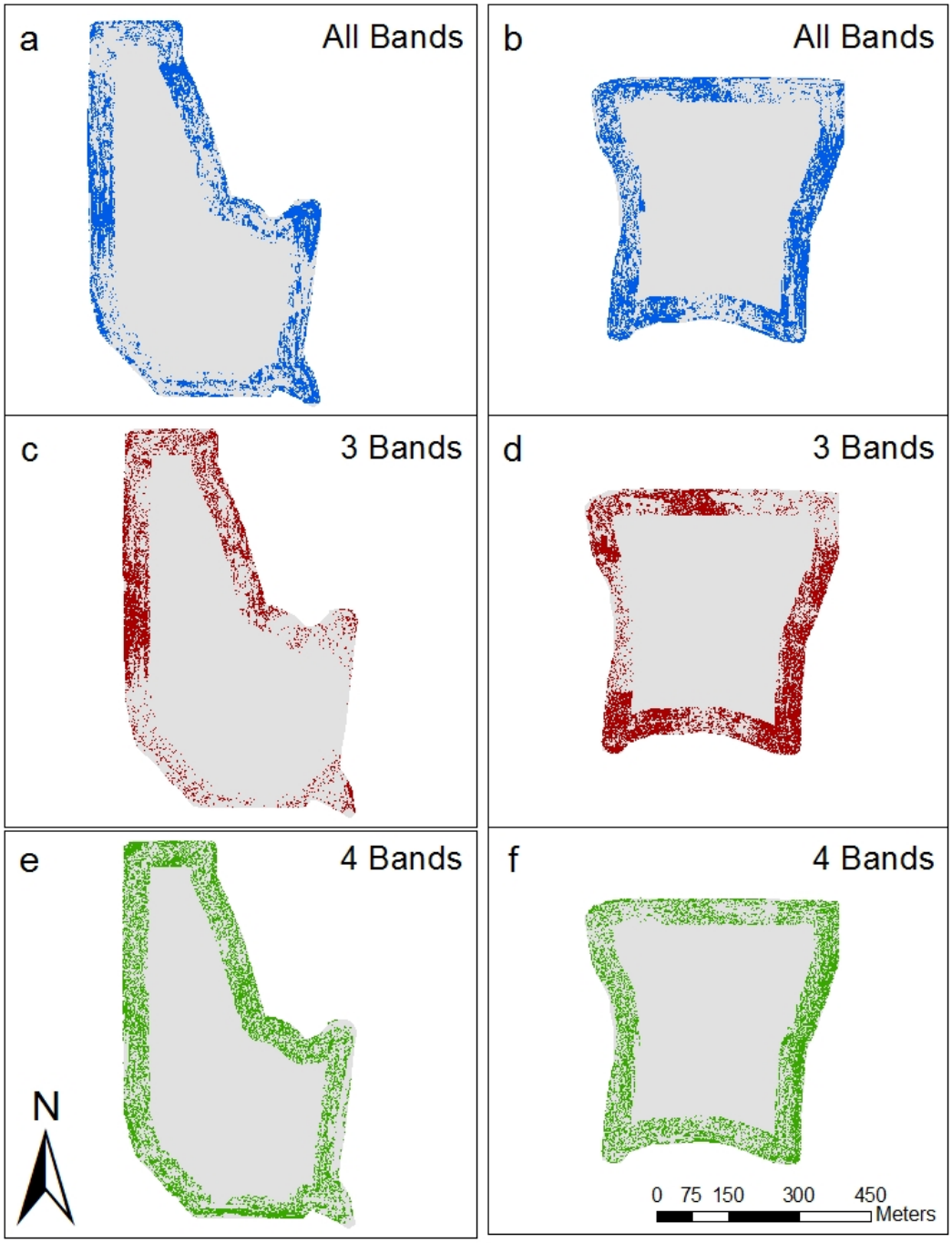

Figure 3.9. Estimated weed map using all bands (*a* and *b*), 3 band Jefferies-Matusita (*c* and *d*), and 4 band transform divergence (*e* and *f*). Colored pixels are classified as infested pixels.

Discussion

Selecting an overall top method for weed locations appropriate for management is not straightforward based on the results above. The results are highly variable based on band selection method and atmospheric correction, making it hard to determine if differences in results represent estimated accuracy of band combinations or variation as an artifact of processing. The reduced band combinations generally are lower than using all 80 bands, however, approximately half the time three or four bands could achieve results with no statistically significant difference in kappa statistics from the use of all bands.

Looking at output weed maps, patterns indicate that some variation in wheat may be affecting results. The percent weed cover estimated is higher than expected in a managed field, supporting the idea that wheat is being identified as a weed. Sampling across various wheat conditions to create various wheat spectra might be necessary in further research.

Atmospheric Correction

Variation in results across atmospheric correction are small until three and four band averages are examined separately. The LaSRC processing showed a large variation, with the highest and lowest recorded results. Both the MFFC and ASTM results demonstrated stability when changing between three and four bands, with MFFC highest on average.

The LaSRC correction technique is a new method that holds some potential as a tool. It does not require placing in-field targets like the MFFC. This could be important if

data collection did not include viable spectral targets and further time could not be allocated to spectral correction targets.

LaSRC had multiple issues with its use; imagery collection is not flexible and cannot be changed for mission requirements. The Landsat image used in this case was collected the day before the hyperspectral flight. The difference between the LaSRC and hyperspectral image could be very high due to cloudy conditions on the flight date, leading to varying results. It was fortuitous to have LaSRC coverage so close to the flight date, but it is possible that this will not happen every time narrow spectral bands need to be determined. Consistency in atmospheric conditions between the LaSRC and hyperspectral image cannot be guaranteed. LaSRC contains error introduced in the processing of Landsat data unknown to the end user (McCann et al., 2017).

The results from the LaSRC correction were either very accurate, the best result found, or very inaccurate, the worst result found. This inconsistency leaves the question of results being band combination related or an artifact of processing. Accuracies might change when placed on-tractor, making the band combination a poor choice.

The ASTM based correction method is a generic correction technique. The model could be customized to the location of interest with further ancillary data, but the data might not be available, limiting its use. It also produced the most inaccurate results, with all bands and the lowest average estimated accuracy of reduced optimal bands.

The MFFC shows a few benefits when taking into account the requirements of weed spraying. The MFFC has the highest estimated accuracy with all 80 bands, leaving a better chance of higher results with band reduction. The MFFC calculation corrects the

pixels based on actual conditions at the moment the data was collected, most representing a ground-based sensor. The other correction techniques do not have this customized approach to data collection.

The estimated accuracy and stability of the MFFC indicates it as the best overall atmospheric correction for these fields. The MFFC provides more flexible mission planning at the cost of more field work. The LaSRC correction could provide a better but inconsistent result than the ASTM correction in case of loss of MFFC capability.

Optimization Technique

Band selection based on transformed divergence and Jeffries-Matusita were tied for optimal bands across all correction methods and in this case the increased required processing power for Jeffries-Matusita did not slow analysis. Both Euclidean and divergence showed overall relatively poor results, with one-third of the results showing undetectable differences in estimated accuracy from use of all 80 bands.

Euclidean and divergence consistently performed poorly with MFFC, the best overall atmospheric correction method. Transform divergence and Jeffries-Matusita worked well in all cases with MFFC. The result for MFFC with a Jeffries-Matusita band selection were among some of the highest accuracies, 73% for 3 bands and 71% for 4 bands. Transformed divergence band selection with MFFC had 70% estimated accuracy for both 3 and 4 bands.

Jeffries-Matusita had the overall highest average estimated accuracy with 3 bands, and transform divergence was the highest average estimated accuracy with 4 bands. Transform divergence and Jeffries-Matusita provide accuracies at least above 85% in

other research selecting optimal bands and classifying targets and in most cases above 95% with various classification algorithms (Riedmann and Milton, 2003; Su et al., 2014; Yang et al., 2011).

Conclusion

The band combinations from transform divergence and Jeffries-Matusita band selection methods, when run on an image corrected using ground based spectral data, showed results similar to use of all 80 bands. The selection of bands played an important role in the estimated accuracies, while some band combinations showed no statistically significant reduction in accuracies some bands did show a significant loss. This possibility of poor accuracies from band combinations means that the usefulness of any band combination must be measured in multiple fields before wider use, but the accuracies associated with hyperspectral sensors can be attained with only a few bands. This has the ability to revolutionize the multispectral sensors used for on-tractor spot spraying, potentially enabling results comparable to the high classification accuracies seen in historical studies of weed mapping with hyperspectral data. The accuracy of our results did not match the level of infestation expected in the output weed maps, an indication that our results may not be applicable to areas outside our data collection. The next step is to test the robustness of these results across other fields and settings with additional data

Reference Cited

Bandos, T.V., Bruzzone, L., Camps-Valls, G., 2009. Classification of Hyperspectral Images With Regularized Linear Discriminant Analysis. IEEE Transactions on Geoscience and Remote Sensing 47, 862–873. doi:10.1109/TGRS.2008.2005729

Breiman, L., 2001. Random Forests. Machine Learning 45, 5–32. doi:10.1023/A:1010933404324

Breiman, L., 1996. Out-of-bag estimation. Technical report, Statistics Department, University of California Berkeley, Berkeley CA 94708, 1996b. 33, 34.

Davis, S.M., Landgrebe, D.A., Phillips, T.L., Swain, P.H., Hoffer, R.M., Lindenlaub, J.C., Silva, L.F., 1978. Remote sensing: The quantitative approach. McGraw-Hill International Book Company.

Deng, W., Huang, Y., Zhao, C., Chen, L., Wang, X., 2016. Bayesian discriminant analysis of plant leaf hyperspectral reflectance for identification of weeds from cabbages. AJAR 11, 551–562. doi:10.5897/AJAR2015.10395

Du, Q., Yang, H., 2008. Similarity-Based Unsupervised Band Selection for Hyperspectral Image Analysis. IEEE Geoscience and Remote Sensing Letters 5, 564–568. doi:10.1109/LGRS.2008.2000619

Goetz, A.F.H., Vane, G., Solomon, J.E., Rock, B.N., 1985. Imaging Spectrometry for Earth Remote Sensing. Science 228, 1147–1153. doi:10.1126/science.228.4704.1147

Herrmann, I., Shapira, U., Kinast, S., Karnieli, A., Bonfil, D.J., 2013. Ground-level hyperspectral imagery for detecting weeds in wheat fields. Precision Agric 14, 637–659. doi:10.1007/s11119-013-9321-x

Holland Scientific, 2017. CROP CIRCLE ACS470 [WWW Document]. Holland Scientific. URL http://hollandscientific.com/portfolio/crop-circle-acs-470/ (accessed 7.24.17).

Horler, D.N.H., Dockray, M., Barber, J., 1983. The red edge of plant leaf reflectance. International Journal of Remote Sensing 4, 273–288. doi:10.1080/01431168308948546

Huete, A.R., Jackson, R.D., Post, D.F., 1985. Spectral response of a plant canopy with different soil backgrounds. Remote Sensing of Environment 17, 37–53.

King, M.D., Kaufman, Y.J., Menzel, W.P., Tanre, D., 1992. Remote sensing of cloud, aerosol, and water vapor properties from the moderate resolution imaging spectrometer (MODIS). IEEE Transactions on Geoscience and Remote Sensing 30, 2–27. doi:10.1109/36.124212

Knipling, E.B., 1970. Physical and physiological basis for the reflectance of visible and near-infrared radiation from vegetation. Remote Sensing of Environment 1, 155–159. doi:10.1016/S0034-4257(70)80021-9

Lass, L.W., Thill, D.C., Shafii, B., Prather, T.S., 2002. Detecting Spotted Knapweed (Centaurea maculosa) with Hyperspectral Remote Sensing Technology. Weed Technology 16, 426–432. doi:10.1614/0890-037X(2002)016[0426:DSKCMW]2.0.CO;2

Lawrence, R., 2004. Classification of remotely sensed imagery using stochastic gradient boosting as a refinement of classification tree analysis. Remote Sensing of Environment 90, 331–336. doi:10.1016/j.rse.2004.01.007

Lawrence, R.L., Wood, S.D., Sheley, R.L., 2006. Mapping invasive plants using hyperspectral imagery and Breiman Cutler classifications (randomForest). Remote Sensing of Environment 100, 356–362. doi:10.1016/j.rse.2005.10.014

Lord, D., Desjardins, R.L., Dubé, P.A., 1988. Sun-Angle Effects on the Red and near Infrared Reflectances of Five Different Crop Canopies. Canadian Journal of Remote Sensing 14, 46–55. doi:10.1080/07038992.1988.10855118

Maggiori, E., Tarabalka, Y., Charpiat, G., Alliez, P., 2017. Convolutional Neural Networks for Large-Scale Remote-Sensing Image Classification. IEEE Transactions on Geoscience and Remote Sensing 55, 645–657. doi:10.1109/TGRS.2016.2612821

Marchant, J.A., Onyango, C.M., 2002. Spectral invariance under daylight illumination changes. JOSA A 19, 840–848.

McCann, C., Repasky, K.S., Morin, M., Lawrence, R.L., Powell, S., 2017. Using Landsat Surface Reflectance Data as a Reference Target for Multiswath Hyperspectral Data Collected Over Mixed Agricultural Rangeland Areas. IEEE Transactions on Geoscience and Remote Sensing PP, 1–13. doi:10.1109/TGRS.2017.2699618

NTech Industies, Inc., 2017. Data Sheet Model 650 Sensor.

Okamoto, H., Murata, T., Kataoka, T., Hata, S.-I., 2007. Plant classification for weed detection using hyperspectral imaging with wavelet analysis. Weed Biology and Management 7, 31–37. doi:10.1111/j.1445-6664.2006.00234.x

Pantazi, X.-E., Moshou, D., Bravo, C., 2016. Active learning system for weed species recognition based on hyperspectral sensing. Biosystems Engineering 146, 193–202. doi:10.1016/j.biosystemseng.2016.01.014

Riedmann, M., Milton, E.J., 2003. Supervised band selection for optimal use of data from airborne hyperspectral sensors, in: IGARSS 2003 IEEE International. Presented at the Geoscience and Remote Sensing Symposium, pp. 1770–1772. doi:10.1109/IGARSS.2003.1294245

Seibert, J.A., Boone, J.M., Lindfors, K.K., 1998. Flat-field correction technique for digital detectors. Presented at the Medical Imaging 1998: Physics of Medical Imaging, International Society for Optics and Photonics, pp. 348–355. doi:10.1117/12.317034

Stafford, J.V., Miller, P.C.H., 1996. Spatially Variable Treatment of Weed Patches. Precision Agriculture 465–474. doi:10.2134/1996.precisionagproc3.c50

Su, H., Du, Q., Chen, G., Du, P., 2014. Optimized Hyperspectral Band Selection Using Particle Swarm Optimization. IEEE Journal of Selected Topics in Applied Earth Observations and Remote Sensing 7, 2659–2670. doi:10.1109/JSTARS.2014.2312539

Sun, K., Geng, X., Ji, L., 2015. A New Sparsity-Based Band Selection Method for Target Detection of Hyperspectral Image. IEEE Geoscience and Remote Sensing Letters 12, 329–333. doi:10.1109/LGRS.2014.2337957

Topcon Positioning Systems, Inc., 2017. Cropspec Brochure.

Wang, C., Zhou, B., Palm, H.L., 2008. Detecting Invasive Sericea Lespedeza (Lespedeza cuneata) in Mid-Missouri Pastureland Using Hyperspectral Imagery. Environmental Management 41, 853–862. doi:10.1007/s00267-008-9092-8

Wendel, A., Underwood, J., 2016. Self-supervised weed detection in vegetable crops using ground based hyperspectral imaging, in: 2016 IEEE International Conference on Robotics and Automation. Presented at the 2016 IEEE International Conference on Robotics and Automation (ICRA), pp. 5128–5135. doi:10.1109/ICRA.2016.7487717

Xia, X., Che, H., Zhu, J., Chen, H., Cong, Z., Deng, X., Fan, X., Fu, Y., Goloub, P., Jiang, H., Liu, Q., Mai, B., Wang, P., Wu, Y., Zhang, J., Zhang, R., Zhang, X., 2016. Ground-based remote sensing of aerosol climatology in China: Aerosol optical properties, direct radiative effect and its parameterization. Atmospheric Environment, Air Pollution in the Beijing – Tianjin – Hebei (BTH) region, China 124, 243–251. doi:10.1016/j.atmosenv.2015.05.071

Yang, H., Du, Q., Su, H., Sheng, Y., 2011. An Efficient Method for Supervised Hyperspectral Band Selection. IEEE Geoscience and Remote Sensing Letters 8, 138–142. doi:10.1109/LGRS.2010.2053516

Zwiggelaar, R., 1998. A review of spectral properties of plants and their potential use for crop/weed discrimination in row-crops. Crop Protection 17, 189–206. doi:10.1016/S0261-2194(98)00009-X

CHAPTER FOUR

EFFECTS OF BANDWIDTH ON CLASSIFICATION ACCURACY OF INVASIVE WEEDS USING FIELD HYPERSPECTRAL IMAGERY

Introduction

Spectral resolution, including the number and spectral width of bands, is one of the key characteristics distinguishing imaging sensors from each other. Relatively wider bands might not have sufficient spectral resolution for differentiation of similar targets, such as the ability to detect narrow absorption features present in one target but absent in another. Narrow bands have shown the ability to differentiate similar targets in different settings and could be applied to current technology to improve accuracies of similar target classes. There appears to be no universally accepted definition, but hyperspectral data tends to refer to narrow, continuous bands and multispectral tends to refer to broad, discrete band sensors (Lillesand et al., 2014). Narrow bands tend to be more expensive due to the high cost of hyperspectral sensors and required processing (Du and Yang, 2008). Broad bands are more common due to the relatively cheaper sensors and lower data processing requirements. The cost of narrow spectral bands from hyperspectral sensors is not warranted if narrow bands do not provide an increase in accuracy, however if narrow bands do improve accuracies then implementation of narrow spectral filters on existing technology might improve sensor accuracy and justify increased costs.

Hyperspectral sensors allow narrow sections of spectral responses to be analyzed using continues narrow bands across a portion of the EM spectrum (Goetz et al., 1985).

Hyperspectral data allows targets with narrow absorption bands to be located with analysis of narrow sections of the reflectance curve. The successful use of hyperspectral imagery in aerial reconnaissance surveys for feature extraction purposes and environmental monitoring has been demonstrated repeatedly in the literature (Sorenson et al., 2017; Scafutto et al., 2017; Davies and Calvin, 2017; Scafutto et al., 2016; Richter et al., 2016; Resmini et al., 1997; Chen et al., 2009). Three examples that rely on the narrow bands found in the hyperspectral sensors are detection of potential mineral deposits, hydrocarbon seepage in soils, and acidic mine leakage.

Hyperspectral sensor bands selected based on lab spectra were used on an aerial platform to classify minerals including alunite, kaolinite, and calcite (Resmini et al., 1997). A satellite borne hyperspectral sensor, Hyperion, was compared to an established aerial sensor, AVIRIS (Swayze, 1997), across a total of seven minerals containing four separate mineral species in Cuprite, NV, and Northern Death Valley, CA. Satellite collected hyperspectral data were capable of classifying the four mineral species to within 95% of aerial sensors (Kruse et al., 2003).

Hydrocarbons that leak into soils as crude oil and petroleum products were shown to have diagnostic absorption features centered on 1742 and 2329 nm in the short wave infrared (SWIR) region. These bandwidths were found to not only define presence and absence of hydrocarbons but possible groups based on densities and contamination (Scafutto et al., 2016). The ability to monitor for potential leaks from pipelines, refineries, processing stations, and natural oil seeps with spectra from libraries is a new

technology being developed for industry usage (Asadzadeh and de Souza Filho, 2017; Scafutto et al., 2017).

Hyperspectral imagery has also been used to detect high potential areas of acidic mine waste that could enter waterways through weathering (Davies and Calvin, 2017). The Leviathan mine was mapped looking at the potential of hyperspectral data for locating and dispatching remediation efforts to potentially high acidic mine waste. The hyperspectral data was able to classify six separate acidic distinctive features, with each feature showing individual absorption and reflectance bands around 700 nm and above 2000 nm.

Hyperspectral sensors have also been shown to locate and classify weed species, although the published literature does not tend to rely on the presence of unique absorption or reflectance features as necessarily the basis of successful classification. Aerial monitoring of weeds has allowed researchers to identity weed species like; Chinese bushclover (*Lespedeza cuneate L.),* leafy spurge (*Euphorbia esula*), spotted knapweed (*Centaurea maculosa*), Barnyard grass (Echinochloa crusgalli) , green foxtail *(Setaria viridis),* goose grass (*Galium aparine),* and small quinoa (*Chenopodium quinoa)* with accuracies ranging from 84% to 100% in associated range, pasture, and agricultural lands (Wang et al., 2008; Lawrence et al., 2006; Deng et al., 2016; Lass et al., 2002).

On-ground sensors have had similar or higher accuracies identifying weed species in crops. Recognition of creeping buttercup (*Ranunculus repens),* Canada thistle *(Cirsium arvense),* wild mustard *(Sinapis arvensis),* common chickweed *(Stellaria media),* common dandelion *(Tarraxacum officinale),* annual bluegrass *(Poa annua),* lady's thumb

(Poligonum persicaria), common nettle *(Urtica dioica),* common yellow woodsorrel *(Oxalis europaea),* and black medick *(Medicago lupulina)* in corn (*zea mays*) showed accuracies as high as 94% in a comparison of various machine learning techniques using hyperspectral data (Pantazi et al., 2016). Classification of caltrop (Tribulus terrestris), curly dock (Rumex crispus), red dock (rumex sanguineus), and barnyard grass in corn with a hyperspectral sensor reached accuracies over 95% (Wendel and Underwood, 2016). Classification accuracies as high as 97% were found for wild buckwheat (*Fallopia convolvulus),* field horsetail *(Equisetum arvense),* green foxtail, and common chickweed in a field of sugar beets (*Beta vulgaris* subsp. *Vulgaris)* (Okamoto et al., 2007). What is not established from these studies with respect to weed species (in contrast to minerology studies, for example), however, is whether or not similar accuracies could have been achieved with multispectral sensors. Hyperspectral data sensor design and components and be costly relative to multispectral sensors, and data processing requirements are high compared to multispectral sensors; therefore, it is important to determine to what extent there are tradeoffs in classification accuracy between alternative sensor designs.

Multispectral sensors with lower associated costs and processing and the ability for multispectral sensors to collect wide bands in the visible, red edge, NIR, and SWIR has led to their use in vegetation identification, particularly weed species (Goel et al., 2002; Feyaerts and van Gool, 2001; Alchanatis et al., 2005). The Canon s110 camera has been adopted for use in the eBee from sensyFly to image in the near infrared (NIR) and red edge portions of the EM spectrum for agricultural purposes (SenseFly Ltd., 2017). The relatively inexpensive and compact multispectral sensors have seen a growth in use

with UAV technology and have shown accuracies as high as 98% mapping weeds (Pantazi et al., 2017).

Current commercial tractor-mounted spot spraying sensors rely on multispectral bands most likely centered in the visible red and NIR only, allowing use in fallow, between row, and pre-emergent crops where vegetation can be assumed to be weeds (Topcon Positioning Systems, Inc., 2017; NTech Industies, Inc., 2017; Holland Scientific, 2017). We are not aware of any commercial on-tractor sensors that use hyperspectral data or narrow bands. The ability of hyperspectral sensors to analyze specific sections of the EM spectrum potentially could allow improved differentiation of plant species based on differences in internal characteristics of plant structures and canopy absorption dynamics (Knipling, 1970; Lord et al., 1988; Huete et al., 1985; Marchant and Onyango, 2002).

The application of either hyperspectral data or narrow band multispectral data for on-tractor sensor weed identification necessitates a determination of whether these data types are sufficiently superior to wider, multispectral bands to justify their cost and implementation. Our objective was to provide initial insight into this question by analyzing broadleaf weed identification in wheat fields. We used airborne hyperspectral data to address two specific questions: (1) what were the comparative accuracies between narrow and progressively wider contiguous spectral bands and (2) what were the comparative accuracies using either three or four discrete wider or narrow bands. The first question was addressed to evaluate the potential advantages for on-tractor

hyperspectral instruments. The second question was addressed to evaluate the potential for modifying current multispectral approaches with narrower spectral bands.

Methods

Location

The study site included two agricultural fields southwest of Bozeman, Montana at approximately 1675 m above sea level, in the north foothills of the Gallatin Range (Figure 4.1). Winter wheat was planted in both fields fall of 2015 and harvested in August of 2016. Fields were on well drained stream terraces in a mix of clay and silt loam soils. The Bozeman area receives approximately 41 cm of rain a year with highest average rain falls being concentrated in the spring and early summer months of April, May, and June based on 2017 U.S. climate data (U.S. Climate Data, 2017). The frost free growing season is late May to middle of September, just over 100 days based on averages from 1981 through 2010. The weed infested areas were dominated by broadleaf weeds; Canada thistle (*Cirsium arvense*), prickly lettuce (*Lactuca serriola*), and bedstraw (*Galium aparine*). No grass weed locations large enough to be mapped from the air were found.

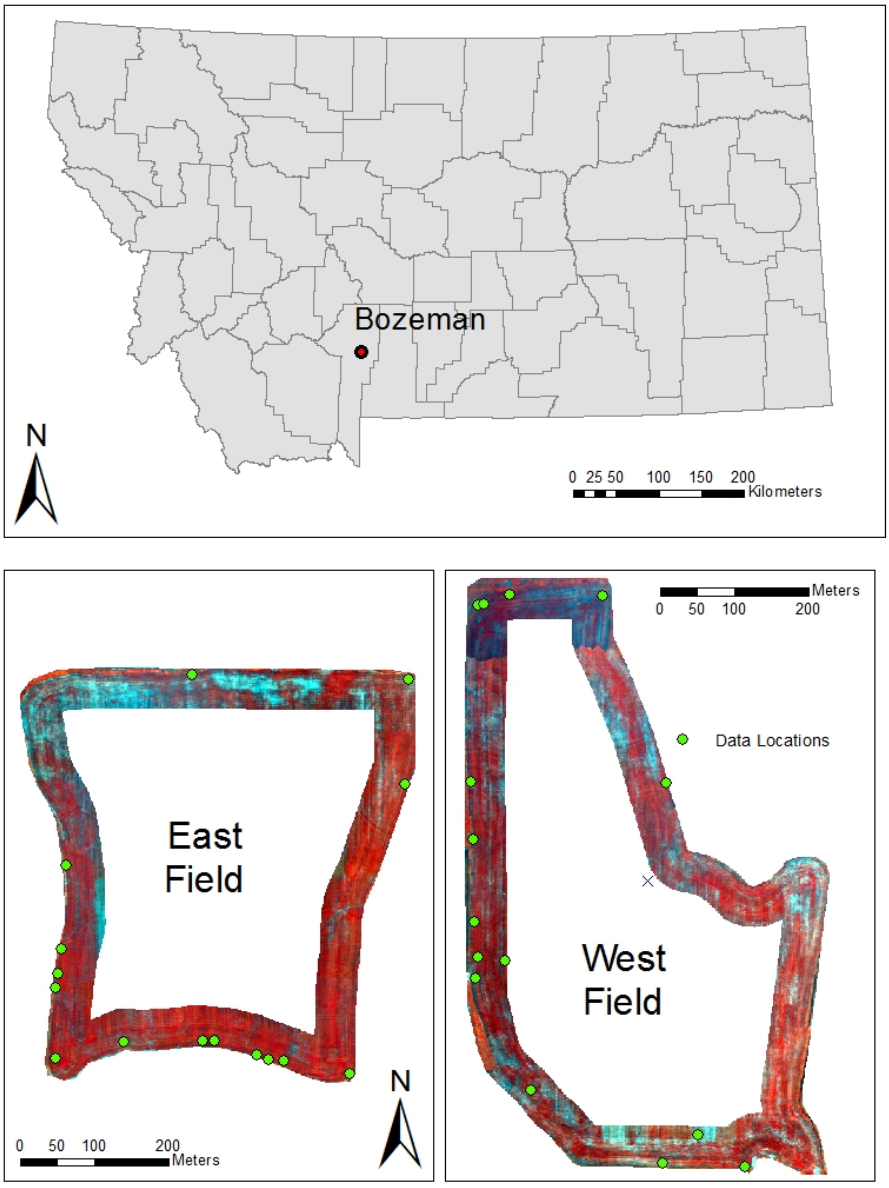

Figure 4.1. Research fields 15 km southwest of Bozeman, Montana where flights to collect hyperspectral data was conducted on June 2, 2016. Fields shown in false color infrared and data collection points in green.

Reference data

Weed locations were not selected randomly due to the requirements for visibility from the air. Locations had to be large enough that 0.5-m pixels contained weeds. Roll, pitch, and yaw caused uncertainty in geolocation error of individual pixels, requiring tarps be placed as reference to locate the weed locations in the image. Weed infested locations within the wheat field large enough to be sensed were within 50 m of the field edges, concentrating weed infestation data collection and analysis to this area.

Locations were visually selected as having at least a 2x2-m area of more than 75% weed coverage for infested locations (hereafter referred to as infested) and 2x2-m area free of weeds for uninfested locations (hereafter referred to as uninfested). Blue tarps were centered among locations (Figure 4.2). Each tarp identified four locations, two identified as infested and two uninfested, when such variation was present within several meters of a tarp (in some cases only infested or uninfested locations were present near a given tarp). Additional uninfested locations away from field edges were identified to account for some of the variability in wheat growth across the fields. Tarp center points were the reference for field data collection.

The infested and uninfested locations were documented as a distance and azimuth from tarp center (Figure 4.3) and marked with an orange flag. The azimuth was taken with a Lietz pocket transit in degrees from north from the tarp center.

Figure 4.2. Tarp placed in field to locate data points on hyperspectral data. Blue tarps also provided reference for atmospheric correction.

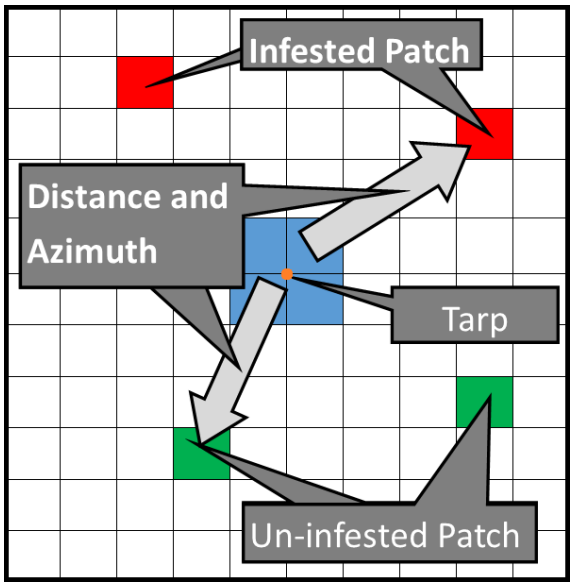

Figure 4.3. Distance and azimuth recorded for each infested and uninfested area from the tarp center point. Field data allowed specific pixels to be selected as infested and uninfested signatures in the image for analysis.

Image Collection

A Pika II imaging spectrometer (Resonon, Inc., Bozeman, MT, USA) was flown at approximately 800 m above the ground on June 2nd, 2016, collecting 0.5-m resolution hyperspectral data. The flight date was selected to minimize shifting light conditions and coincide with the farmer's weed spraying schedule. Flight paths were planned to collect swaths that overlapped 50%, allowing common ground control points to be identified. The Pika collects 80 spectral bands with 6.39-nm spectral resolution from 425–925 nm. The imaging spectrometer was calibrated in the factory at the time of manufacture.

Processing

Data from the spectrometer was post processed as outlined by McCann et al. (2017), using data collected by the global positioning and internal navigation systems. Swaths were radiometrically normalized using overlapping areas to smooth irradiance values. Each swath was georeferenced to a 2015 NAIP image of the area, projected, and mosaicked to create a single image for each field. The centers of fields where data was not collected was removed.

The method for atmospheric correction was a model correction using field-based tarp spectra. Tarp spectral responses were collected with a FieldSpec Pro spectrometer (ASD Inc., Longmont, Colorado, USA). A Modified Flat Field Correction (MFFC) technique compared each tarp pixel collected by the Pika to the tarp irradiance from the FieldSpec to correct the image (Seibert et al., 1998).

Narrow hyperspectral data bands were combined into increasingly wider bands to simulated increased bandwidth. No specific sensor was being imitated, so bands were

simply averaged in order, based on the principle that filters can isolate that section of the EM spectrum for sensors that contain the necessary bands. Band data layers were averaged to create new wider bandwidth values, and each new band was stacked to create a new image. Hyperspectral data was combined from 80 6-nm bands and simulated bands widths were accomplished by adding two, three, four, six, eight, and sixteen bands for 12, 16, 24, 36, 48, and 96-nm bandwidths, respectively.

Spectral Extraction and Analysis

Four pixels closest to each infested or uninfested identified location were selected and spectral signatures extracted. The 528 pixels were identified as either infested or uninfested. The spectral samples from 224 infested pixels were merged to represent one infested spectrum and 304 uninfested spectral samples were merged to represent one uninfested spectrum. These merged spectra potentially masked spectral variability within each class, but was appropriate for the purpose of the analysis, which intended to distinguish infested from uninfested locations as a two class problem.

Optimal band selection for analyses of reduced numbers of bands, regardless of bandwidth, is important because removal of bands can reduce accuracy (Su et al., 2014). Band selection is achieved by measuring the spectral separability between target signatures to select bands that best differentiate groups (Davis et al., 1978). The distance between spectral responses can be evaluated using various measurements. We used the Jeffries-Matusita method, because it consistently performed better than other measures (Chapter 3). Jeffries-Matusita measures statistical separability using the distance between density functions and contains a negative exponential to create a saturating effect. The

saturating effect creates an exponential decrease as distance values get smaller, so that, when averaged, a few widely separated outlier values in a cluster do not make a disproportionate difference in the distance metric.

Each of the bandwidth datasets was classified using the random forest algorithm. The entire dataset was used for training, and accuracies were assessed using out-of-bag error estimations (Breiman, 1996, 2001; Lawrence, 2004). Comparisons were made based on overall accuracy of the classification. Statistical significance between classifications was based on comparisons of kappa statistics at an alpha of 0.05 (Congalton and Green, 2008). Output maps were also visually compared for correspondence with field observations.

Results

Classifications using all available bands resulted in all cases in overall accuracies above 75% regardless of bandwidth (Table 4.1), with neither a positive or negative trend as bandwidths were increased (Figure 4.4). Results had a range of 1.6% and averaged 77% (Table 4.2). The selection of four narrow bands maintained a similar trend to all bands with accuracies staying above 70%, however the three band combination showed a statistically detectable drop in accuracy from 12 to 18 nm and a 10.5% variation in accuracies. Comparison of the resulting maps from classifications using different bandwidths (Figure 4.5) revealed that the majority of pixels classified as infested were classified the same regardless of bandwidth (seen in green in the Comparison image at the top of Figure 4.5). The west side of the image showed more pixels where only one or two bandwidths classified these areas as infested. The northwest corner and east side of

the field showed relatively more areas that were classified as infested by three or four bandwidths. Agreement among all bandwidths in the east field was 68% and 67% in the west field (Table 4.3). The west field however showed the majority of areas all bandwidths agreed on infestation except in the southern end of the field were one of the five bandwidths classified pixels as infested the majority of the time (Figure 4.7).

Table 4.1. Estimated accuracies for three, four, and all available bands by bandwidth.

	Accuracies		
	3 Bands	4 Bands	All Bands
6 nm	73.3%	71%	77%
12 nm	75.4%	73%	76%
18 nm	65%	76%	78%
24 nm	68.7%	75%	77%
36 nm	71%	75%	77%
48 nm	74.9%	77%	77%
96 nm	77.0%	73%	76%

Table 4.2. The estimated accuracy values for three, four, and all available bands averaged for all band widths. The range of values shows the level of variation in results for each number of bands used.

	3 Bands	4 Bands	All Bands
Average	72.2%	74.3%	77.0%
Range of Values	12.1%	5.8%	1.6%

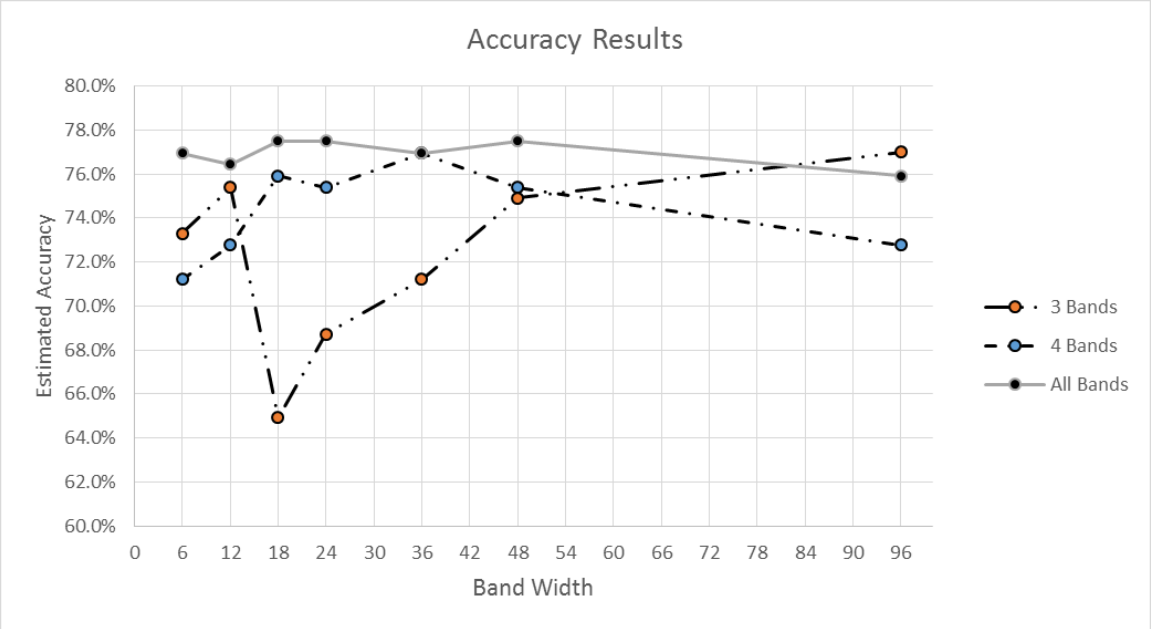

Figure 4.4. Estimated accuracies for the seven bandwidths tested.

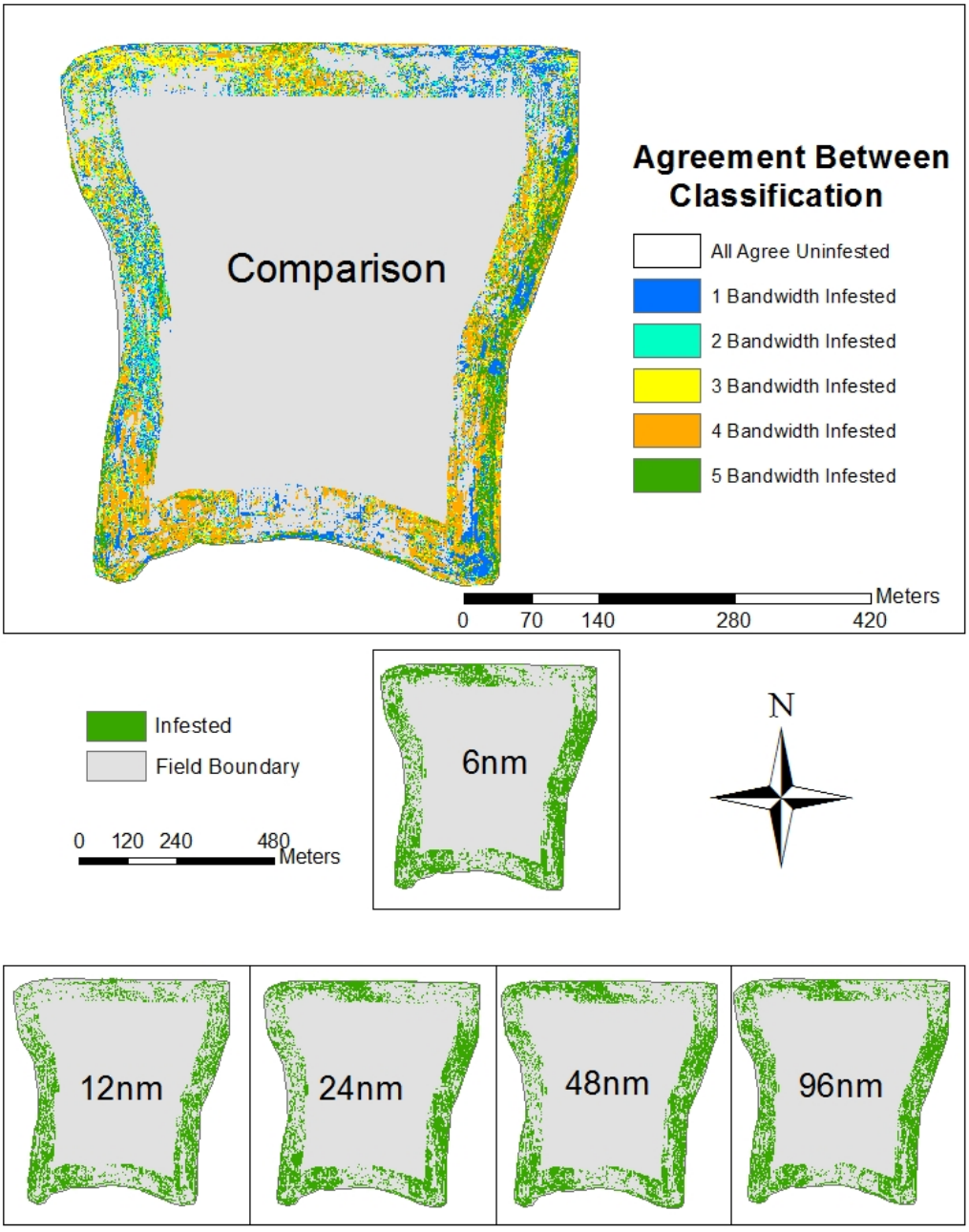

Figure 4.5. Comparison map and weed maps for 6-, 12-, 24-, 48-, and 96-nm bandwidths of the east field. General spatial locations of infestations were consistent across bandwidths, although number of predicted infested pixels noticeably varied.

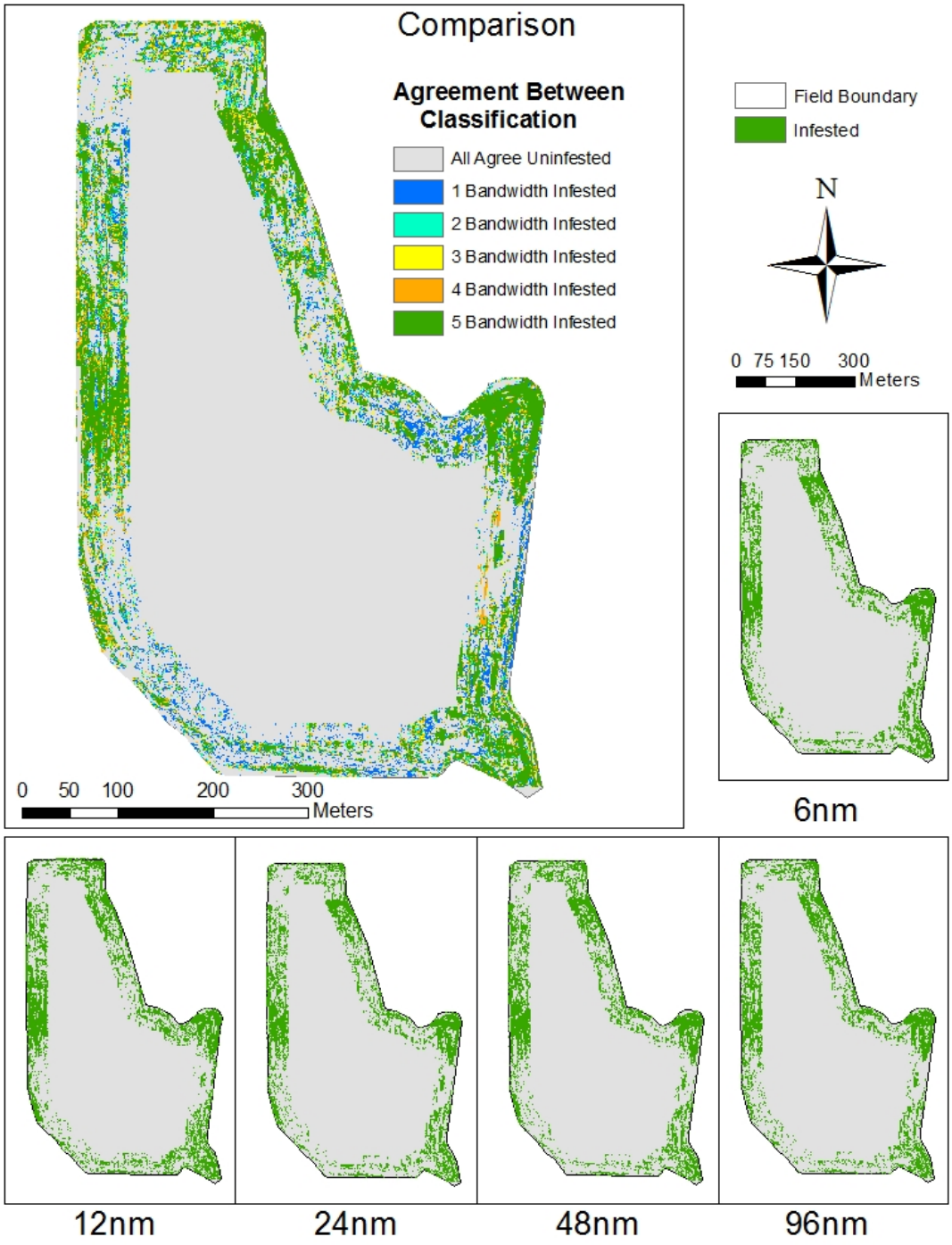

Figure 4.6. Comparison map and weed maps for 6-, 12-, 24-, 48-, and 96-nm bandwidths of the west field. General spatial locations of infestations were consistent across bandwidths, although number of predicted infested pixels noticeably varied.

Table 4.3. This table shows the percent agreement of pixels classified infested using all available 6-, 12-, 24-, 48-, and 96-nm bandwidths.

Percent Agreement of Pixels Classified Infested Using All Bands		
	East Field	West Field
No Bandwidths Classifies Infested	44.6%	60.3%
1 Bandwidths Classifies Infested	9.6%	10.0%
2 Bandwidths Classifies Infested	4.9%	4.1%
3 Bandwidths Classifies Infested	5.0%	3.7%
4 Bandwidths Classifies Infested	12.7%	4.6%
All Bandwidths Classifies Infested	23.1%	17.4%

Reduced Band Results

The results for both three and four band combinations averaged 74% (Table 4.2). Both three and four band results were lower, but with no statistically significant difference, than accuracies using all available bands. The three band accuracies generally resulted in an increase in accuracy with increasing bandwidth (Figure 4.4), however there was a decrease of 10.5% when bands were widened to 24 nm from 12 nm. The four band accuracies also demonstrated an increasing trend in accuracies as bandwidth was widened, except for the final increase to 96 nm from 48 nm. The highest and lowest results, 6 nm and 36 nm respectively for four bands, had a difference of 6%.

The east and west fields showed similar patterns of infestation to all bands. The east maps show the most variation and were examined for differences in classification as infested for different bandwidths. East maps output for reduced bands show dense weed populations around the outside edges of the fields (Figure 4.7).

A comparison of the maps resulting from different bandwidths revealed that the 12-nm and 96-nm bandwidth maps had similar patterns of infested pixels. The south side, particularly at the corners, show pixels only classified by three bands. The west side was dominated by pixels classified by only 4 bands. The northwest corner show areas only classified by all bands. The 6-nm bandwidth map is dominated by locations of pixels classified singly by either three, four, or all bands. The 24-nm bandwidth agreement map shows a majority of pixels only classified by three bands and the 48-nm bandwidth agreement map has pixels classified by either all bands or classified by both three and four bands.

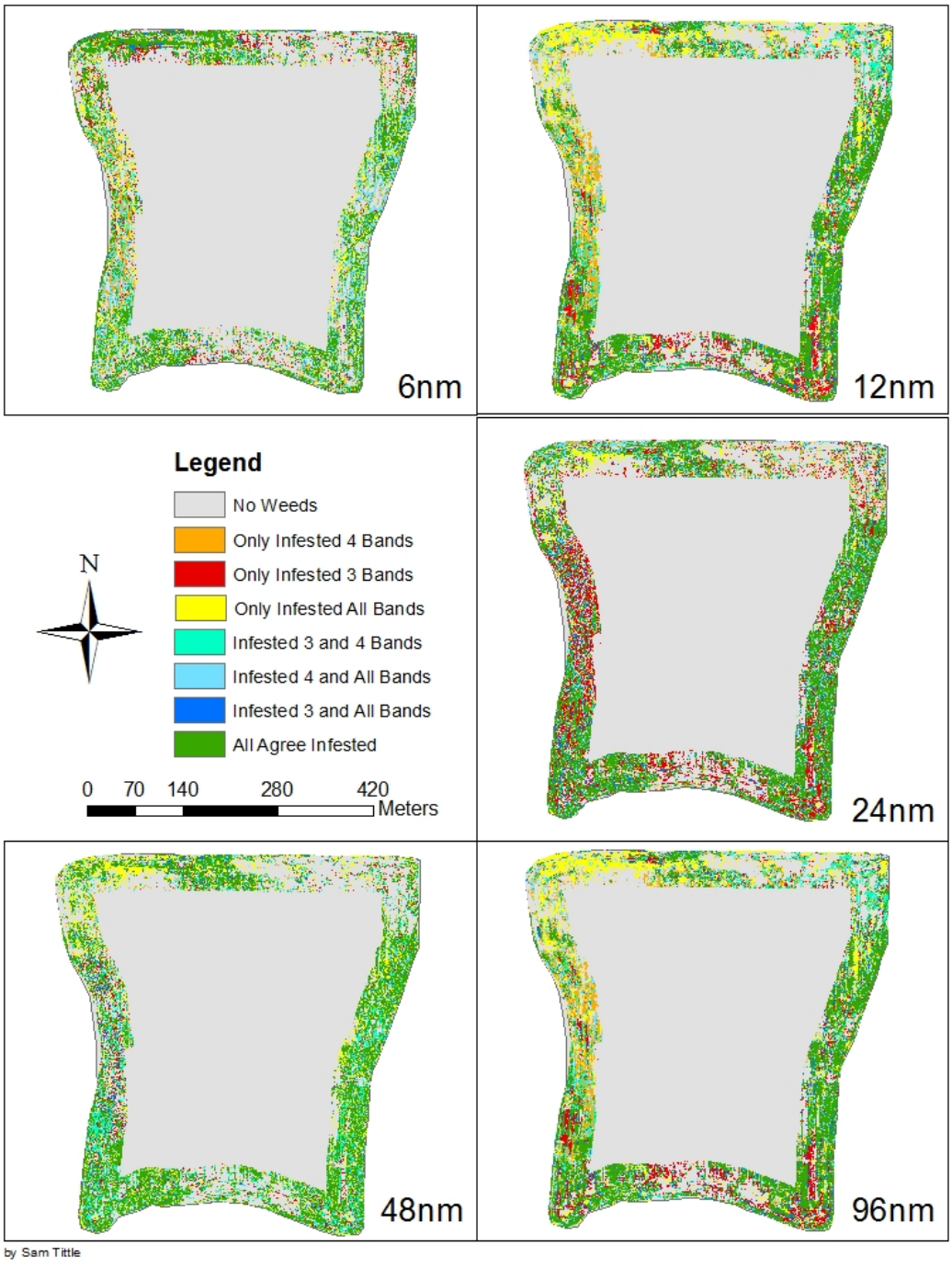

Figure 4.7. Comparison of weed maps output by each bandwidth for agreement between number of bands used; three bands, four bands, or all 80 available bands.

Discussion

Using all available bands from the sensor showed similar results as bands were widened, with no detectable change in accuracy from narrow to wider bands. Bands were artificially widened by averaging with no weight put on certain bands, this could mask high or low absorption bands. There was no detectable advantage in using the narrowest possible bands for this particular application, and potentially a slight disadvantage based on our results. The Jefferies Matusita band selection method showed results at or above 70% for all bandwidths for both three and four band combinations. The accuracies did increase as bands were widened but were not as high as all bands in most cases, showing that even select narrow bands do not have a statistical advantage over similar wider bands.

The lack of a statistically significant differences between three and four bands could be two possible explanations. The first is that enough information is contained in three bands and the addition of a fourth band does not add significant new information. The second is that we lack the number of samples to see the fine variations in accuracy based on number of bands used. The random variation is also not separable from variation present in wide versus narrow bands. The lack of statistical differences mean that the patterns seen might only be a function of random variability. The reduction of random variability would require collection of more sampling and validation field data.

Wide bands were not proven to be as accurate as narrow bands, only that we did not detect a difference. The maps clearly show there was a difference in predicted infested locations, but statistically we were not able to determine which maps were more

accurate, indicating a limitation in training and validation data. The wide bands associated with multispectral were not statistically better than narrower bands found in hyperspectral when wider bands were specifically selected for this dataset. This should be distinguished from current on-tractor sensors, which use pre-selected spectral bands for all applications. We do not know if the reduced bands selected here have broader applicability beyond this study. Wide bands might be as effective as narrow bands in classification of weed infested locations in wheat, but a full range of bands might be necessary to identify bands needed for accurate use. Hyperspectral data, therefore, might be necessary to determine which reduced bands provide optimal classifications and therefore obviate the advantages of being able to use reduced bands. A broader study is needed to determine whether a particular set of reduced bands might have wider applicability.

A broader study would allow the collection of further data to separate confounding variables or processing artifacts demonstrated by the variation in infested pixel destiny as bands were widened. The east field showed much higher variation then the west field, indicating variations in and between fields need to be taken into account. Large sections in both fields were classified by every bandwidth. The classification of an area as heavily infested by a majority of classifications but known to be limited in infestation showed that same areas were difficult to differentiate infestation from wheat.

Variation within classes could be caused by different species of weeds and infestation levels. This was a binary classification to answer the question of producers; infested or not infested, spray or don’t spray. There is, however, merit in looking at the

level of infestation. Areas with only a few plants could lead to increasing weed populations in the future. A continuous classification that is then converted with a threshold level to create a binary spray or don't spray decision could record percent cover of weed species. Weed species differentiation is also a potential source of added information that should be examined.

A brief analysis of the economic benefits of spot spraying technology shows that it holds potential. Compared to spraying an entire field, the bands selected by Jefferies-Matusita identified 27% of pixels were infested. The use of these bands to spray a field would potentially reduce the area sprayed by 73%. Herbicide application cost can vary with tax, permits, equipment, labor, maintenance, and the herbicide. The savings precision weed spraying can provide depends on this variability along with sensor design. Savings in barley have been shown between $8 and $22 per acre depending on the amount of the boom turned on when weeds are detected (e.g. 40m or 100% of boom, 20m, 10m, 5m, 2m, 1m) (Franco et al., 2017). The level of precision adds savings but additional complication and cost of the system. The 124 acres within our field would equal a savings of $1357 with herbicide costing $15/acre and reducing spraying by 73%. A system costing $70,000, an estimate based off the current cost of similar systems like WeedIt not capable of in crop spraying, and no increase in maintenance costs for the new system would take 51 years to recuperate the costs of the system in savings. This would indicated an in-depth study on the viability of systems for individual users is needed as small acreage landowners may not see a reasonable return. The cost of herbicide seems to have the largest effect on the time for system cost to be returned in savings (Figure 4.8)

compared to the changes in system overall cost (Figure 4.9). Even the cost of the most expensive system ($85,000) can be recuperated in three years at herbicide costs of $15/acre managing 2,000 acres. The USDA statistics for Montana show that 2,350,000 acres of winter wheat were planted in 2015 (USDA, 2016). A 73% reduction in herbicide application at $15/acre would be over $25.6 million in savings. These are rough numbers and variation in herbicide application rate, weed infestation level, maintenance costs, and the farmer's individual needs can change the savings seen from a system.

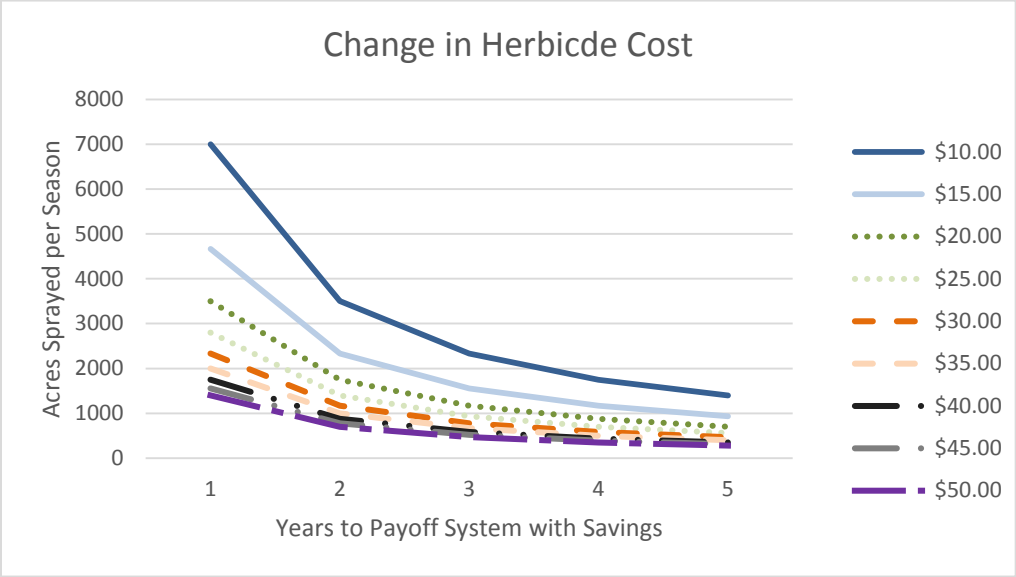

Figure 4.8 Analysis of how increasing application costs in $5 steps effects the years it takes to recuperate cost of the system. The x-axis represents the number of years necessary to pay of the spraying system with the expected savings generated spraying the different levels of acreage on the y-axis. Change in cost of herbicide application is represent by induvial lines.

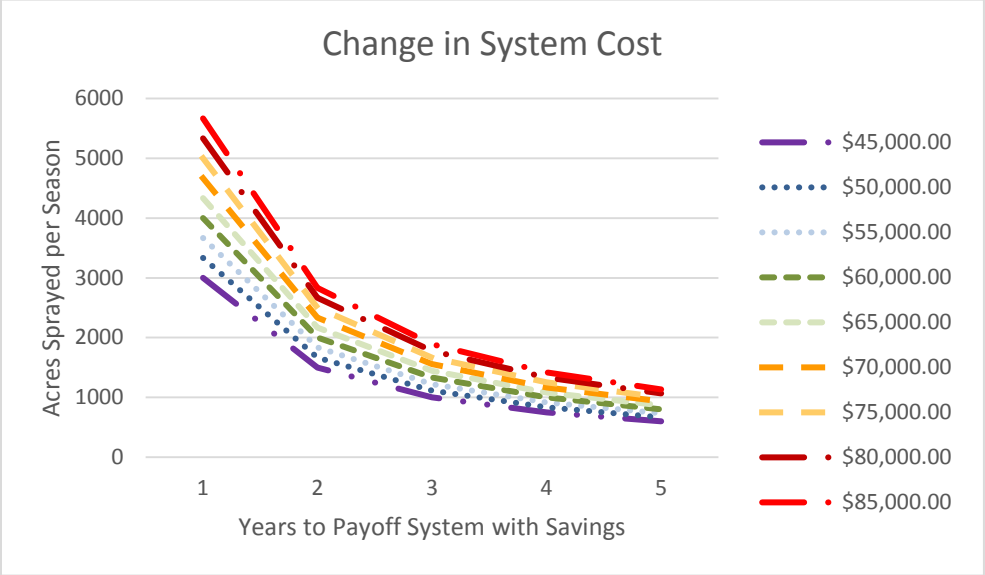

Figure 4.9 Analysis of how system overall cost effects the years it takes to recuperate cost of the system. The x-axis represents the number of years necessary to pay of the spraying system with the expected savings generated spraying the different levels of acreage on the y-axis. Change in system cost is represent by induvial lines.

A system were only select areas are sprayed created a risk that infestations will be missed and cause increasing populations, thereby increasing cost of management in the future and negating any savings. Locations in our research could only be classified as infested or uninfested. Four possible outcomes exist for a pixel; infested classified as infested, infested classified as uninfested, uninfested classified as uninfested, and uninfested classified as infested, of the two possible errors the infested areas mistaken for uninfested are of greater concern. Areas mistaken as infested that in reality contain no weed species are areas that are sprayed unnecessarily and do not risk the increase of weed populations. Removal of these errors can further savings of spot spraying but reduced herbicide application is achieved with these errors present compared to current uniform application methods. The number of times infested locations were misclassified as

uninfested in our results (Table 4.4) was similar or lower than the error of uninfested locations classified as infested.

Table 4.4 Error matrixes for 96 and 6 nm three bands with the calculated omission error for both classes.

96nm Bands	Estimated Uninfested	Estimated Infested		6nm Bands	Estimated Uninfested	Estimated Infested	
Uninfested	77	27	104	Uninfested	76	28	104
Infested	17	70	87	Infested	23	64	87
	94	97	191		99	92	191
Uninfested Error of Omission			26%	Uninfested Error of Omission			27%
Infested Error of Omission			20%	Infested Error of Omission			26%

Conclusion

Narrowing bands, even to 6 nm, as compared to 96 nm, did not improve weed classification accuracies for our study site, either for hyperspectral, continuous bands or for multispectral, discrete bands. There was limited evidence that reduced bands might lead to slightly reduced accuracies, but the evidence was not statistically significant, indicating that reduced bands, if properly selected, might be able to maintain or come close to accuracies achieved with full hyperspectral data. It is unknown, however, whether such reduced bands can be selected *a priori* or whether such reduced band selection is site and/or scene specific. These results do indicate that perceived advantages of hyperspectral data for weed mapping should be subjected to rigorous analysis and that the added cost and complexity of using hyperspectral data needs to be justified by comparison to multispectral options.

References Cited

Alchanatis, V., Ridel, L., Hetzroni, A., and Yaroslavsky, L., 2005, Weed detection in multi-spectral images of cotton fields: Computers and Electronics in Agriculture, v. 47, p. 243–260, doi: 10.1016/j.compag.2004.11.019.

Asadzadeh, S., and de Souza Filho, C.R., 2017, Spectral remote sensing for onshore seepage characterization: A critical overview: Earth-Science Reviews, v. 168, p. 48–72, doi: 10.1016/j.earscirev.2017.03.004.

Breiman, L., 1996, Out-of-bag estimation: Technical report, Statistics Department, University of California Berkeley, Berkeley CA 94708, 1996b. 33, 34, http://www.stat.berkeley.edu/~breiman/OOBestimation.pdf (accessed October 2017).

Breiman, L., 2001, Random Forests: Machine Learning, v. 45, p. 5–32, doi: 10.1023/A:1010933404324.

Chen, J., Gu, S., Shen, M., Tang, Y., and Matsushita, B., 2009, Estimating aboveground biomass of grassland having a high canopy cover: an exploratory analysis of in situ hyperspectral data: International Journal of Remote Sensing, v. 30, p. 6497–6517, doi: 10.1080/01431160902882496.

Congalton, R.G., and Green, K., 2008, Assessing the Accuracy of Remotely Sensed Data: Principles and Practices, Second Edition: CRC Press, 210 p.

Davies, G.E., and Calvin, W.M., 2017, Mapping acidic mine waste with seasonal airborne hyperspectral imagery at varying spatial scales: Environmental Earth Sciences, v. 76, p. 432, doi: 10.1007/s12665-017-6763-x.

Davis, S.M., Landgrebe, D.A., Phillips, T.L., Swain, P.H., Hoffer, R.M., Lindenlaub, J.C., and Silva, L.F., 1978, Remote sensing: The quantitative approach: McGraw-Hill International Book Company, 396 p., http://adsabs.harvard.edu/abs/1978mhi..book.....D (accessed August 2017).

Deng, W., Huang, Y., Zhao, C., Chen, L., and Wang, X., 2016, Bayesian discriminant analysis of plant leaf hyperspectral reflectance for identification of weeds from cabbages: African Journal of Agricultural Research, v. 11, p. 551–562, doi: 10.5897/AJAR2015.10395.

Du, Q., and Yang, H., 2008, Similarity-Based Unsupervised Band Selection for Hyperspectral Image Analysis: IEEE Geoscience and Remote Sensing Letters, v. 5, p. 564–568, doi: 10.1109/LGRS.2008.2000619.

Feyaerts, F., and van Gool, L., 2001, Multi-spectral vision system for weed detection: Pattern Recognition Letters, v. 22, p. 667–674, doi: 10.1016/S0167-8655(01)00006-X.

Franco, C., Pedersen, S.M., Papaharalampos, H., and Ørum, J.E., 2017, The value of precision for image-based decision support in weed management: Precision Agriculture, v. 18, p. 366–382, doi: 10.1007/s11119-017-9520-y.

Goel, P.K., Prasher, S.O., Patel, R.M., Smith, D.L., and DiTommaso, A., 2002, Use of airborne multi–spectral imagery for weed detection in field crops: Transactions of the ASAE, v. 45, p. 443.

Goetz, A.F.H., Vane, G., Solomon, J.E., and Rock, B.N., 1985, Imaging Spectrometry for Earth Remote Sensing: Science, v. 228, p. 1147–1153, doi: 10.1126/science.228.4704.1147.

Holland Scientific, 2017, CROP CIRCLE ACS470: Holland Scientific, http://hollandscientific.com/portfolio/crop-circle-acs-470/ (accessed July 2017).

Huete, A.R., Jackson, R.D., and Post, D.F., 1985, Spectral response of a plant canopy with different soil backgrounds: Remote Sensing of Environment, v. 17, p. 37–53.

Knipling, E.B., 1970, Physical and physiological basis for the reflectance of visible and near-infrared radiation from vegetation: Remote Sensing of Environment, v. 1, p. 155–159, doi: 10.1016/S0034-4257(70)80021-9.

Kruse, F.A., Boardman, J.W., and Huntington, J.F., 2003, Comparison of airborne hyperspectral data and EO-1 Hyperion for mineral mapping: IEEE Transactions on Geoscience and Remote Sensing, v. 41, p. 1388–1400, doi: 10.1109/TGRS.2003.812908.

Lass, L.W., Thill, D.C., Shafii, B., and Prather, T.S., 2002, Detecting Spotted Knapweed (Centaurea maculosa) with Hyperspectral Remote Sensing Technology: Weed Technology, v. 16, p. 426–432, doi: 10.1614/0890-037X(2002)016[0426:DSKCMW]2.0.CO;2.

Lawrence, R., 2004, Classification of remotely sensed imagery using stochastic gradient boosting as a refinement of classification tree analysis: Remote Sensing of Environment, v. 90, p. 331–336, doi: 10.1016/j.rse.2004.01.007.

Lawrence, R.L., Wood, S.D., and Sheley, R.L., 2006, Mapping invasive plants using hyperspectral imagery and Breiman Cutler classifications (randomForest): Remote Sensing of Environment, v. 100, p. 356–362, doi: 10.1016/j.rse.2005.10.014.

Lillesand, T., Kiefer, R.W., and Chipman, J., 2014, Remote Sensing and Image Interpretation: John Wiley & Sons, 768 p.

Lord, D., Desjardins, R.L., and Dubé, P.A., 1988, Sun-Angle Effects on the Red and near Infrared Reflectances of Five Different Crop Canopies: Canadian Journal of Remote Sensing, v. 14, p. 46–55, doi: 10.1080/07038992.1988.10855118.

Marchant, J.A., and Onyango, C.M., 2002, Spectral invariance under daylight illumination changes: Journal of the Optical Society of AmericaA, v. 19, p. 840–848.

NTech Industies, Inc., 2017, Data Sheet Model 650 Sensor:, http://www.agrioptics.co.nz/wp-content/uploads/2013/03/DataSheetModel650Sensor.pdf (accessed July 2017).

Okamoto, H., Murata, T., Kataoka, T., and Hata, S.-I., 2007, Plant classification for weed detection using hyperspectral imaging with wavelet analysis: Weed Biology and Management, v. 7, p. 31–37, doi: 10.1111/j.1445-6664.2006.00234.x.

Pantazi, X.-E., Moshou, D., and Bravo, C., 2016, Active learning system for weed species recognition based on hyperspectral sensing: Biosystems Engineering, v. 146, p. 193–202, doi: 10.1016/j.biosystemseng.2016.01.014.

Pantazi, X.E., Tamouridou, A.A., Alexandridis, T.K., Lagopodi, A.L., Kashefi, J., and Moshou, D., 2017, Evaluation of hierarchical self-organising maps for weed mapping using UAS multispectral imagery: Computers and Electronics in Agriculture, v. 139, p. 224–230, doi: 10.1016/j.compag.2017.05.026.

Resmini, R.G., Kappus, M.E., Aldrich, W.S., Harsanyi, J.C., and Anderson, M., 1997, Mineral mapping with HYperspectral Digital Imagery Collection Experiment (HYDICE) sensor data at Cuprite, Nevada, U.S.A.: International Journal of Remote Sensing, v. 18, p. 1553–1570, doi: 10.1080/014311697218278.

Richter, R., Reu, B., Wirth, C., Doktor, D., and Vohland, M., 2016, The use of airborne hyperspectral data for tree species classification in a species-rich Central European forest area: International Journal of Applied Earth Observation and Geoinformation, v. 52, p. 464–474, doi: 10.1016/j.jag.2016.07.018.

Scafutto, R.D.M., de Souza Filho, C.R., and de Oliveira, W.J., 2017, Hyperspectral remote sensing detection of petroleum hydrocarbons in mixtures with mineral substrates: Implications for onshore exploration and monitoring: ISPRS Journal of Photogrammetry and Remote Sensing, v. 128, p. 146–157, doi: 10.1016/j.isprsjprs.2017.03.009.

Scafutto, R.D.M., Souza Filho, C.R. de, and Rivard, B., 2016, Characterization of mineral substrates impregnated with crude oils using proximal infrared

hyperspectral imaging: Remote Sensing of Environment, v. 179, p. 116–130, doi: 10.1016/j.rse.2016.03.033.

Seibert, J.A., Boone, J.M., and Lindfors, K.K., 1998, Flat-field correction technique for digital detectors, *in* International Society for Optics and Photonics, v. 3336, p. 348–355, doi: 10.1117/12.317034.

SenseFly Ltd., 2017, SenseFly eBee:, https://www.sensefly.com/drones/accessories.html (accessed October 2017).

Sorenson, P.T., Small, C., Tappert, M.C., Quideau, S.A., Drozdowski, B., Underwood, A., and Janz, A., 2017, Monitoring organic carbon, total nitrogen, and pH for reclaimed soils using field reflectance spectroscopy: Canadian Journal of Soil Science, v. 97, p. 241–248, doi: 10.1139/cjss-2016-0116.

Su, H., Du, Q., Chen, G., and Du, P., 2014, Optimized Hyperspectral Band Selection Using Particle Swarm Optimization: IEEE Journal of Selected Topics in Applied Earth Observations and Remote Sensing, v. 7, p. 2659–2670, doi: 10.1109/JSTARS.2014.2312539.

Swayze, G.A., 1997, The hydrothermal and structural history of the Cuprite mining district, southwestern Nevada: An integrated geological and geophysical approach [Ph.D.]: University of Colorado at Boulder, 399 p., https://search.proquest.com/docview/304359978/abstract/54274CE5AADD4B21PQ/1 (accessed September 2017).

Topcon Positioning Systems, Inc., 2017, Cropspec Brochure:, https://www.topconpositioning.com/sites/default/files/product_files/cropspec_broch_7010-0957_revf_sm_2.pdf (accessed July 2017).

U.S. Climate Data, 2017, Climate Bozeman: U.S. Climate Data, http://www.usclimatedata.com/climate/bozeman/montana/united-states/usmt0040 (accessed August 2017).

USDA, 2016, Montana Annual Bulletin 2016: USDA 1095-7278 LIII, https://www.nass.usda.gov/Statistics_by_State/Montana/Publications/Annual_Statistical_Bulletin/2016/Montana_Annual_Bulletin_2016.pdf (accessed November 2017).

Wang, C., Zhou, B., and Palm, H.L., 2008, Detecting Invasive Sericea Lespedeza (Lespedeza cuneata) in Mid-Missouri Pastureland Using Hyperspectral Imagery: Environmental Management, v. 41, p. 853–862, doi: 10.1007/s00267-008-9092-8.

Wendel, A., and Underwood, J., 2016, Self-supervised weed detection in vegetable crops using ground based hyperspectral imaging, *in* 2016 IEEE International

Conference on Robotics and Automation, p. 5128–5135, doi: 10.1109/ICRA.2016.7487717.

CHAPTER FIVE

CONCLUSION

Infestation Classification of Weeds Using Narrow Bands

This research addressed two questions with the potential to improve on-tractor sensing of weeds for mapping and precision herbicide application. First, could a few select narrow bands match the success in detecting reported in previous research from full hyperspectral sensors? Three and four band selections were used to match the number of bands commonly found in commercial multispectral sensors, which could potentially be modified from multispectral broad-band sensors to multispectral narrow band sensors. Related to this was the second question, whether narrow-band sensors were more successful in detecting weeds than broad-band sensors.

The results demonstrated reasonable abilities at weed detection for reduced bands and broader bands comparable to the full hyperspectral dataset. None of the best results from reducing the bands or broadening the bands, however, resulted in statistically significantly different results, meaning that we were unable to detect differences based on the data available. Resulting weed prediction maps, however, demonstrated strikingly different predictions. These seemingly contradictory results indicate that this study lacked the statistical power to detect very real differences among these methods that were present. We do know that there were substantial differences in the predictive abilities of the various band permutations, but we were unable to determine which were actually closer to the truth.

It is unknown whether bands and bandwidths can be selected *a priori* or whether band selection is specific to individual fields. A combination of farmers' herbicide spraying schedules, sensor failure during a flight, and weather conditions resulted in being able to collect data from only two of eight fields that were identified prior to the field campaign. This made it impossible to evaluate the robustness of bands selected based on one field or other limited conditions. The ability exists to revolutionize the multispectral sensors used for on-tractor spot spraying if results from this research hold true after rigorous analysis. Results indicate the added cost and complexity of using hyperspectral data needs to be justified by comparison to multispectral options. Potentially high classification accuracies results seen in historical studies of weed mapping with hyperspectral data are possible with limited spectral bands. The next step is to test the robustness of these results across other fields and conditions. The research explained is only a start and definitive band combinations and selection methods cannot be given, however our findings can direct further research. The results, however, also indicate the conclusions drawn in previous studies with respect to the value of hyperspectral imaging for weed detection need to be tempered, because previous studies fail to evaluate whether similar results could have been achieved with multispectral data.

Future Research

This research supports a progression of methods that should be followed for wider application. The nature of our data caused uncertainty in results and a limit to inferences that could be drawn. Collection of more data to account for variation in spectra found in

wheat, or other crops, is needed. Uncertainty in results due to the nature of variation in vegetation is possible, but limiting uncertainty is the next step in this research. Control of uncertainty found in real world fields is challenging, so creation of an artificial dataset is needed. This would allow a comparison of band selection methods and classifications algorithms in a controlled environment as a first step to fully functional in–crop, on-tractor weed sensors.

Justification and Objectives for Future Research

The limitations of the study reported in this thesis are indicated by two results. First, we were unable to determine whether certain band permutations were better than others because we were unable to find statistically significant differences. Second, predicted weed maps demonstrated strong differences, even where there were no statistically different findings, leaving open the question of which band permutations were most accurate, as clearly some were more accurate than others. Both of these issues can be resolved by an adequately sized reference dataset. An optimal dataset would consist of an adequate sample (based on a statistical power test) covering both within field variability for sampled fields and among field variability within a defined region for which a sensor might be developed. The short time, however, between plant emergence and herbicide spraying, combined with typically unsettled spring weather with high cloud presence, made the collection of such a reference set impractical, and would likely do so in the future. An alternative, therefore, is to develop a set of simulated fields based on known plant spectra and variance, which can be used for a wide range of analysis and for which true values would be known.

Building the Dataset

Pixels values for the test dataset would be based on field data of crop and weed species collect with a spectrometer, such as the ASD Fieldspec Pro, that collects data in a large portion of the EM spectrum. The FieldSpec provides data from the ultraviolet region into the SWIR, 350 nm to 2500 nm, in 3-nm bands for the VNIR (350 - 1000nm) and 10 nm in the SWIR (1001 – 2500nm). The sensor unit is carried in a backpack and can be used to collect data on single plants to medium sized weed patches, depending on the height the sensor optic (a fiber optic cable) is held above the object, giving flexibility to collect specific and high spatial resolution data at the cost of broad coverage of the field. Research is focused on improving on-tractor sensors and atmospheric conditions of data collection should reflect these conditions, which ASD ground data does. The data collected with the FieldSpec from a stationary positon limits the collection of incorrect spectral data and use of a Spectralon calibration target panel allows absolute reflectance to be recorded. This allows the dataset to be flexible to data needs with repeat data collection (time-series) and the data collected on multiple days reasonably compared. The addition of data is possible to fill gaps, cover unforeseen variables, or replace bad data without starting over with all new data. Observations should be collected across multiple fields based on a stratified random sampling design (stratified by fields), with a sample size determined by a statistical power test.

Spectral data for sub-classes is paramount to ascertain what is causing variation in infestation classifications. Different spectra for healthy plants, nitrogen variation, percent cover, soil, weed species, and other sources of variance would allow controlling for

potential confounding variables, allowing evaluation of classification results on more than a binary bases. Simulation of percent cover for the test dataset can be created as well, however collection of the percent cover of true in-field spectra is need to verify the created spectra.

Data once collected would be used to create an individual spectral curve for each sample. Multiple curves for each target (e.g., wheat) would result in a family of curves that could be used to produce a theoretical distribution of spectral curves for each target. A random sample could be drawn from the distribution of curves based on the probability function created by the variation in the spectra for the target. The random sampling of this probability function, when applied to a map, would simulate the distribution of spectral responses observed in the field.

The spatial distribution of areas of weed infestation can be set based on first-hand knowledge, randomly placed, or modeled. Creating a weed map with set spatial distribution should be based on answering a specific field condition problem or recreating a previous field study. Assignment of pixels should start simple as a proof of concept before complexity is added to data generation. Ideally modeling would allow the creation of complex weed maps, limit researcher bias, and mimic real world conditions (López and Stokes, 2016; Magarey et al., 2017; Pelikan et al., 2015; Somerville et al., 2017). An appropriately chosen model could control for the spatial distribution of weed presence, as well as density per pixel.

The resulting simulated weed maps would represent a realistic spatial and spectral distribution of weeds, but with the value of all pixels known. This simulated dataset

would enable a repeat of the analyses contained in this thesis, but with notable advantages. Statistical significance of differences would not be an issue, because the entire population would be known (statistical significance attempts to quantify the relation to an unknown population). Spatial distributions could be expressly compared and quantified. Replication for additional locations or crop/weed systems would require separate parameterization.

Research Questions

The overarching concept is that this dataset can provide analysis and comparison before band combinations and classification algorithms are used in the field. New algorithms can be compared under the same conditions as previous algorithms and conditions can be altered to simulate and test field data requirements before data collection starts.

The research questions that should be addressed first to form a base line database of band combinations and results are; best overall band combination, the effect of band width, multiple weed species effect on select bands, nitrogen variation effect on select bands, algorithm sensitivity for infestation levels, current viable sensors, applicability of spectral libraries, and method's sensitivity to training data.

Band combinations might be site specific, but this study can act as a guide. We expect that Jefferies-Matusita and transform divergence methods will outperform Euclidean and divergence based on our band selection results. Bands selected using Jefferies-Matusita and transform divergence showed no statistically significant difference from the use of all bands in all but two cases. Sample sizes, however, were small and

atmospheric corrections might have introduced bias. The usefulness of a band combination should be determined by beginning with the simplest possible array of pixels. This can then act as a baseline to which classifications with added complexity and variation can be compared. Various methods might select separate bands, but these bands might exist in the same region of the spectrum, helping to focus research efforts.

The next question that should be addressed is the effect on accuracy of bandwidth. Research performed here used bandwidths of 6, 12, 18, 24, 36, 48, and 96 nm and no detectable difference was found, except for one band combination, for these band combinations compared to the use of the full hyperspectral dataset. Increasing trends with increased bandwidth was seen, but the conclusion that this is true outside of the study sample cannot be made. Results could indicate a paradigm shift in remote sensing and the ability to build sensors with little compromise in accuracy compared to hyperspectral sensors if a random sample were taken from a larger area, and the same conclusions reached. Permutations of bands should be automated in R or a similar program. The output bands should include all available bandwidths, with the ASD this would be divisions of 3-nm bands in the VNIR (*e.g.* 3-,6-,9-,12-,15-,…, 96-nm bands) and 10-nm bands in the SWIR (*e.g.* 10-, 20-, 30-,…,100-nm bands).

The weed species in this research were Canada thistle (*Cirsium arvense*), prickly lettuce (*Lactuca serriola*), and bedstraw (*Galium aparine*), however no attempt at separation of spectral signatures of these species or there effect on positive classification was attempted. Species specific spectral data should be collected, including grass species. Grass species could not be collected due to the limited amount, patch size, and

geolocation errors in our research; these issues should not be a limiting factor in the research outlined here, allowing for their inclusion. The collection of ASD data with a reflectance target allows multiple agricultural fields and dates of data collection to be used. Presence of only a few species in a field should not limit the spectra collected or the comparison between species.

The question of sensitivity to infestation level is important to end users, since areas of low infestation could be missed and spread in following seasons. Band combination and classification algorithm sensitivity to infestation level can be tested by including incremented infestation levels. Collection of the full range of infestation levels is generally not practical, but pure crop and weed spectra can be combined to simulate mixed signals. The class accuracy of these levels will indicate the limits of an algorithm or band combination. The levels can be arbitrarily selected or focused by research into the economic threshold of weed spraying. The economic level would be the point at which an increase in the ability to classify lower density weeds is marked with an unacceptable increase in cost of the sensors required to make the classification. Graphically this can be shown with classification accuracy for each infestation level class.

The design, testing, and implementation of new sensors creates a further burden on the timely integration of in–crop, on-tractor spot spraying sensors to the market. This is not the case if current sensors can be repurposed or retrofitted to meet the needs of these on-tractor sensors. To test this, a list of currently available sensors should be created. Spectral bands available for each of these sensors can be generated by combining

associated ASD bands for each sensor band. The sensor specific datasets can be used to collect training data for band selection and classification. Results can be compared for each sensor, looking for sensors that provide the highest overall accuracy, best accuracy to cost ratio, least accurate sensor that meets industry requirements, and least expensive sensors that meets industry requirements.

Beyond simulated field data, if spectral libraries could be used this would increase the application and acquisition of data. Library data for crops and weeds from areas not locally available can be added. Spectra from libraries can add variability to the family of curves to create training datasets. Increase of variability may decrease the overall accuracy of bands, however if this variability accounts for an entire region or country of interest, band combinations might be found that do not need to be changed for application to a wider area.

Time and money are at a premium in research and collecting training data in the field was one of the most time-consuming aspects of our research. Understanding the effect that training data has on the classification of weed infestation is important to using this time wisely. Different levels of training data are possible to “collect” with a simulated dataset where every pixel value is known. Variation of field conditions and the extent to which training data needs to be increased to account for it can be analyzed for effects on accuracy. Training data using the same spectral variability can be collected for multiple training sample levels and graphed to see if a trend in accuracies exists.

There are many questions of spectral variation caused by field conditions and the bands necessary to address changes in field conditions. The creation of simulated

infestation in crops can be used to address questions related to spectral variability, however, manual analysis will limit the amount of processing and analysis that can be made. The application of a Monte Carlo simulation to automate the creation of datasets, collection of training samples, band selection, and classification can be performed (Fehske et al., 2005; Rubinstein and Kroese, 2016). A high number of iterations can allow graphing of the distribution of accuracy for changing field conditions and provide probability functions for band combinations and classification techniques. Output of automated results can save both time and money that can be allocated to further a research project. The application of this research has the potential to save farmers thousands of dollars and as a country millions of dollars while reducing potentially damaging ecological substances leaving farm’s fields.

References Cited

Fehske, A., Gaeddert, J., Reed, J.H., 2005. A new approach to signal classification using spectral correlation and neural networks, in: First IEEE International Symposium on New Frontiers in Dynamic Spectrum Access Networks, 2005. DySPAN 2005. Presented at the First IEEE International Symposium on New Frontiers in Dynamic Spectrum Access Networks, 2005. DySPAN 2005., pp. 144–150. doi:10.1109/DYSPAN.2005.1542629

López, S., Stokes, D.L., 2016. Modeling the Invasion of Holly (Ilex aquifolium): Spatial Relationships and Spread Trajectories. The Professional Geographer 68, 399–413. doi:10.1080/00330124.2015.1102029

Magarey, R., Newton, L., Hong, S.C., Takeuchi, Y., Christie, D., Jarnevich, C.S., Kohl, L., Damus, M., Higgins, S.I., Millar, L., Castro, K., West, A., Hastings, J., Cook, G., Kartesz, J., Koop, A.L., 2017. Comparison of four modeling tools for the prediction of potential distribution for non-indigenous weeds in the United States. Biol Invasions 1–16. doi:10.1007/s10530-017-1567-1

Pelikan, S., Heywood, S.N., Rogstad, S.H., 2015. Weed Suppression Success Can Depend on Removal Pattern and Gene Dispersal Distance: Modeling Callery Pear. Weed Science 63, 703–709. doi:10.1614/WS-D-14-00100.1

Rubinstein, R.Y., Kroese, D.P., 2016. Simulation and the Monte Carlo Method. John Wiley & Sons.

Somerville, G.J., Powles, S.B., Walsh, M.J., Renton, M., 2017. How do spatial heterogeneity and dispersal in weed population models affect predictions of herbicide resistance evolution? Ecological Modelling 362, 37–53. doi:10.1016/j.ecolmodel.2017.08.002

REFERENCES CITED

Alchanatis, V., Ridel, L., Hetzroni, A., and Yaroslavsky, L., 2005, Weed detection in multi-spectral images of cotton fields: Computers and Electronics in Agriculture, v. 47, p. 243–260, doi: 10.1016/j.compag.2004.11.019.

Andújar, D., Fernández-Quintanilla, C., and Dorado, J., 2015, Matching the Best Viewing Angle in Depth Cameras for Biomass Estimation Based on Poplar Seedling Geometry: Sensors, v. 15, p. 12999–13011, doi: 10.3390/s150612999.

Asadzadeh, S., and de Souza Filho, C.R., 2017, Spectral remote sensing for onshore seepage characterization: A critical overview: Earth-Science Reviews, v. 168, p. 48–72, doi: 10.1016/j.earscirev.2017.03.004.

Aspinall, R.J., Marcus, W.A., and Boardman, J.W., 2002, Considerations in collecting, processing, and analysing high spatial resolution hyperspectral data for environmental investigations: Journal of Geographical Systems, v. 4, p. 15–29, doi: 10.1007/s101090100071.

Bandos, T.V., Bruzzone, L., and Camps-Valls, G., 2009, Classification of Hyperspectral Images With Regularized Linear Discriminant Analysis: IEEE Transactions on Geoscience and Remote Sensing, v. 47, p. 862–873, doi: 10.1109/TGRS.2008.2005729.

Barrero, O., Rojas, D., Gonzalez, C., and Perdomo, S., 2016, Weed detection in rice fields using aerial images and neural networks, *in* 2016 XXI Symposium on Signal Processing, Images and Artificial Vision (STSIVA), p. 1–4, doi: 10.1109/STSIVA.2016.7743317.

Bauer, M.E., 1985, Spectral inputs to crop identification and condition assessment: Proceedings of the IEEE, v. 73, p. 1071–1085, doi: 10.1109/PROC.1985.13238.

Berberoglu, S., and Akin, A., 2009, Assessing different remote sensing techniques to detect land use/cover changes in the eastern Mediterranean: International Journal of Applied Earth Observation and Geoinformation, v. 11, p. 46–53, doi: 10.1016/j.jag.2008.06.002.

Berni, J.A.J., Zarco-Tejada, P.J., Suarez, L., and Fereres, E., 2009, Thermal and Narrowband Multispectral Remote Sensing for Vegetation Monitoring From an Unmanned Aerial Vehicle: IEEE Transactions on Geoscience and Remote Sensing, v. 47, p. 722–738, doi: 10.1109/TGRS.2008.2010457.

Bongiovanni, R., and Lowenberg-Deboer, J., 2004, Precision Agriculture and Sustainability: Precision Agriculture, v. 5, p. 359–387, doi: 10.1023/B:PRAG.0000040806.39604.aa.

Breiman, L., 1996, Out-of-bag estimation: Technical report, Statistics Department, University of California Berkeley, Berkeley CA 94708, 1996b. 33, 34, http://www.stat.berkeley.edu/~breiman/OOBestimation.pdf (accessed October 2017).

Breiman, L., 2001, Random Forests: Machine Learning, v. 45, p. 5–32, doi: 10.1023/A:1010933404324.

Brown, R.B., and Noble, S.D., 2005, Site-specific weed management: sensing requirements— what do we need to see? Weed Science, v. 53, p. 252–258, doi: 10.1614/WS-04-068R1.

Brown, R.B., and Steckler, J.-P.G.A., 1993, Weed Patch Identification in No-Till Corn Using Digital Imagery: Canadian Journal of Remote Sensing, v. 19, p. 088–091, doi: 10.1080/07038992.1993.10855155.

Campbell, J.B., and Wynne, R.H., 2011, Introduction to Remote Sensing, Fifth Edition: New York, The Guilford Press, 667 p.

Casbeer, D.W., Beard, R.W., McLain, T.W., Li, S.-M., and Mehra, R.K., 2005, Forest fire monitoring with multiple small UAVs, *in* American Control Conference, 2005. Proceedings of the 2005, p. 3530–3535 vol. 5, doi: 10.1109/ACC.2005.1470520.

Chan, J.C.-W., and Paelinckx, D., 2008, Evaluation of Random Forest and Adaboost tree-based ensemble classification and spectral band selection for ecotope mapping using airborne hyperspectral imagery: Remote Sensing of Environment, v. 112, p. 2999–3011, doi: 10.1016/j.rse.2008.02.011.

Chang, C.-I., and Wang, S., 2006, Constrained band selection for hyperspectral imagery: IEEE Transactions on Geoscience and Remote Sensing, v. 44, p. 1575–1585, doi: 10.1109/TGRS.2006.864389.

Chappelle, E.W., Kim, M.S., and McMurtrey, J.E., 1992, Ratio analysis of reflectance spectra (RARS): An algorithm for the remote estimation of the concentrations of chlorophyll A, chlorophyll B, and carotenoids in soybean leaves: Remote Sensing of Environment, v. 39, p. 239–247, doi: 10.1016/0034-4257(92)90089-3.

Chen, J., Gu, S., Shen, M., Tang, Y., and Matsushita, B., 2009, Estimating aboveground biomass of grassland having a high canopy cover: an exploratory analysis of in situ hyperspectral data: International Journal of Remote Sensing, v. 30, p. 6497–6517, doi: 10.1080/01431160902882496.

Colomina, I., and Molina, P., 2014, Unmanned aerial systems for photogrammetry and remote sensing: A review: ISPRS Journal of Photogrammetry and Remote Sensing, v. 92, p. 79–97, doi: 10.1016/j.isprsjprs.2014.02.013.

Colwell, J.E., 1974, Vegetation canopy reflectance: Remote Sensing of Environment, v. 3, p. 175–183, doi: 10.1016/0034-4257(74)90003-0.

Congalton, R.G., and Green, K., 2008, Assessing the Accuracy of Remotely Sensed Data: Principles and Practices, Second Edition: CRC Press, 210 p.

Coppin, P.R., and Bauer, M.E., 1994, Processing of multitemporal Landsat TM imagery to optimize extraction of forest cover change features: IEEE Transactions on Geoscience and Remote Sensing, v. 32, p. 918–927, doi: 10.1109/36.298020.

Czanner, G., Sarma, S.V., Ba, D., Eden, U.T., Wu, W., Eskandar, E., Lim, H.H., Temereanca, S., Suzuki, W.A., and Brown, E.N., 2015, Measuring the signal-to-noise ratio of a neuron: Proceedings of the National Academy of Sciences, v. 112, p. 7141–7146, doi: 10.1073/pnas.1505545112.

Davidson, D.W., Fröjdh, C., O'Shea, V., Nilsson, H.-E., and Rahman, M., 2003, Limitations to flat-field correction methods when using an X-ray spectrum: Nuclear Instruments and Methods in Physics Research Section A: Accelerators, Spectrometers, Detectors and Associated Equipment, v. 509, p. 146–150, doi: 10.1016/S0168-9002(03)01563-8.

Davies, G.E., and Calvin, W.M., 2017, Mapping acidic mine waste with seasonal airborne hyperspectral imagery at varying spatial scales: Environmental Earth Sciences, v. 76, p. 432, doi: 10.1007/s12665-017-6763-x.

Davis, S.M., Landgrebe, D.A., Phillips, T.L., Swain, P.H., Hoffer, R.M., Lindenlaub, J.C., and Silva, L.F., 1978, Remote sensing: The quantitative approach: McGraw-Hill International Book Company, 396 p., http://adsabs.harvard.edu/abs/1978mhi..book.....D (accessed August 2017).

Deng, W., Huang, Y., Zhao, C., Chen, L., and Wang, X., 2016, Bayesian discriminant analysis of plant leaf hyperspectral reflectance for identification of weeds from cabbages: African Journal of Agricultural Research, v. 11, p. 551–562, doi: 10.5897/AJAR2015.10395.

DeNoyelles, F., Kettle, W.D., and Sinn, D.E., 1982, The Responses of Plankton Communities in Experimental Ponds to Atrazine, the Most Heavily Used Pesticide in the United States: Ecology, v. 63, p. 1285–1293, doi: 10.2307/1938856.

Ding, S., Qin, Q., Chen, L., and Zhang, H., 2012, Hyperspectral Classification with Swarm Intelligence Optimization Algorithms: Sensor Letters, v. 10, p. 1759–1767.

Domingues Franceschini, M.H., Bartholomeus, H., van Apeldoorn, D., Suomalainen, J., and Kooistra, L., 2017, Intercomparison of Unmanned Aerial Vehicle and

Ground-Based Narrow Band Spectrometers Applied to Crop Trait Monitoring in Organic Potato Production: Sensors, v. 17, p. 1428, doi: 10.3390/s17061428.

Dozier, J., and Warren, S.G., 1982, Effect of viewing angle on the infrared brightness temperature of snow: Water Resources Research, v. 18, p. 1424–1434, doi: 10.1029/WR018i005p01424.

Du, Q., and Yang, H., 2008, Similarity-Based Unsupervised Band Selection for Hyperspectral Image Analysis: IEEE Geoscience and Remote Sensing Letters, v. 5, p. 564–568, doi: 10.1109/LGRS.2008.2000619.

Fehske, A., Gaeddert, J., and Reed, J.H., 2005, A new approach to signal classification using spectral correlation and neural networks, *in* First IEEE International Symposium on New Frontiers in Dynamic Spectrum Access Networks, 2005. DySPAN 2005., p. 144–150, doi: 10.1109/DYSPAN.2005.1542629.

Feyaerts, F., and van Gool, L., 2001, Multi-spectral vision system for weed detection: Pattern Recognition Letters, v. 22, p. 667–674, doi: 10.1016/S0167-8655(01)00006-X.

Fornace, K.M., Drakeley, C.J., William, T., Espino, F., and Cox, J., 2014, Mapping infectious disease landscapes: unmanned aerial vehicles and epidemiology: Trends in Parasitology, v. 30, p. 514–519, doi: 10.1016/j.pt.2014.09.001.

Franco, C., Pedersen, S.M., Papaharalampos, H., and Ørum, J.E., 2017, The value of precision for image-based decision support in weed management: Precision Agriculture, v. 18, p. 366–382, doi: 10.1007/s11119-017-9520-y.

Fraser, R.S., and Kaufman, Y.J., 1985, The relative importance of aerosol scattering and absorption in remote sensing: IEEE Transactions on Geoscience and Remote Sensing, p. 625–633.

Gao, J., Du, Q., Gao, L., Sun, X., and Zhang, B., 2014, Ant colony optimization-based supervised and unsupervised band selections for hyperspectral urban data classification: Journal of Applied Remote Sensing, v. 8, p. 085094–085094, doi: 10.1117/1.JRS.8.085094.

Gao, L., Gao, J., Li, J., Plaza, A., Zhuang, L., Sun, X., and Zhang, B., 2015, Multiple Algorithm Integration Based on Ant Colony Optimization for Endmember Extraction From Hyperspectral Imagery: IEEE Journal of Selected Topics in Applied Earth Observations and Remote Sensing, v. 8, p. 2569–2582, doi: 10.1109/JSTARS.2014.2371615.

Gao, B.-C., Montes, M.J., Davis, C.O., and Goetz, A.F.H., 2009, Atmospheric correction algorithms for hyperspectral remote sensing data of land and ocean: Remote Sensing of Environment, v. 113, p. S17–S24, doi: 10.1016/j.rse.2007.12.015.

Gibson, K.D., Dirks, R., Medlin, C.R., and Johnston, L., 2004, Detection of Weed Species in Soybean Using Multispectral Digital Images: Weed Technology, v. 18, p. 742–749, doi: 10.1614/WT-03-170R1.

Glenn, N.F., Mundt, J.T., Weber, K.T., Prather, T.S., Lass, L.W., and Pettingill, J., 2005, Hyperspectral data processing for repeat detection of small infestations of leafy spurge: Remote Sensing of Environment, v. 95, p. 399–412, doi: 10.1016/j.rse.2005.01.003.

Goebel, M.E., Perryman, W.L., Hinke, J.T., Krause, D.J., Hann, N.A., Gardner, S., and LeRoi, D.J., 2015, A small unmanned aerial system for estimating abundance and size of Antarctic predators: Polar Biology, v. 38, p. 619–630, doi: 10.1007/s00300-014-1625-4.

Goel, P.K., Prasher, S.O., Landry, J.A., Patel, R.M., Bonnell, R.B., Viau, A.A., and Miller, J.R., 2003, Potential of airborne hyperspectral remote sensing to detect nitrogen deficiency and weed infestation in corn: Computers and Electronics in Agriculture, v. 38, p. 99–124, doi: 10.1016/S0168-1699(02)00138-2.

Goel, P.K., Prasher, S.O., Landry, J.-A., Patel, R.M., and Viau, A.A., 2003, Hyperspectral image classification to detect weed infestations and nitrogen status in corn: Transactions of the ASAE, v. 46, p. 539.

Goel, P.K., Prasher, S.O., Landry, J.-A., Patel, R.M., Viau, A.A., and Miller, J.R., 2003, Estimation of crop biophysical parameters through airborne and field hyperspectral remote sensing: Transactions of the ASAE, v. 46, p. 1235.

Goel, P.K., Prasher, S.O., Patel, R.M., Landry, J.A., Bonnell, R.B., and Viau, A.A., 2003, Classification of hyperspectral data by decision trees and artificial neural networks to identify weed stress and nitrogen status of corn: Computers and Electronics in Agriculture, v. 39, p. 67–93, doi: 10.1016/S0168-1699(03)00020-6.

Goel, P.K., Prasher, S.O., Patel, R.M., Smith, D.L., and DiTommaso, A., 2002a, Use of airborne multi–spectral imagery for weed detection in field crops: Transactions of the ASAE, v. 45, p. 443.

Goel, P.K., Prasher, S.O., Patel, R.M., Smith, D.L., and DiTommaso, A., 2002b, Use of airborne multi–spectral imagery for weed detection in field crops: Transactions of the ASAE, v. 45, p. 443.

Goetz, A.F.H., Vane, G., Solomon, J.E., and Rock, B.N., 1985, Imaging Spectrometry for Earth Remote Sensing: Science, v. 228, p. 1147–1153, doi: 10.1126/science.228.4704.1147.

Goswami, S., Gamon, J., Vargas, S., and Tweedie, C., 2015, Relationships of NDVI, Biomass, and Leaf Area Index (LAI) for six key plant species in Barrow, Alaska: PeerJ PrePrints.

Grains Research & Development Corporation, 2010, WHY WE PURCHASED A HEADER AND WEEDSEEKER: www.grdc.com.au, https://www.grdc.com.au/Research-and-Development/GRDC-Update-Papers/2010/09/WHY-WE-PURCHASED-A-HEADER-AND-WEEDSEEKER (accessed February 2016).

Gray, C.J., Shaw, D.R., Gerard, P.D., and Bruce, L.M., 2008, Utility of Multispectral Imagery for Soybean and Weed Species Differentiation: Weed Technology, v. 22, p. 713–718, doi: 10.1614/WT-07-116.1.

Green, R.O., Conel, J.E., Carrere, V., Bruegg, C.J., Margolis, J.S., Rast, M., and Hoover, G., 1990, Determination of the In-Flight Spectral and Radiometric Characteristics of the Airborne Visible/Infrared Imaging Spectrometer (AVIRIS): AVIRIS Proceedings June 4 - 5, 1990 (JPL Publication), v. 90–54, https://aviris.jpl.nasa.gov/proceedings/workshops/90_docs/2.PDF (accessed October 2017).

Gueymard, C.A., 2004, The sun's total and spectral irradiance for solar energy applications and solar radiation models: Solar Energy, v. 76, p. 423–453, doi: 10.1016/j.solener.2003.08.039.

Guo, Z., Zhang, D., Zhang, L., and Liu, W., 2012, Feature Band Selection for Online Multispectral Palmprint Recognition: IEEE Transactions on Information Forensics and Security, v. 7, p. 1094–1099, doi: 10.1109/TIFS.2012.2189206.

Haboudane, D., Miller, J.R., Pattey, E., Zarco-Tejada, P.J., and Strachan, I.B., 2004, Hyperspectral vegetation indices and novel algorithms for predicting green LAI of crop canopies: Modeling and validation in the context of precision agriculture: Remote Sensing of Environment, v. 90, p. 337–352, doi: 10.1016/j.rse.2003.12.013.

Haggar, R.J., Stent, C.J., and Isaac, S., 1983, A prototype hand-held patch sprayer for killing weeds, activated by spectral differences in crop/weed canopies: Journal of Agricultural Engineering Research, v. 28, p. 349–358, doi: 10.1016/0021-8634(83)90066-5.

Haun, J.R., 1973, Visual Quantification of Wheat Development: Agronomy Journal, v. 65, p. 116–119, doi: 10.2134/agronj1973.00021962006500010035x.

Herrmann, I., Shapira, U., Kinast, S., Karnieli, A., and Bonfil, D.J., 2013, Ground-level hyperspectral imagery for detecting weeds in wheat fields: Precision Agriculture, v. 14, p. 637–659, doi: 10.1007/s11119-013-9321-x.

Holland Scientific, 2017, CROP CIRCLE ACS470: Holland Scientific, http://hollandscientific.com/portfolio/crop-circle-acs-470/ (accessed July 2017).

Horler, D.N.H., Dockray, M., and Barber, J., 1983, The red edge of plant leaf reflectance: International Journal of Remote Sensing, v. 4, p. 273–288, doi: 10.1080/01431168308948546.

Huang, R., and He, M., 2005, Band selection based on feature weighting for classification of hyperspectral data: IEEE Geoscience and Remote Sensing Letters, v. 2, p. 156–159, doi: 10.1109/LGRS.2005.844658.

Huang, W., Lamb, D.W., Niu, Z., Zhang, Y., Liu, L., and Wang, J., 2007, Identification of yellow rust in wheat using in-situ spectral reflectance measurements and airborne hyperspectral imaging: Precision Agriculture, v. 8, p. 187–197, doi: 10.1007/s11119-007-9038-9.

Huang, Y., Lee, M.A., Thomson, S.J., and Reddy, K.N., 2016, Ground-based hyperspectral remote sensing for weed management in crop production: International Journal of Agricultural and Biological Engineering; Beijing, v. 9, p. 98–109, doi: http://dx.doi.org/10.3965/j.ijabe.20160902.2137.

Huete, A.R., Jackson, R.D., and Post, D.F., 1985a, Spectral response of a plant canopy with different soil backgrounds: Remote Sensing of Environment, v. 17, p. 37–53, doi: 10.1016/0034-4257(85)90111-7.

Huete, A.R., Jackson, R.D., and Post, D.F., 1985b, Spectral response of a plant canopy with different soil backgrounds: Remote Sensing of Environment, v. 17, p. 37–53.

Hussain, M., Chen, D., Cheng, A., Wei, H., and Stanley, D., 2013, Change detection from remotely sensed images: From pixel-based to object-based approaches: ISPRS Journal of Photogrammetry and Remote Sensing, v. 80, p. 91–106, doi: 10.1016/j.isprsjprs.2013.03.006.

Jia, S., Tang, G., Zhu, J., and Li, Q., 2016, A Novel Ranking-Based Clustering Approach for Hyperspectral Band Selection: IEEE Transactions on Geoscience and Remote Sensing, v. 54, p. 88–102, doi: 10.1109/TGRS.2015.2450759.

Kelcey, J., and Lucieer, A., 2012, Sensor Correction of a 6-Band Multispectral Imaging Sensor for UAV Remote Sensing: Remote Sensing, v. 4, p. 1462–1493, doi: 10.3390/rs4051462.

Keshava, N., 2004, Distance metrics and band selection in hyperspectral processing with applications to material identification and spectral libraries: IEEE Transactions on Geoscience and Remote Sensing, v. 42, p. 1552–1565, doi: 10.1109/TGRS.2004.830549.

Khokhar, J.S., Sareen, S., Tyagi, B.S., Singh, G., Chowdhury, A.K., Dhar, T., Singh, V., King, I.P., Young, S.D., and Broadley, M.R., 2017, Characterising variation in wheat traits under hostile soil conditions in India: PLOS ONE, v. 12, p. e0179208, doi: 10.1371/journal.pone.0179208.

King, M.D., Kaufman, Y.J., Menzel, W.P., and Tanre, D., 1992, Remote sensing of cloud, aerosol, and water vapor properties from the moderate resolution imaging spectrometer (MODIS): IEEE Transactions on Geoscience and Remote Sensing, v. 30, p. 2–27, doi: 10.1109/36.124212.

Knipling, E.B., 1970, Physical and physiological basis for the reflectance of visible and near-infrared radiation from vegetation: Remote Sensing of Environment, v. 1, p. 155–159, doi: 10.1016/S0034-4257(70)80021-9.

Kondinin Group, 2013, Weedseeker upgrade looks the goods: Farming Ahead, http://www.farmingahead.com.au/articles/1/9196/2013-10-18/news/weedseeker-upgrade-looks-the-goods (accessed February 2016).

Kruse, F.A., Boardman, J.W., and Huntington, J.F., 2003, Comparison of airborne hyperspectral data and EO-1 Hyperion for mineral mapping: IEEE Transactions on Geoscience and Remote Sensing, v. 41, p. 1388–1400, doi: 10.1109/TGRS.2003.812908.

Lamb, D.W., 2000, The use of qualitative airborne multispectral imaging for managing agricultural crops-a case study in south-eastern Australia: Australian Journal of Experimental Agriculture, v. 40, p. 725–738.

Lamb, Weedon, and Rew, 1999, Evaluating the accuracy of mapping weeds in seedling crops using airborne digital imaging: Avena spp. in seedling triticale: Weed Research, v. 39, p. 481–492, doi: 10.1046/j.1365-3180.1999.00167.x.

Lass, L.W., Thill, D.C., Shafii, B., and Prather, T.S., 2002, Detecting Spotted Knapweed (Centaurea maculosa) with Hyperspectral Remote Sensing Technology: Weed Technology, v. 16, p. 426–432, doi: 10.1614/0890-037X(2002)016[0426:DSKCMW]2.0.CO;2.

Laursen, M.S., Jørgensen, R.N., Midtiby, H.S., Jensen, K., Christiansen, M.P., Giselsson, T.M., Mortensen, A.K., and Jensen, P.K., 2016, Dicotyledon Weed Quantification Algorithm for Selective Herbicide Application in Maize Crops: Sensors, v. 16, p. 1848, doi: 10.3390/s16111848.

Lawrence, R., 2004, Classification of remotely sensed imagery using stochastic gradient boosting as a refinement of classification tree analysis: Remote Sensing of Environment, v. 90, p. 331–336, doi: 10.1016/j.rse.2004.01.007.

Lawrence, R.L., Wood, S.D., and Sheley, R.L., 2006a, Mapping invasive plants using hyperspectral imagery and Breiman Cutler classifications (randomForest): Remote Sensing of Environment, v. 100, p. 356–362, doi: 10.1016/j.rse.2005.10.014.

Lawrence, R.L., Wood, S.D., and Sheley, R.L., 2006b, Mapping invasive plants using hyperspectral imagery and Breiman Cutler classifications (randomForest): Remote Sensing of Environment, v. 100, p. 356–362, doi: 10.1016/j.rse.2005.10.014.

Li, W., Prasad, S., Fowler, J.E., and Bruce, L.M., 2012, Locality-Preserving Dimensionality Reduction and Classification for Hyperspectral Image Analysis: IEEE Transactions on Geoscience and Remote Sensing, v. 50, p. 1185–1198, doi: 10.1109/TGRS.2011.2165957.

Liaghat, S., and Balasundram, S.K., 2010, A review: The role of remote sensing in precision agriculture: American journal of agricultural and biological sciences, v. 5, p. 50–55.

Lillesand, T., Kiefer, R.W., and Chipman, J., 2014, Remote Sensing and Image Interpretation: John Wiley & Sons, 768 p.

Lin, F., Zhang, D., Huang, Y., Wang, X., and Chen, X., 2017, Detection of Corn and Weed Species by the Combination of Spectral, Shape and Textural Features: Sustainability, v. 9, p. 1335, doi: 10.3390/su9081335.

López, S., and Stokes, D.L., 2016, Modeling the Invasion of Holly (Ilex aquifolium): Spatial Relationships and Spread Trajectories: The Professional Geographer, v. 68, p. 399–413, doi: 10.1080/00330124.2015.1102029.

López-Granados, F., 2011, Weed detection for site-specific weed management: mapping and real-time approaches: Weed Research, v. 51, p. 1–11, doi: 10.1111/j.1365-3180.2010.00829.x.

López-Granados, F., Peña-Barragán, J.M., Jurado-Expósito, M., Francisco-FERNÁNDEZ, M., Cao, R., Alonso-Betanzos, A., and Fontenla-Romero, O., 2008, Multispectral classification of grass weeds and wheat (Triticum durum) using linear and nonparametric functional discriminant analysis and neural networks: Weed Research, v. 48, p. 28–37, doi: 10.1111/j.1365-3180.2008.00598.x.

López-Granados, F., Torres-Sánchez, J., Serrano-Pérez, A., Castro, A.I. de, Mesas-Carrascosa, F.-J., and Peña, J.-M., 2016, Early season weed mapping in sunflower using UAV technology: variability of herbicide treatment maps against weed thresholds: Precision Agriculture, v. 17, p. 183–199, doi: 10.1007/s11119-015-9415-8.

Lord, D., Desjardins, R.L., and Dubé, P.A., 1988, Sun-Angle Effects on the Red and near Infrared Reflectances of Five Different Crop Canopies: Canadian Journal of Remote Sensing, v. 14, p. 46–55, doi: 10.1080/07038992.1988.10855118.

Lunetta, R.S., Congalton, R.G., Fenstermaker, L.K., ensen, J.R., McGwire, K.C., and Tinney, L.R., 1991, Remote sensing and geographic information system data integration: error sources and research issues: v. 57.

MacDonald, R.B., and Hall, F.G., 1980, Global Crop Forecasting: Science, v. 208, p. 670–679.

Mackinney, G., 1941, Absorption of light by chlorophyll solutions: J. biol. Chem, v. 140, p. 315–322.

Magarey, R., Newton, L., Hong, S.C., Takeuchi, Y., Christie, D., Jarnevich, C.S., Kohl, L., Damus, M., Higgins, S.I., Millar, L., Castro, K., West, A., Hastings, J., Cook, G., et al., 2017, Comparison of four modeling tools for the prediction of potential distribution for non-indigenous weeds in the United States: Biological Invasions, p. 1–16, doi: 10.1007/s10530-017-1567-1.

Maggiori, E., Tarabalka, Y., Charpiat, G., and Alliez, P., 2017, Convolutional Neural Networks for Large-Scale Remote-Sensing Image Classification: IEEE Transactions on Geoscience and Remote Sensing, v. 55, p. 645–657, doi: 10.1109/TGRS.2016.2612821.

Marchant, J.A., and Onyango, C.M., 2002, Spectral invariance under daylight illumination changes: Journal of the Optical Society of AmericaA, v. 19, p. 840–848.

MartÍnez-UsÓMartinez-Uso, A., Pla, F., Sotoca, J.M., and GarcÍa-Sevilla, P., 2007, Clustering-Based Hyperspectral Band Selection Using Information Measures: IEEE Transactions on Geoscience and Remote Sensing, v. 45, p. 4158–4171, doi: 10.1109/TGRS.2007.904951.

McCann, C., Repasky, K.S., Morin, M., Lawrence, R.L., and Powell, S., 2017, Using Landsat Surface Reflectance Data as a Reference Target for Multiswath Hyperspectral Data Collected Over Mixed Agricultural Rangeland Areas: IEEE Transactions on Geoscience and Remote Sensing, v. PP, p. 1–13, doi: 10.1109/TGRS.2017.2699618.

McGwire, K., Minor, T., and Fenstermaker, L., 2000, Hyperspectral Mixture Modeling for Quantifying Sparse Vegetation Cover in Arid Environments: Remote Sensing of Environment, v. 72, p. 360–374, doi: 10.1016/S0034-4257(99)00112-1.

Moshou, D., Kateris, D., Pantazi, X.E., and Gravalos, I., 2013, Crop and weed species recognition based on hyperspectral sensing and active learning: Precision Agriculture, p. 555–561.

Mouginot, J., Rignot, E., Scheuchl, B., and Millan, R., 2017, Comprehensive Annual Ice Sheet Velocity Mapping Using Landsat-8, Sentinel-1, and RADARSAT-2 Data: Remote Sensing, v. 9, p. 364, doi: 10.3390/rs9040364.

Natividade, J., Prado, J., and Marques, L., 2017, Low-cost multi-spectral vegetation classification using an Unmanned Aerial Vehicle, *in* 2017 IEEE International Conference on Autonomous Robot Systems and Competitions (ICARSC), p. 336–342, doi: 10.1109/ICARSC.2017.7964097.

Nieto, H.J., Brondo, M.A., and Gonzalez, J.T., 1968, Critical Periods of the Crop Growth Cycle for Competition from Weeds: International Journal of Pest Management: Part C, v. 14, p. 159–166, doi: 10.1080/05331856809432576.

NTech Industies, Inc., 2017, Data Sheet Model 650 Sensor:, http://www.agrioptics.co.nz/wp-content/uploads/2013/03/DataSheetModel650Sensor.pdf (accessed July 2017).

Okamoto, H., Murata, T., Kataoka, T., and Hata, S.-I., 2007, Plant classification for weed detection using hyperspectral imaging with wavelet analysis: Weed Biology and Management, v. 7, p. 31–37, doi: 10.1111/j.1445-6664.2006.00234.x.

Pantazi, X.-E., Moshou, D., and Bravo, C., 2016, Active learning system for weed species recognition based on hyperspectral sensing: Biosystems Engineering, v. 146, p. 193–202, doi: 10.1016/j.biosystemseng.2016.01.014.

Pantazi, X.E., Tamouridou, A.A., Alexandridis, T.K., Lagopodi, A.L., Kashefi, J., and Moshou, D., 2017, Evaluation of hierarchical self-organising maps for weed mapping using UAS multispectral imagery: Computers and Electronics in Agriculture, v. 139, p. 224–230, doi: 10.1016/j.compag.2017.05.026.

Pelikan, S., Heywood, S.N., and Rogstad, S.H., 2015, Weed Suppression Success Can Depend on Removal Pattern and Gene Dispersal Distance: Modeling Callery Pear: Weed Science, v. 63, p. 703–709, doi: 10.1614/WS-D-14-00100.1.

Peña, J.M., Torres-Sánchez, J., Castro, A.I. de, Kelly, M., and López-Granados, F., 2013, Weed Mapping in Early-Season Maize Fields Using Object-Based Analysis of Unmanned Aerial Vehicle (UAV) Images: PLOS ONE, v. 8, p. e77151, doi: 10.1371/journal.pone.0077151.

Plant, R.E., 2001, Site-specific management: the application of information technology to crop production: Computers and Electronics in Agriculture, v. 30, p. 9–29, doi: 10.1016/S0168-1699(00)00152-6.

Resmini, R.G., Kappus, M.E., Aldrich, W.S., Harsanyi, J.C., and Anderson, M., 1997, Mineral mapping with HYperspectral Digital Imagery Collection Experiment (HYDICE) sensor data at Cuprite, Nevada, U.S.A.: International Journal of Remote Sensing, v. 18, p. 1553–1570, doi: 10.1080/014311697218278.

Resonon Inc., 2016, Hyperspectral Imaging Cameras Datasheet: www.resonon.com, http://www.resonon.com/data-sheets/ResononHyperspectralCameras.Datasheet.pdf (accessed February 2016).

Richter, R., Reu, B., Wirth, C., Doktor, D., and Vohland, M., 2016, The use of airborne hyperspectral data for tree species classification in a species-rich Central European forest area: International Journal of Applied Earth Observation and Geoinformation, v. 52, p. 464–474, doi: 10.1016/j.jag.2016.07.018.

Riedmann, M., and Milton, E.J., 2003, Supervised band selection for optimal use of data from airborne hyperspectral sensors, *in* IGARSS 2003 IEEE International, v. 3, p. 1770–1772, doi: 10.1109/IGARSS.2003.1294245.

Rohr, J.R., and Crumrine, P.W., 2005, Effects of an herbicide and an insecticide on pond community structure and processes: Ecological Applications, v. 15, p. 1135–1147, doi: 10.1890/03-5353.

Röser, H.P., and von Schönermark, M., 1996, Comparison of remote sensing experiments from airborne and space platforms: Acta Astronautica, v. 39, p. 855–862, doi: 10.1016/S0094-5765(97)00070-2.

Rouse, J.H., Shaw, J.A., Lawrence, R.L., Lewicki, J.L., Dobeck, L.M., Repasky, K.S., and Spangler, L.H., 2010, Multi-spectral imaging of vegetation for detecting CO2 leaking from underground: Environmental Earth Sciences, v. 60, p. 313–323, doi: 10.1007/s12665-010-0483-9.

Roy, P.S., and Ravan, S.A., 1996, Biomass estimation using satellite remote sensing data—an investigation on possible approaches for natural forest: Journal of biosciences, v. 21, p. 535–561.

Rubinstein, R.Y., and Kroese, D.P., 2016, Simulation and the Monte Carlo Method: John Wiley & Sons, 436 p.

Sankey, J.B., Ravi, S., Wallace, C.S.A., Webb, R.H., and Huxman, T.E., 2012, Quantifying soil surface change in degraded drylands: Shrub encroachment and effects of fire and vegetation removal in a desert grassland: Journal of Geophysical Research: Biogeosciences, v. 117, p. G02025, doi: 10.1029/2012JG002002.

Sankey, T.T., Sankey, J.B., Weber, K.T., and Montagne, C., 2009, Geospatial Assessment of Grazing Regime Shifts and Sociopolitical Changes in a Mongolian

Rangeland: Rangeland Ecology & Management, v. 62, p. 522–530, doi: 10.2111/.1/REM-D-09-00014.1.

Scafutto, R.D.M., de Souza Filho, C.R., and de Oliveira, W.J., 2017, Hyperspectral remote sensing detection of petroleum hydrocarbons in mixtures with mineral substrates: Implications for onshore exploration and monitoring: ISPRS Journal of Photogrammetry and Remote Sensing, v. 128, p. 146–157, doi: 10.1016/j.isprsjprs.2017.03.009.

Scafutto, R.D.M., Souza Filho, C.R. de, and Rivard, B., 2016, Characterization of mineral substrates impregnated with crude oils using proximal infrared hyperspectral imaging: Remote Sensing of Environment, v. 179, p. 116–130, doi: 10.1016/j.rse.2016.03.033.

Schmidt, K.S., and Skidmore, A.K., 2003, Spectral discrimination of vegetation types in a coastal wetland: Remote Sensing of Environment, v. 85, p. 92–108, doi: 10.1016/S0034-4257(02)00196-7.

Scotford, I.M., and Miller, P.C.H., 2005, Applications of Spectral Reflectance Techniques in Northern European Cereal Production: A Review: Biosystems Engineering, v. 90, p. 235–250, doi: 10.1016/j.biosystemseng.2004.11.010.

Seibert, J.A., Boone, J.M., and Lindfors, K.K., 1998, Flat-field correction technique for digital detectors, *in* International Society for Optics and Photonics, v. 3336, p. 348–355, doi: 10.1117/12.317034.

Senay, G.B., Ward, A.D., Lyon, J.G., Fausey, N.R., and Nokes, S.E., 1998, Manipulation of high spatial resolution aircraft remote sensing data for use in site-specific farming: Transactions of the ASAE, v. 41, p. 489.

SenseFly Ltd., 2017, SenseFly eBee:, https://www.sensefly.com/drones/accessories.html (accessed October 2017).

Skakun, S., Vermote, E., Roger, J.-C., Franch, B., 1 Department of Geographical Sciences, University of Maryland, College Park, MD 20742, USA, and 2 NASA Goddard Space Flight Center Code 619, 8800 Greenbelt Road, Greenbelt, MD 20771, USA, 2017, Combined Use of Landsat-8 and Sentinel-2A Images for Winter Crop Mapping and Winter Wheat Yield Assessment at Regional Scale: AIMS Geosciences, v. 3, p. 163–186, doi: 10.3934/geosci.2017.2.163.

Slater, P.N., and Jackson, R.D., 1982, Atmospheric effects on radiation reflected from soil and vegetation as measured by orbital sensors using various scanning directions: Applied Optics, v. 21, p. 3923–3931, doi: 10.1364/AO.21.003923.

Solomon, K.R., Baker, D.B., Richards, R.P., Dixon, K.R., Klaine, S.J., La Point, T.W., Kendall, R.J., Weisskopf, C.P., Giddings, J.M., Giesy, J.P., and others, 1996,

Ecological risk assessment of atrazine in North American surface waters: Environmental Toxicology and Chemistry, v. 15, p. 31–76.

Somers, B., Asner, G.P., Tits, L., and Coppin, P., 2011, Endmember variability in Spectral Mixture Analysis: A review: Remote Sensing of Environment, v. 115, p. 1603–1616, doi: 10.1016/j.rse.2011.03.003.

Somerville, G.J., Powles, S.B., Walsh, M.J., and Renton, M., 2017, How do spatial heterogeneity and dispersal in weed population models affect predictions of herbicide resistance evolution? Ecological Modelling, v. 362, p. 37–53, doi: 10.1016/j.ecolmodel.2017.08.002.

Sorenson, P.T., Small, C., Tappert, M.C., Quideau, S.A., Drozdowski, B., Underwood, A., and Janz, A., 2017, Monitoring organic carbon, total nitrogen, and pH for reclaimed soils using field reflectance spectroscopy: Canadian Journal of Soil Science, v. 97, p. 241–248, doi: 10.1139/cjss-2016-0116.

Spectral Imaging Ltd., 2014, SPECIM Datasheets:, http://www.specim.fi/files/pdf/aisa/datasheets/AisaOWL_ver1-2014.pdf (accessed February 2016).

Staab, E.S., Slaughter, D.C., Zhang, Y., and Giles, D.K., 2009, Hyperspectral imaging system for precision weed control in processing tomato, *in* 2009 Reno, Nevada, June 21-June 24, 2009, American Society of Agricultural and Biological Engineers, p. 1.

Stafford, J.V., and Miller, P.C.H., 1996, Spatially Variable Treatment of Weed Patches: Precision Agriculture, p. 465–474, doi: 10.2134/1996.precisionagproc3.c50.

Steven, M.D., 1993, Satellite remote sensing for agricultural management: opportunities and logistic constraints: ISPRS Journal of Photogrammetry and Remote Sensing, v. 48, p. 29–34, doi: 10.1016/0924-2716(93)90029-M.

Su, H., Du, Q., Chen, G., and Du, P., 2014, Optimized Hyperspectral Band Selection Using Particle Swarm Optimization: IEEE Journal of Selected Topics in Applied Earth Observations and Remote Sensing, v. 7, p. 2659–2670, doi: 10.1109/JSTARS.2014.2312539.

Sugiyama, M., 2007, Dimensionality reduction of multimodal labeled data by local fisher discriminant analysis: Journal of machine learning research, v. 8, p. 1027–1061.

Sui, R., Thomasson, J.A., Hanks, J., and Wooten, J., 2008, Ground-based sensing system for weed mapping in cotton: Computers and Electronics in Agriculture, v. 60, p. 31–38, doi: 10.1016/j.compag.2007.06.002.

Sun, K., Geng, X., and Ji, L., 2015, A New Sparsity-Based Band Selection Method for Target Detection of Hyperspectral Image: IEEE Geoscience and Remote Sensing Letters, v. 12, p. 329–333, doi: 10.1109/LGRS.2014.2337957.

Swain, P., and King, R., 1973, Two Effective Feature Selection Criteria for Multispectral Remote Sensing: LARS Technical Reports, https://docs.lib.purdue.edu/larstech/39.

Swayze, G.A., 1997, The hydrothermal and structural history of the Cuprite mining district, southwestern Nevada: An integrated geological and geophysical approach [Ph.D.]: University of Colorado at Boulder, 399 p., https://search.proquest.com/docview/304359978/abstract/54274CE5AADD4B21PQ/1 (accessed September 2017).

Thenkabail, P., 2017, Hyperspectral Remote Sensing of Vegetation and Agricultural Crops: Photogrammetric Engineering & Remote Sensing (PE&RS);80,(2014) Pagination 697,723, http://repo.mel.cgiar.org/handle/20.500.11766/5374 (accessed October 2017).

Thenkabail, P.S., Enclona, E.A., Ashton, M.S., and Van Der Meer, B., 2004, Accuracy assessments of hyperspectral waveband performance for vegetation analysis applications: Remote Sensing of Environment, v. 91, p. 354–376, doi: 10.1016/j.rse.2004.03.013.

Thenkabail, P.S., Smith, R.B., and De Pauw, E., 2002, Evaluation of narrowband and broadband vegetation indices for determining optimal hyperspectral wavebands for agricultural crop characterization: Photogrammetric Engineering and Remote Sensing, v. 68, p. 607–622.

Thenkabail, P.S., Smith, R.B., and De Pauw, E., 2000, Hyperspectral Vegetation Indices and Their Relationships with Agricultural Crop Characteristics: Remote Sensing of Environment, v. 71, p. 158–182, doi: 10.1016/S0034-4257(99)00067-X.

Thorp, K.R., and Tian, L.F., 2004, A Review on Remote Sensing of Weeds in Agriculture: Precision Agriculture, v. 5, p. 477–508, doi: 10.1007/s11119-004-5321-1.

Tidemann, B.D., Hall, L.M., Harker, K.N., and Alexander, B.C.S., 2016, Identifying Critical Control Points in the Wild Oat (Avena fatua) Life Cycle and the Potential Effects of Harvest Weed-Seed Control: Weed Science, v. 64, p. 463–473, doi: 10.1614/WS-D-15-00200.1.

Todd, S.W., Hoffer, R.M., and Milchunas, D.G., 1998, Biomass estimation on grazed and ungrazed rangelands using spectral indices: International Journal of Remote Sensing, v. 19, p. 427–438, doi: 10.1080/014311698216071.

Topcon Positioning Systems, Inc., 2017, Cropspec Brochure:, https://www.topconpositioning.com/sites/default/files/product_files/cropspec_broch_7010-0957_revf_sm_2.pdf (accessed July 2017).

Torres-Sánchez, J., López-Granados, F., Castro, A.I.D., and Peña-Barragán, J.M., 2013, Configuration and Specifications of an Unmanned Aerial Vehicle (UAV) for Early Site Specific Weed Management: PLOS ONE, v. 8, p. e58210, doi: 10.1371/journal.pone.0058210.

Toutin, T., 2004, Review article: Geometric processing of remote sensing images: models, algorithms and methods: International Journal of Remote Sensing, v. 25, p. 1893–1924, doi: 10.1080/0143116031000101611.

U.S. Climate Data, 2017, Climate Bozeman: U.S. Climate Data, http://www.usclimatedata.com/climate/bozeman/montana/united-states/usmt0040 (accessed August 2017).

USDA, 2016, Montana Annual Bulletin 2016: USDA 1095-7278 LIII, https://www.nass.usda.gov/Statistics_by_State/Montana/Publications/Annual_Statistical_Bulletin/2016/Montana_Annual_Bulletin_2016.pdf (accessed November 2017).

Uto, K., Seki, H., Saito, G., Kosugi, Y., and Komatsu, T., 2016, Development of a Low-Cost, Lightweight Hyperspectral Imaging System Based on a Polygon Mirror and Compact Spectrometers: IEEE Journal of Selected Topics in Applied Earth Observations and Remote Sensing, v. 9, p. 861–875, doi: 10.1109/JSTARS.2015.2472293.

Vanderlip, R.L., and Reeves, H.E., 1972, Growth Stages of Sorghum [Sorghum bicolor, (L.) Moench.]: Agronomy Journal, v. 64, p. 13–16, doi: 10.2134/agronj1972.00021962006400010005x.

Verrelst, J., Rivera, J.P., Gitelson, A., Delegido, J., Moreno, J., and Camps-Valls, G., 2016, Spectral band selection for vegetation properties retrieval using Gaussian processes regression: International Journal of Applied Earth Observation and Geoinformation, v. 52, p. 554–567, doi: 10.1016/j.jag.2016.07.016.

Villa, T.F., Gonzalez, F., Miljievic, B., Ristovski, Z.D., and Morawska, L., 2016, An Overview of Small Unmanned Aerial Vehicles for Air Quality Measurements: Present Applications and Future Prospectives: Sensors, v. 16, p. 1072, doi: 10.3390/s16071072.

Wang, C., Zhou, B., and Palm, H.L., 2008, Detecting Invasive Sericea Lespedeza (Lespedeza cuneata) in Mid-Missouri Pastureland Using Hyperspectral Imagery: Environmental Management, v. 41, p. 853–862, doi: 10.1007/s00267-008-9092-8.

Weis, M., Gutjahr, C., Ayala, V.R., Gerhards, R., Ritter, C., and Schölderle, F., 2008, Precision farming for weed management: techniques: Gesunde Pflanzen, v. 60, p. 171–181, doi: 10.1007/s10343-008-0195-1.

Wendel, A., and Underwood, J., 2016, Self-supervised weed detection in vegetable crops using ground based hyperspectral imaging, *in* 2016 IEEE International Conference on Robotics and Automation, p. 5128–5135, doi: 10.1109/ICRA.2016.7487717.

Xia, X., Che, H., Zhu, J., Chen, H., Cong, Z., Deng, X., Fan, X., Fu, Y., Goloub, P., Jiang, H., Liu, Q., Mai, B., Wang, P., Wu, Y., et al., 2016, Ground-based remote sensing of aerosol climatology in China: Aerosol optical properties, direct radiative effect and its parameterization: Atmospheric Environment, v. 124, p. 243–251, doi: 10.1016/j.atmosenv.2015.05.071.

Yang, H., Du, Q., and Chen, G., 2012, Particle Swarm Optimization-Based Hyperspectral Dimensionality Reduction for Urban Land Cover Classification: IEEE Journal of Selected Topics in Applied Earth Observations and Remote Sensing, v. 5, p. 544–554, doi: 10.1109/JSTARS.2012.2185822.

Yang, H., Du, Q., Su, H., and Sheng, Y., 2011a, An Efficient Method for Supervised Hyperspectral Band Selection: IEEE Geoscience and Remote Sensing Letters, v. 8, p. 138–142, doi: 10.1109/LGRS.2010.2053516.

Yang, H., Du, Q., Su, H., and Sheng, Y., 2011b, An Efficient Method for Supervised Hyperspectral Band Selection: IEEE Geoscience and Remote Sensing Letters, v. 8, p. 138–142, doi: 10.1109/LGRS.2010.2053516.

Yang, C., Everitt, J.H., and Bradford, J.M., 2007, Airborne hyperspectral imagery and linear spectral unmixing for mapping variation in crop yield: Precision Agriculture, v. 8, p. 279–296, doi: 10.1007/s11119-007-9045-x.

Ye, X., Sakai, K., Garciano, L.O., Asada, S.-I., and Sasao, A., 2006, Estimation of citrus yield from airborne hyperspectral images using a neural network model: Ecological Modelling, v. 198, p. 426–432, doi: 10.1016/j.ecolmodel.2006.06.001.

Yuan, C., Zhang, Y., and Liu, Z., 2015, A survey on technologies for automatic forest fire monitoring, detection, and fighting using unmanned aerial vehicles and remote sensing techniques: Canadian Journal of Forest Research, v. 45, p. 783–792, doi: 10.1139/cjfr-2014-0347.

Zhang, L., and Weng, Q., 2016, Annual dynamics of impervious surface in the Pearl River Delta, China, from 1988 to 2013, using time series Landsat imagery: ISPRS Journal of Photogrammetry and Remote Sensing, v. 113, p. 86–96, doi: 10.1016/j.isprsjprs.2016.01.003.

Zheng, B., Myint, S.W., Thenkabail, P.S., and Aggarwal, R.M., 2015, A support vector machine to identify irrigated crop types using time-series Landsat NDVI data: International Journal of Applied Earth Observation and Geoinformation, v. 34, p. 103–112, doi: 10.1016/j.jag.2014.07.002.

Zhu, Z., Wang, S., and Woodcock, C.E., 2015, Improvement and expansion of the Fmask algorithm: cloud, cloud shadow, and snow detection for Landsats 4–7, 8, and Sentinel 2 images: Remote Sensing of Environment, v. 159, p. 269–277, doi: 10.1016/j.rse.2014.12.014.

Zwiggelaar, R., 1998, A review of spectral properties of plants and their potential use for crop/weed discrimination in row-crops: Crop Protection, v. 17, p. 189–206, doi: 10.1016/S0261-2194(98)00009-X.